Dopaminergic modulation of odor responses by local interneurons in the olfactory bulb

Inauguraldissertation

zur

Erlangung der Würde eines Doktors der Philosophie

vorgelegt der

Philosophisch-Naturwissenschaftlichen Fakultät

der Universität Basel

von

Sebastian Tylman Bundschuh

aus Friedberg / Hessen, Deutschland

Basel, 2011

creative commons

Namensnennung-Keine kommerzielle Nutzung-Keine Bearbeitung 2.5 Schweiz

Sie dürfen:

das Werk vervielfältigen, verbreiten und öffentlich zugänglich machen

Zu den folgenden Bedingungen:

Namensnennung. Sie müssen den Namen des Autors/Rechteinhabers in der von ihm festgelegten Weise nennen (wodurch aber nicht der Eindruck entstehen darf, Sie oder die Nutzung des Werkes durch Sie würden entlohnt).

Keine kommerzielle Nutzung. Dieses Werk darf nicht für kommerzielle Zwecke verwendet werden.

Keine Bearbeitung. Dieses Werk darf nicht bearbeitet oder in anderer Weise verändert werden.

- Im Falle einer Verbreitung müssen Sie anderen die Lizenzbedingungen, unter welche dieses Werk fällt, mitteilen. Am Einfachsten ist es, einen Link auf diese Seite einzubinden.

- Jede der vorgenannten Bedingungen kann aufgehoben werden, sofern Sie die Einwilligung des Rechteinhabers dazu erhalten.

- Diese Lizenz lässt die Urheberpersönlichkeitsrechte unberührt.

Quelle: http://creativecommons.org/licenses/by-nc-nd/2.5/ch/   Datum: 3.4.2009

Genehmigt von der Philosophisch-Naturwissenschaftlichen Fakultät auf Antrag von:

PD Dr. Rainer W. Friedrich
(Dissertationsleiter)

Prof. Dr. Andreas Lüthi
(Korreferent)

Prof. Dr. Silvia Arber
(Fakultätsverantwortliche)

Basel, den 26. April 2011

<div align="right">

Prof. Dr. Martin Spiess
(Dekan)

</div>

Abbreviations

AP	Action potential
AP5	D-(-)-2-Amino-5-phosphonopentanoic acid
CGP 54626	[S-(R*,R*)]-[3-[[1-(3,4-Dichlorophenyl)ethyl]amino]-2-hydroxypropyl](cyclohexylmethyl) phosphinic acid
ChR2	Channelrhodopsin-2
Dihydrexidine	(±)-trans-10,11-Dihydroxy-5,6,6a,7,8,12b-hexahydrobenzo[a]phenanthridine hydrochloride
Dopamine	2-(3,4-Dihydroxyphenyl)ethylamine hydrochloride, 3,4-Dihydroxyphenethylamine hydrochloride, 3-Hydroxytyramine hydrochloride, 4-(2-Aminoethyl)-1,2-benzenediol hydrochloride
Gabazine	6-Imino-3-(4-methoxyphenyl)-1(6H)-pyridazinebutanoic acid hydrobromide
IR DIC	Infrared differential interference contrast
Kynurenic acid	4-Hydroxyquinoline-2-carboxylic acid
LED	Light-emitting diode
MPTP	1-methyl-4-phenyl-1,2,3,6-tetrahydropyridine
NBQX	2,3-Dioxo-6-nitro-1,2,3,4-tetrahydro-benzo[f] quinoxaline-7-sulfonamide disodium salt
ON	Olfactory nerve
ORN	Olfactory receptor neuron
PBS	phosphate buffered saline
PMT	photomultiplier
PSTH	Peristimulus time histogram
Quinpirole	(4aR-trans)-4,4a,5,6,7,8,8a,9-Octahydro-5-propyl-1H-pyrazolo[3,4-g]quinoline hydrochloride
SN	Substantia nigra
Sulpiride	(S)-5-Aminosulfonyl-N-[(1-ethyl-2-pyrrolidinyl)methyl]-2-methoxybenzamide
TH	Tyrosine hydroxylase
VTA	Ventral tegmental area

Abstract

The olfactory bulb is one of the few regions in the brain where dopamine is provided locally by an intrinsic population of GABAergic interneurons but their role in processing of sensory information remains ambiguous. I examined the function of dopamine in processing of natural odors within the intact olfactory bulb of zebrafish by a combination of calcium-sensitive dye imaging and electrophysiological recordings in conjunction with traditional pharmacological manipulations and optogenetic stimulation. My results demonstrate that dopamine does not exert a prominent effect on olfactory nerve input. Instead, it directly modulates mitral cell properties by means of D2 receptors. Bath application of dopamine had a direct hyperpolarizing effect on mitral cells, resulting in an increase in neuronal response threshold and a suppression of spontaneous firing. As a direct consequence of the shift in response threshold, weak excitatory and inhibitory odor responses were abolished, whereas strong odor responses were enhanced. Therefore, the contrast within odor responses was enhanced, while the general pattern of activity remained rather stable. To directly analyze endogenous dopamine release I stimulated periglomerular cells using optogenetic tools. Experiments revealed a very slow dopaminergic effect that gradually built up over several seconds. It is therefore unlikely that dopamine directly participates in initial odor processing, but rather provides a mechanism to adapt the system to slow changes in the environment. Potential functions could be a channel-autonomous background subtraction or a global contrast enhancement.

Introduction

The dopaminergic system is traditionally associated with brain stem nuclei such as the substantia nigra (SN) or the ventral tegmental area (VTA) (Wise, 2004; Björklund and Dunnett, 2007). These mesencephalic systems provide neuromodulatory input by long-distance projections to most of the telencephalon and have been linked to reward learning (VTA) and motor behavior (SN). However, the by far larger number of dopaminergic neurons is located within a telencephalic structure itself: the olfactory bulb (Björklund and Lindvall, 1984; McLean and Shipley, 1988). In contrast to the brain stem systems, in the olfactory bulb dopamine is provided exclusively by an intrinsic population of GABAergic interneurons and is thought to participate in local computations (Halász et al, 1977a, 1977b; Halász et al, 1978; Kosaka et al, 1985, 1995; Gall et al, 1987). However, little is known about its role in early sensory processing. Furthermore, to date its function in olfactory computations in the intact network remains highly speculative since most studies used slice preparations or cell cultures with unnatural electrical stimulation. I therefore investigated the role of dopamine in the intact zebrafish olfactory bulb as this system is one of the few vertebrate models that allows for a comprehensive analysis of a large proportion of the intact microcircuit using natural odor stimuli (Yaksi and Friedrich, 2006).

The olfactory system

The olfactory bulb is a telencephalic structure that receives direct input from olfactory receptor neurons (ORNs) in the nose. Each ORN expresses a single odorant receptor out of a repertoire of approximately 1000 different receptors in rodents and about 100 – 200 in teleosts (Mombaerts, 1999). ORNs expressing the same

receptor are scattered throughout the epithelium, but their axons converge in the olfactory bulb onto one or a few discrete glomeruli (Buck, 2000). The total number of glomeruli is approximately 2000 in mice and 200 in zebrafish. Within glomeruli, ORN axons form synapses with the principal cells of the olfactory bulb, the mitral cells, and with inhibitory interneurons. Mitral cells not only project to higher brain areas, but also interact within the olfactory bulb with two classes of inhibitory interneurons: the periglomerular cells that are part of the juxtaglomerular system, and the granule cells that are located in the deep layers of the olfactory bulb (Fig. 1).

Information processing in the olfactory bulb

Each odorant receptor can bind multiple different odor molecules, and each odorant is recognized by multiple types of odorant receptors. Consequently, a given odor molecule is initially represented in the olfactory bulb by the activation of a specific combination of glomeruli (Friedrich and Korsching, 1997; Rubin and Katz, 1999; Wachowiak and Cohen, 2001). As shown in zebrafish by calcium- (Friedrich and Korsching, 1997) and voltage-sensitive dye imaging (Friedrich and Korsching, 1998), odors belonging to the same category cause excitation in defined regions of the olfactory bulb. In zebrafish, three different natural classes of odorants have been studied: amino acids, bile acids, and nucleotides. Amino acids are represented in the ventro-lateral region of the olfactory bulb, bile acids in the medial, and nucleotides in the posterior-lateral region of the olfactory bulb (Friedrich and Korsching, 1998). Within the amino acid-sensitive region, glomeruli activated by short-chain neutral amino acids cluster in a different part than those activated by long-chain neutral or basic amino acids (Friedrich and Korsching, 1997). Hence, chemical features of odor stimuli are spatially mapped onto the array of glomeruli in a coarse fashion that is referred to as

"chemotopy". This functional topography of the primary sensory map is, however, less prominent than in other sensory systems. A potential reason might be the lack of feature continuity in odor-space (Friedrich and Stopfer, 2001).

Temporal response patterns of ORNs are relatively simple. Firing frequency rises upon odor stimulation and adapts slowly during stimulation (Friedrich and Laurent, 2001, 2004). Mitral cell responses, in contrast, exhibit a prominent temporal structure on at least two different timescales. First, mitral cell firing frequencies are modulated dynamically over hundreds of milliseconds (Friedrich and Laurent, 2001, 2004; Laurent, 2002). Responses are sometimes multiphasic and can include both sequences of increased as well as decreased activity. These dynamics have been termed slow temporal patterns and are both cell- and odor-dependent. After a few hundred milliseconds, mitral cell activity patterns converge onto a steady-state. When comparing odor representations by ensembles of mitral cells, activity patterns are initially very similar to each other for odors within the same category, but become continuously more dissimilar as the steady-state is approached (Friedrich and Laurent, 2001). Morphing of one odor into a similar but molecularly different odor leads to aprupt changes of mitral cell activity patterns. Hence, neuronal circuits in the olfactory bulb decorrelate activity patterns evoked by similar odors and classify them into discrete network states similar to attractor network models (Niessing and Friedrich, 2010). This decorrelation and discretization of odor representations may facilitate the discrimination of similar odors and avoid interference between odor representations stored in associative memory circuits. Furthermore, it has been shown that inhibitory interactions are crucial for spatio-temporal patterning of the olfactory bulb output (Yokoi et al, 1995; Friedrich and Laurent, 2004; Lagier et al, 2004; Tabor et al. 2008). An analytical study has demonstrated

both mathematically and by computational modeling that pattern decorrelation in the olfactory bulb is likely to dependent on mitral cell spontaneous activity (Wiechert et al, 2010).

As first reported by Adrian (1942), odors evoke prominent oscillations in the beta and gamma range in the local field potential (LFP) of the olfactory bulb (Gray, 1994; Laurent, 2002). Fast odor-evoked subthreshold oscillations are also observed in mitral cells (Friedrich and Laurent, 2001; Friedrich et al. 2004) and reflect the synchronized activity of odor-specific subsets of mitral cells (Friedrich and Laurent, 2001). In insects, it has been proposed that information conveyed by the synchronization of action potentials (APs) is involved in the discrimination of different cell assemblies (Wehr and Laurent, 1996; Stopfer et al, 1997). Data by Friedrich et al (2004) in zebrafish show that phase-locking of odor-specific mitral cell subsets provides a means to simultaneously convey complementary stimulus information by the same activity pattern. As temporal modulations are lacking in the ORN input patterns (Friedrich and Korsching, 1997; Friedrich and Laurent 2001, 2004), these oscillations must emerge from intrinsic properties of the network in the olfactory bulb. The most likely mechanism to generate them is the interaction between mitral cells and granule cells via recurrent and lateral inhibition (Friedrich et al, 2004).

In summary, mitral cells exhibit prominent spatio-temporal activity patterns on different time scales. Slow temporal patterning causes a decorrelation of mitral cell responses over time and has been associated with odor discrimination and memory formation. Mitral cells also exhibit fast odor-evoked subthreshold oscillations that are thought to enhance the bandwidth of information transmission to the telencephalon (Friedrich et al, 2004). Furthermore, the olfactory bulb is also involved in other computations such as processing of odor

mixtures (Tabor et al, 2004) and population gain control (Friedrich and Laurent, 2004). Inhibitory interactions with local interneurons are important for all of these processes (Yokoi et al, 1995; Friedrich and Laurent, 2004; Lagier et al, 2004).

Functional architecture of the olfactory bulb

Within the glomeruli the ORN projections innervate only a subdivision of each glomerulus termed the olfactory nerve (ON) zone, where ORN fibers form excitatory glutamatergic synapses with the principal neurons of the olfactory bulb, the mitral cells. The intraglomerular regions devoid of ORN axons are termed non-ON zones. Each mitral cell extends its apical dendrite into the glomerular layer where it ramifies within one to a few glomeruli. In contrast to the ORN terminals, however, the mitral cell dendrites are not limited to the ON zones (Kasowski et al, 1999; Kosaka et al, 2001). Furthermore, the ORN fibers also contact inhibitory periglomerular cells that are part of the juxtaglomerular system.

The mitral cells interact with two different sets of local inhibitory interneurons. The most numerous group are the granule cells whose somata are located in the central region of the olfactory bulb. Being approximately 10 – 100 times more numerous than mitral cells, granule cells account for the largest subpopulation of neurons within the olfactory bulb. Granule cells do not possess axonal processes but form reciprocal dendrodendritic synapses with the dendrites of mitral cells (Pinching and Powell, 1971a, 1971b, Satou, 1990). APs within mitral cell dendrites or axon collaterals cause release of glutamate that excites postsynaptic granule cells via alpha-amino-3-hydroxy-5-methylisoxazole-4-proprionic acid (AMPA) and N-methyl-D-aspartate (NMDA) receptors. This, in return, triggers the release of
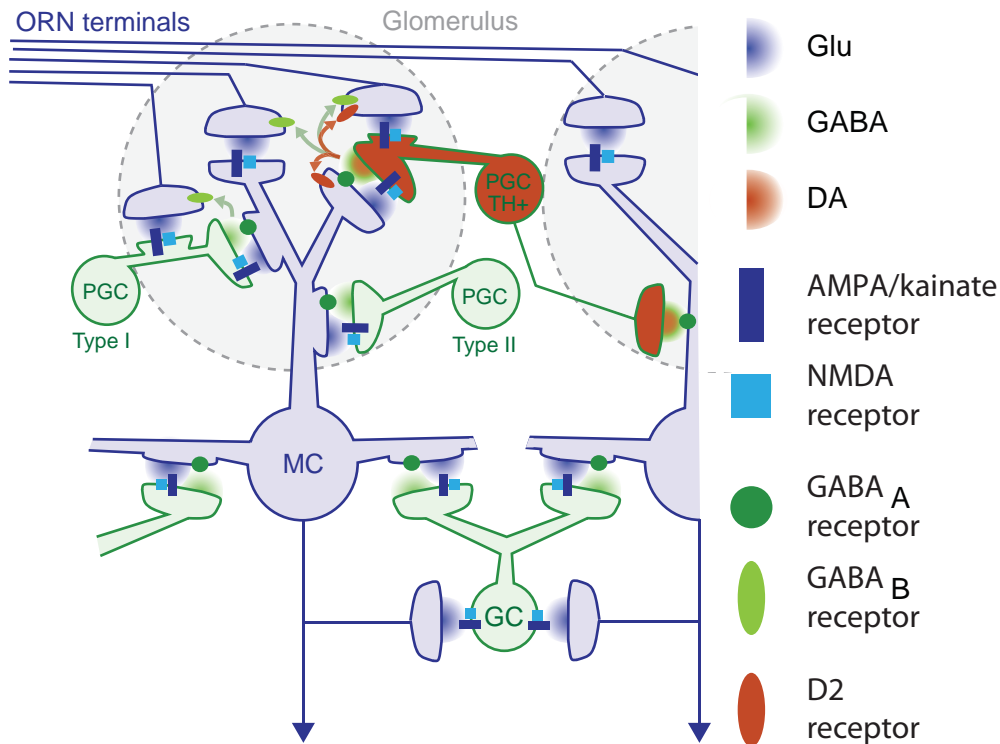
Figure 1: Simplified diagram of the olfactory bulb microcircuit. In the glomerular layer, olfactory receptor neurons form excitatory glutamatergic synapses on mitral cells and type 1 periglomerular cells including the TH-positive dopaminergic subpopulation. All types of periglomerular cells also receive excitatory glutamatergic input from mitral cells and provide GABAergic inhibition to the same mitral cells. In addition, periglomerular cells also inhibit presynaptic nerve terminals by activation of GABA receptors via spillover. Dopaminerigic periglomerular cells co-release dopamine as a neurotransmitter that has been shown to target olfactory receptor neurons and/or mitral cells by D2 receptors. In addition, it has been suggested that dopaminergic neurons participate in an interglomerular network. In deeper layers mitral cells provide excitatory glutamatergic input to granule cells by reciprocal dendro-dendritic synapses and axon collaterals. In turn granule cells release GABA from dendro-dendritic synapses causing recurrent inhibition of the same mitral cells and lateral inhibition of neighboring mitral cells. Abbreviations: ORN: olfactory receptor neuron; MC: mitral cell; PGC: periglomerular cell; GC: granule cell; TH+: tyrosine hydroxylase positive. (Figure modified with permission of Tabor and Friedrich, 2008)

gamma-aminobutyric-acid (GABA) from granule cell dendrites that inhibits mitral cells via $GABA_A$-receptors. The dendritic granule cells synapses are thought to be capable of releasing neurotransmitters at subthreshold membrane potentials (Chen et al, 2000; Egger et al, 2003, 2005), triggered by calcium influx through either NMDA receptors (Chen et al, 2000; Halabisky et al, 2000) or a combination of NMDA and high voltage-activated (HVA) calcium channels (Isaacson and Strowbridge, 1998; Schoppa et al, 1998; Isaacson JS, 2001). It has been shown that brief stimulation of mitral cells often triggers barrages of inhibitory postsynaptic currents (IPSCs) lasting hundreds of milliseconds (Isaacson and Strowbridge, 1998; Schoppa et al, 1998). Thus, transmitter release from granule cell dendrites is termed "asynchronous" as it substantially outlasts the triggering event.

It has been proposed that granule cells may operate in three different modes: first, small focal depolarizations in the dendrites cause influx of calcium restricted to a single reciprocal synaptic site and, consequently, evoke highly localized release of GABA. This mechanism would result in recurrent inhibition of individual mitral cells (Chen et al, 2000; Egger et al, 2005). Second, stronger dendritic activation can elicit calcium spikes in dendrites that invade the entire dendritic tree and trigger global transmitter release, which is thought to result in lateral inhibition of neighboring mitral cells. Third, somatic APs, which are presumably initiated at the soma, can also invade the entire dendritic tree, providing an additional mechanism for lateral inhibition (Egger et al, 2003, 2005).

Periglomerular cells, the second class of inhibitory interneurons, are located within the glomerular layer. They are known to interact with mitral cell dendrites as well as with the ORN terminals. In many species their somata are located around the outer layer of a

glomerulus (Pinching and Powell, 1971a, 1971b; Schneider and Macrides, 1978). In rats, most periglomerular cells have only one primary dendrite that enters a single glomerulus and arborizes extensively to form a short bushy tree (Pinching and Powell, 1971a, 1971b). Periglomerular cells receive excitatory input from the ORN terminals and form inhibitory reciprocal dendrodendritic synapses with mitral cells, similar to the synaptic conncetions between mitral and granule cells (Pinching and Powell, 1971a, 1971b, Schneider and Macrides, 1978). An electrophysiological study (Murphy et al, 2005) indicates that single action potentials evoked by small depolarizations fail to evoke substantial transmitter release from periglomerular neurons. Stronger depolarizations, however, result in an L-type mediated calcium spike that triggers strong and long-lasting ("asynchronous") GABA release.

Periglomerular cells also contact other periglomerular cells within the same glomerulus and in neighboring glomeruli. They are likely to be linked both by dendrodendritic synapses (Pinching and Powell, 1971a, 1971b; Kosaka et al, 2001) and by axonal projections within the periglomerular neuropil (Pinching and Powell, 1971c). At least a subset of these projections is GABAergic (Murphy et al, 2005) and acts via $GABA_A$-receptors that are expressed on the surface of periglomerular cells (Laurie et al, 1992; Fritschy and Mohler, 1995). This is particularly intriguing as the chloride concentration is increased in a subpopulation of periglomerular cells (Siklos et al, 1995; Smith and Jahr, 2002). Smith and Jahr (2002) reported that GABA depolarizes periglomerular cells, and yet exerts an inhibitory effect by shunting inhibition. In addition, these authors found that periglomerular cells exhibit a strong self-inhibition driven by $GABA_A$-receptors in close vicinity to the presynaptic sites that causes tonic inhibition at rest. GABAergic inhibition might therefore act on other

periglomerular cells by spillover during odor stimulation (but see Murphy et al, 2005).

While the existence of functional GABAergic synapses is well established, recent immunocytochemical and electron microscopy studies suggest that periglomerular cells are in fact very heterogeneous. Based on the combinatorial expression of GABA, calretinin, and calbindin, Kosaka et al, (1995, 1998) discriminated three major classes of periglomerular cells and concluded that further subclasses may exist. Periglomerular cells also differ with respect to their connectivity patterns and are classified into two different subpopulations, one spreading its dendrites throughout the glomerulus (type 1), and one extending its dendrites only to the non-ON zones (type 2) (Kosaka et al, 1997; Kosaka et al, 1998). Type 1 periglomerular cells receive ORN input and form unidirectional dendrodendritic synapses onto mitral cells, whereas type 2 periglomerular cells do not receive ORN input but establish reciprocal dendrodendritic synapses with mitral cells. In addition, type 1 and type 2 periglomerular cells are also neurochemically distinct: the dendritic structure of GABAergic periglomerular cells (Kosaka et al, 1997; Kosaka et al, 1998) resembles the type 1 pattern, while calretinin- and calbindin-positive periglomerular cells exhibit a type 2 pattern (Toida et al, 1998). Therefore, it is likely that the two subpopulations serve different tasks, providing either feed-forward (type 1) or feedback (type 2) inhibition to the mitral cells.

Despite of the absence of direct synaptic contacts on the ORN terminals there is also inhibitory feedback from the periglomerular cells to ORN terminals. This mechanism is driven by GABA spillover that exerts a tonic suppression of ORN terminals at rest and presynaptic inhibition of odor-evoked synaptic input to glomeruli (Wachowiak and Cohen, 1999; Aroniadou-Aderjaska et al, 2000;

Duchamp-Viret et al, 2000; Tabor et al, 2008). The inhibitory effect is mediated by GABA$_B$-receptors that are expressed on the ORN terminals (Chu et al, 1990; Bonino et al, 1999).

The basic synaptic circuitry described above appears to be conserved, albeit not identical, throughout all vertebrate classes including fish (Andres, 1970; Satou, 1990; Byrd and Brunjes, 1995). One dominant feature of the olfactory bulb of both vertebrates and invertebrates is that interactions between mitral cells are predominantly or exclusively inhibitory in nature. Inhibitory interactions occur over multiple spatial scales and are mediated by different types of interneurons with distinct physiological properties. Therefore, it is likely that these populations are involved in different computational tasks. It is unknown, however, in which way the individual inhibitory pathways contribute to information processing in the olfactory bulb.

The dopaminergic network in the olfactory bulb

It is long known that tyrosine hydroxylase (TH), the rate limiting enzyme for catecholamine synthesis, is expressed by local neurons in the olfactory bulb. Furthermore, as these cells also express aromatic L-amino acid decarboxylase, but not dopamine-β-hydroxylase, they have been identified as dopaminergic neurons (Halász et al, 1977, 1978; Gonzales and Smeets, 1991). It has been demonstrated that these neurons form a subpopulation of periglomerular cells and utilize GABA as a co-transmitter (Gall et al, 1987; Kosaka et al, 1985; Kosaka et al, 1995). Several studies revealed that the dendrites of this subpopulation spread throughout the entire volume of the innervated glomeruli thus resembling the dendritic pattern of type 1 periglomerular cells (Kosaka et al, 1997; Kosaka et al, 1998). As confirmed by electron-microscopy, TH-

positive neurons receive glutamatergic synaptic contacts from ON terminals, accounting for about 80% of all synapses (Kosaka et al, 1997; Toida et al, 2000). A second source of glutamatergic input are mitral cells. However, so far no typical reciprocal synapses have been observed (Toida et al, 2000). In addition, dopaminergic neurons are also subject to GABAergic control, presumably by other periglomerular cells (Toida et al, 2000).

Several different targets of dopaminergic periglomerular cells have been identified by anatomical studies: first, neurons form direct dendrodendritic synapses onto mitral cells. Second, in mammals a high density of dopaminergic D2 receptors has been consistently found in the ON and glomerular layers by radioactive ligand binding assays (Palacios et al, 1981; Boyson et al, 1986; Camps et al, 1990; Mansour el al, 1990; Coronas et al, 1997), in situ hybridization studies (Mansour el al, 1990; Coronas et al, 1997; Koster et al, 1999), and antibody stainings (Levey et al, 1993) and has been attributed to the ORNs. However, there are also contradicting findings. In amphibians, radioligand binding and immunohisto-chemistry data have suggested that mitral cells might be the primary target of dopamine (Duchamp-Viret et al, 1997; Davison et al, 2004). In mammals, several studies have supported the existence of D2 receptors in mitral cells as well (Mansour et al, 1990; Levey et al, 1993; Davida et al, 2003). A more recent study in rats has confirmed the existence of D2 receptors on the afferent terminals by electron-microscopy using immunogold labeling (Gutièrrez-Mecinas et al, 2005), but also provided evidence for D2 receptors on mitral cell dendrites near presynaptic sites as well as on dopaminergic periglomerular cells, thus supporting a more complex action of dopamine in the olfactory bulb. As no direct synaptic contacts onto the afferent nerve fibers have been observed, dopamine is expected to act on presynaptic terminals by spillover effects (Pinching and

Powell, 1971b). However, little is known about the release sites for dopamine and how they relate to GABAergic release from the same neurons. Furthermore, recent studies have identified the dopaminergic periglomerular cell as the major source of interglomerular connections (Aungst et al, 2003; Kosaka and Kosaka, 2008; Kiyokage et al, 2010; Kosaka and Kosaka, 2011). It has been shown that their axons can innervate tens to even hundreds of glomeruli (Aungst et al, 2003; Kiyokage et al, 2010). In the zebrafish olfactory bulb the existence of dopaminergic neurons has been confirmed by several studies (Byrd and Brunjes, 1995; Kaslin and Panula, 2001). However, little is known about the precise morphology of these cells.

While there is strong evidence for the existence of dopamine receptors in the olfactory bulb, their functional implications are less well studied. Early experiments have demonstrated that dopamine decreases extracellular field potential responses to stimulation of the ON (Nowycky et al, 1983; Gurski and Hamilton, 1996; Hsia et al, 1999; Ennis et al, 2001). In rats, dopamine also reduces paired-pulse depression of field potential responses and, hence, the effect has been attributed to modulation of presynaptic afferent terminals (Hsia et al, 1999; Ennis et al, 2001). Studies in non-mammalian systems, however, have reported similar effects for extracellular field potentials evoked by stimulation of the olfactory tract suggesting at least a contribution of postsynaptic targets (Nowycky et al, 1983; Gurski and Hamilton, 1996).

It has been demonstrated that dopamine as well as D2 receptor agonists can suppress adenylyl cyclase activity in ORNs (Vargas and Lucero, 1999, 2002; Mania-Farnell et al, 1993; Coronas et al, 1999). In rat cell cultures this has been shown to cause a hyperpolarization of receptor neurons by modulation of a hyperpolarization-activated

inward-rectifying current (Vargas and Lucero, 1999, 2002). Furthermore, calcium-sensitive dye imaging experiments in hemisected turtle brains revealed a D2 receptor-mediated suppression of calcium influx in the afferent terminals (Wachowiak and Cohen, 1999). In line with these findings Berkowicz and Trombley (2000) reported a dopamine-induced decrease in excitatory postsynaptic responses to nerve stimulation using patch-clamp recordings, but failed to identify any effect onto mitral cells directly. Similar results were also obtained in acute slices from rats (Ennis et al, 2001). However, there is also some evidence for an effect of dopamine onto mitral cells targeting lateral interactions with interneurons by reducing transmitter release from mitral cells (Davida et al, 2003; Davison et al, 2004) or by augmenting GABA-mediated currents (Brünig et al, 1999).

While the existence of D2 receptors in the olfactory bulb is generally accepted, evidence for D1 receptors in the olfactory bulb remains ambiguous. A few anatomical studies in mammals have reported the existence of D1 receptors at low density (Diop et al, 1988; Camps et al, 1990; Mansour et al, 1990; Nickell et al, 1991; Levey et al, 1993; Coronas et al, 1997). However, most of these studies relied on radioligand binding assays using [^{3}H]SCH 23390 or [^{125}I]SCH 23982. Both agents are known to also exhibit potent binding to 5-HT1c and 5-HT2 receptors (Hoyer and Karpf, 1988; Briggs et al, 1991; Woodward et al, 1992) that are expressed in the rat olfactory bulb (Morilak et al, 1993; Hardy et al, 2005, Petzold et al, 2009). Only two studies utilized other methods (immunohistochemistry: Levey et al, 1993; in situ hybridization: Coronas et al, 1997). In addition, several studies have failed to detect D1 receptors in the olfactory bulb (Monsma et al, 1990; Mengod et al, 1991; Guthrie et al, 1991). Functional evidence is weak and purely based on experiments in cell

culture and isolated cell membranes, respectively (Brünig et al, 1999; Coronas et al, 1999; Davida et al, 2003).

Little is known about the characteristics of dopaminerigic periglomerular cells. Recent data in mice have demonstrated that these neurons exhibit prominent pacemaker currents and are spontaneously active at rest (Pignatelli et al, 2005; Puopolo et al, 2005). However, to date only a single study has addressed dopamine and GABA co-release (Maher and Westbrook, 2008). While the authors provide clear evidence for GABAergic autoinhibition in TH-positive neurons they failed to measure dopaminergic currents in response to direct electrical stimulation. Furthermore, to date no data are available on the role of dopamine within the intact system.

In my doctoral thesis I therefore studied the role of dopamine in processing of natural odors within the intact olfactory bulb of zebrafish. By employing calcium-sensitive dye imaging and electrophysiological recordings in combination with traditional pharmacological manipulations and optogenetic stimulation I found that dopamine does not exert a prominent control of the afferent sensory input. Rather, dopamine influences principal neurons directly by means of D2 receptors as had been suggested in the amphibian system (Duchamp-Viret et al, 1997). Bath application of dopamine has a direct hyperpolarizing effect and suppresses spontaneous firing in mitral cells. As a consequence, the response threshold of the input-output function is elevated. In addition, also the gain of the transfer function is increased. Similar results are also obtained for natural odor stimuli: inhibitory and weak excitatory odor responses in mitral cells are abolished while strong excitatory responses get amplified. Nevertheless, the general population response pattern remains rather stable. When evoking endogenous dopamine release directly by optogenetic stimulation it becomes apparent that

dopaminergic effects exhibit very slow temporal dynamics rendering it unlikely that dopamine will play a prominent role in initial odor processing. From my data it is therefore more probable that dopamine provides a modulatory mechanism to adapt the system to slow changes in the environment. Possible functions could be a correction for tonic background stimuli or a contrast enhancement. While initial experiments emphasize a large expansion of individual neurons none of the above mentioned functions can be excluded to date. Further experiments will be required to elucidate the exact role of the dopaminergic network in the olfactory bulb.

Material and Methods

Animals, preparation and odor stimulation

All experiments were performed in accordance with the official guidelines for animal care and approved by the Veterinary Department of the Canton of Basel-Stadt (Switzerland).

Zebrafish (Danio rerio) were kept in the laboratory at 24–27°C at a light/dark cycle of 13/11 hours. All physiological recordings were performed in an explant preparation of adult (≥ 6 months old) zebrafish comprising the entire brain and nose (Friedrich and Laurent, 2001; Yaksi and Friedrich, 2006) Briefly, zebrafish were anesthetized by cooling in fish water. Animals were then transferred into teleost artifical cerebrospinal fluid (ACSF, Mathieson and Maler, 1988) and decapitated. Eyes and lower jaw were removed and the palate plate was opened to expose the ventral forebrain. For better access to the tissue, the dura marter was routinely removed. The preparation was then mounted in a custom-made flow chamber and transferred to the microscope.

All experiments were performed at room temperature (~22° C). Throughout the experiment, the tissue was continuously perfused with ACSF containing (in mM): 124 NaCl, 2 KCl, 1.6 $MgSO_4$, 2 $CaCl_2$, 1.25 KH_2PO_4, 24 $NaHCO_3$, 22 Glucose (Mathieson and Maler, 1988), and aerated with carbogen (O2: 95%, CO2: 5%). To unambiguously identify mitral cells in the intact tissue, a zebrafish line was used that expresses the transgenic calcium indicator yellow cameleon (YC) under the control of the HuC promoter (Miyawaki et al, 1997; Higashijima et al, 2003; Li et al, 2005). For optogenetic stimulation of specific subpopulations with blue light, two zebrafish lines were utilized (Zhu et al, 2009). Both fish lines express channelrhodopsin-2

(ChR2) by employing the iTet-Off system to enhance gene expression (Gossen and Bujard, 1992; Huang et al, 2005; Schonig and Bujard, 2003; Bockamp et al, 2008). One line expressed ChR2 under control of a HuC promoter fragment that directs expression to mitral cells (HuC:itTA/Ptet:ChR2YFP Line 03). The other line expressed ChR2 under the Dlx4/6 promoter, which targets GABAergic interneurons (Zerucha et al, 2000; Li et al, 2005). It has been shown that one of the transgenic fish lines exhibits preferential expression in the glomerular layer of the olfactory bulb (Dlx4/6:itTA/Ptet:ChR2YFP Line 01, Zhu el al, 2009). In mice, several studies have demonstrated that dopaminergic periglomerular cells express Dlx5/6, the murine orthologs of Dlx4/6 (Allen et al, 2007; Kohwi et al, 2007). For immunohistochemical stainings a zebrafish line expressing GFP under control of the Dlx4/6 promoter was used (Dlx4/6:GFP, Zerucha et al, 2000; Ghanem et al, 2003). A total of 72 zebrafish were used for experiments.

Odor stimulation and pharmacological agents

For odor stimulation, Teflon tubing (1 mm inner diameter) was directed to the naris of the fish. Odors were introduced into a constant stream of ACSF by a computer-controlled, pneumatically actuated HPLC injection valve (Rheodyne, Rohnert Park, CA, USA). The volume of the applied odor solution was adjusted to the velocity of the flow to obtain a stimulus duration of ~2.4 s. Amino acids of highest available purity ($\geq$ 99.0% (NT), Fluka, Neu-Ulm, Germany or Sigma Aldrich, Munich, Germany) were used as odorants. Solutions were prepared freshly from frozen stocks (10 mM) and used at a final concentration of 10 µM. In some experiments several amino acids were mixed to increase the chance to evoke an odor response in the recorded cells, resulting in a final concentration of 30 – 60 µM. Amino acids are natural stimuli for teleosts (Carr, 1988; Hara, 1994). The

concentrations used in the experiments are in the intermediate physiological range (Carr, 1988) and do not saturate glomerular responses (Friedrich and Korsching, 1997; Friedrich and Korsching, 1998).

Stock solutions of pharmacological agents were kept frozen and diluted in ACSF to their final concentrations just before the experiment. Concentrations were similar to those used previously in other studies (Hsia et al, 1999; Ennis et al, 2001; Gorelova et al, 2002; Davison et al, 2004; Tabor and Friedrich, 2008; Tabor et al, 2008). In experiments employing dopamine, ascorbic acid was added to prevent oxidative degradation of dopamine (Uchida et al, 2000). For concentrations see table 1:

Table 1: Concentrations of agonists / antagonists				
Pharmacological agent	**Stock**	**Solvent**	**Dilution**	**Final concentration**
Dopamine + Ascorbic acid	50 mM 50 mM	H_2O	1:500-1:1,000	50-100 µM
Dihydrexidine	10 mM	H_2O	1:1,000	10 µM
Quinpirole	10 mM	H_2O	1:1,000	10 µM
Sulpiride	100 mM	DMSO	1:2,000	50 µM
NBQX	50 mM	H_2O	1:10,000	5 µM
AP5	100 mM	H_2O	1:2,000	50 µM
Gabazine	20 mM	H_2O	1:2,000-1:4,000	5-10 µM
CGP 54626	50 mM	DMSO	1:10,000	5 µM
Kynurenic acid	Prepared freshly in ACSF			2 mM

Dopamine, kynurenic acid and sulpiride were obtained from Sigma Aldrich (Munich, Germany). All other agents were purchased from Tocris Bioscience (Bristol, UK).

Imaging

Microscope

Physiological recordings were performed using a custom-built two-photon microscope based on an Olympus BX51WI torso (Olympus, Hamburg, Germany, for a schematic diagram of the beam path see Fig. 2). The microscope was equipped with a mode-locked Ti:Sapphire laser (SpectraPhysics, Mountain View, CA, USA). Fluorescence evoked by two-photon stimulation (Denk et al, 1990) was separated from excitation light by a dichroic mirror (735 nm longpass) and detected externally by two photomultipliers (PMTs; Hamamatsu Photonics, Hamamatsu City, Japan). To protect the PMTs from back-scattered excitation light an infrared blocking filter (Calflex X, Qioptiq Photonics, Munich, Germany) was installed in the detection beam path.

In addition, the microscope featured a modified double port magnification change unit (WI-DPMC, Olympus) for transmission light and infrared differential interference contrast (IR DIC) microscopy. Illumination was provided by conventional transmission light equipped with a filter for IR illumination (730-830 nm) and a digital video camera (Basler AG, Ahrensburg, Germany) was used for monitoring the image on the computer screen. To allow for simultaneous IR DIC and two-photon imaging, the original dichroic mirror in the WI-DPMC unit was replaced with an 800 nm longpass filter to separate two-photon excitation from IR DIC emission light. In addition, a 740/80 nm bandpass filter was mounted in front of the

camera port to protect it from laser light. The microscope was also equipped with an epifluorescence condensor (BX-RFA, Olympus) for whole-field fluorescence imaging. A 150 W xenon arc lamp (Opti-Quip, Highland Mills, NY, USA) was used for fluorescence illumination. Signals were detected by a sensitive cooled CCD camera (CoolSnapEZ, Photometrics, Tucson, AZ, USA).

For optical stimulation of ChR2 with blue light by whole-field illumination, the arc lamp was exchanged for a strong blue light-emitting diode (LED; Philips Lumileds, San Jose, CA, USA). A 470/22 nm bandpass filter was employed as an excitation filter. To permit rapid computer-controlled switching of the LED a self-made microcircuit based on a BuckPuck driver (LEDdynamics, Randolph, VT, USA) was utilized to drive the LED. A 700 nm longpass dichroic was used to feed the LED light into the beam path to prevent interference with NIR laser light excitation. To prevent excess stimulation of the tissue, the illumination area was restricted to the field of view using the field and aperture iris diaphragms, respectively. When combining two-photon targeted patching with blue light stimulation the 735 nm dichroic mirror was exchanged for a 725 nm dichroic with a second transmission band in the range between 450 – 500 nm (approximately 50% transmission efficacy), allowing for simultaneous transmission of blue LED and NIR laser stimulation light. In this case an additional blocking filter for blue light (Razoredge 488 nm longpass filter) was introduced into the detection beam path to protect the PMTs. For two-photon activation of ChR2, the field of view was scanned with the laser using a conventional frame scan pattern. During flyback laser light was blocked using a Pockel's cell (Conoptics, Danbury, CT, USA).

All imaging experiments were performed using a 20x water immersion objective (NA 0.95, Olympus). For patch-clamp

experiments in some instances a 60x water immersion objective (NA 1.1) was used (both Olympus, Hamburg, Germany). If not specified otherwise, filters and mirrors were obtained from AHF (Tübingen, Germany).

For stimulation with patterns of blue light, a movable objective microscope (Sutter, Novato, CA, USA) was used. The microscope was customized for two-photon laser scanning microscopy (Niesing and Friedrich, 2010) and equipped with a blue laser (RGB Lasersysteme, Kelheim, Germany) to provide collimated light for stimulation of ChR2. To generate spatial patterns of light a digital micromirror device (DMD, Texas Instruments, Dallas, TX, USA) was utilized to project the blue laser light onto the dichroic mirror. This device consists of an array of 1024x768 individually controlled mirrors that can flip with sub-millisecond precision thereby either feeding the blue excitation light into the beam path of the microscope ('on' state) or into a beam trap ('off' state).

Conventional calcium-sensitive dye imaging

To visualize odor evoked activity in the afferent axon terminals, receptor neurons were selectively loaded with the calcium indicator Oregon Green 488 BAPTA-1-dextran (OGB1-dextran, 10 kD; Invitrogen, Carlsbad, CA, USA) as described previously (Friedrich and Korsching, 1997). In summary, zebrafish were anesthetized using 0.01% tricaine methanesulfonate (MS-222). Fish were then transferred to a dissecting microscope and fixated in a wet paper towel. A tube was placed in their mouth for continuous perfusion with fresh fish tank water containing 0.01% MS-222. Nasal cavities were injected with a solution containing 3% OGB1-dextran, 0.1% Triton-X, and 1 mM NaCl (0.5 – 1.5 µl per side). After 4 – 6 minutes the solution was rinsed and fishes were moved to a fish tank to recover

from anaesthesia. To allow the olfactory cilia to regenerate, fishes were only used 3 – 7 days after injection.

Fluorescence signals were recorded with the microscope as described above using a xenon arc lamp for whole-field illumination in combination with a CCD camera. Filter sets were used as following: 495/30 nm bandpass excitation filter, 515 nm longpass dichroic mirror, and a 545/50 nm bandpass emission filter. Excitation light intensity was adjusted with neutral density filters to minimize bleaching. Series of images were recorded for 15 s at a rate of 4 Hz and were digitized at 12 bits. A spatial binning of 2x2 pixels was applied yielding a final image resolution of 696x520 pixels. Data were acquired using custom-written software based on IGOR (Wavemetrics, Lake Oswego, OR, USA) and analyzed offline. Raw OGB1-fluorescence signals were converted to fractional change in pixel intensity relative to pre-stimulus baseline ($\Delta F/F$). The baseline fluorescence F was obtained by averaging the raw pixel values over 3.5 s before onset of the stimulus. Spatial odor response maps were calculated by averaging the $\Delta F/F$ images over a period of 5.25 s starting 0.5 s after stimulus onset. To analyze odor response patterns, presumed glomeruli were outlined manually from the $\Delta F/F$ images by identifying the local maxima. The mean response amplitude was calculated for each individual region of interest for a 3.75 s time window starting 1 s after stimulus onset using a 1 s pre-stimulus baseline as a reference. Individual experiments were aligned to the earliest response observed throughout the recordings. Each odor was applied twice and responses were averaged for analysis. Pharmacological agents were washed-in for at least 10 minutes before recording odor-evoked responses. Similarly, drugs were washed out for at least 15 minutes. Frequently, additional measurements at later times were taken to confirm that responses remained stable throughout each condition (data not shown).

Two-photon calcium-sensitive dye imaging

For two-photon calcium imaging experiments the olfactory bulb was loaded with the cell permeable dye Rhod2-AM by bolus injections as described (Brustein et al, 2003, Stosiek et al, 2003, Yaksi and Friedrich, 2006). Briefly, 50 µg of Rhod2-AM were dissolved in 16 µl DMSO/Pluronic Acid F-127 (80/20) and stored at -20° C. For each experiment, the solution was prepared freshly from the stocks by diluting 3 µl in 27 µl oxygenated ACSF (1:10). Dye was injected into the ventrolateral region of the olfactory bulb with a glass pipette. To obtain a uniform staining of the tissue, dye was injected at 4 – 5 planes and at several sites (usually three) per plane with a distance of approximately 30 µm between sites. Experiments started approximately 30 – 60 minutes after injection of the dye to achieve stable dye levels in the cells and to allow tissue to recover from the injection procedure. To identify mitral cells, experiments were performed in transgenic zebrafish expressing HuC:YC.

Fluorophores were excitied by two-photon excitation at 860 nm. Laser power was optimized to minimize noise and photobleaching. Rhod-2 and YC signals were detected simultaneously through emission filters (Rhod-2: 610/75 nm bandpass; YC: 515/30 nm or 510/50 nm bandpass filters). Image series were acquired for ~13.8 s at a frame rate of approximately 3.26 Hz (256x256 pixels, 1.2 ms/line). Data were digitized using a National Instruments data acquisition card (Austin, TX, USA) and recorded with SCANIMAGE (Svoboda Lab, Cold Spring Harbor Laboratory and Janelia Farm Research Campus; https://openwiki.janelia.org/wiki/display/ SvobodaLab/; Pologruto et al, 2003). Raw fluorescence values for image series were converted pixel-wise into ΔF/F values as described for conventional whole-field fluorescence imaging using a 2.8 s pre-stimulus baseline. To calculate time-averaged maps a 4.9 s
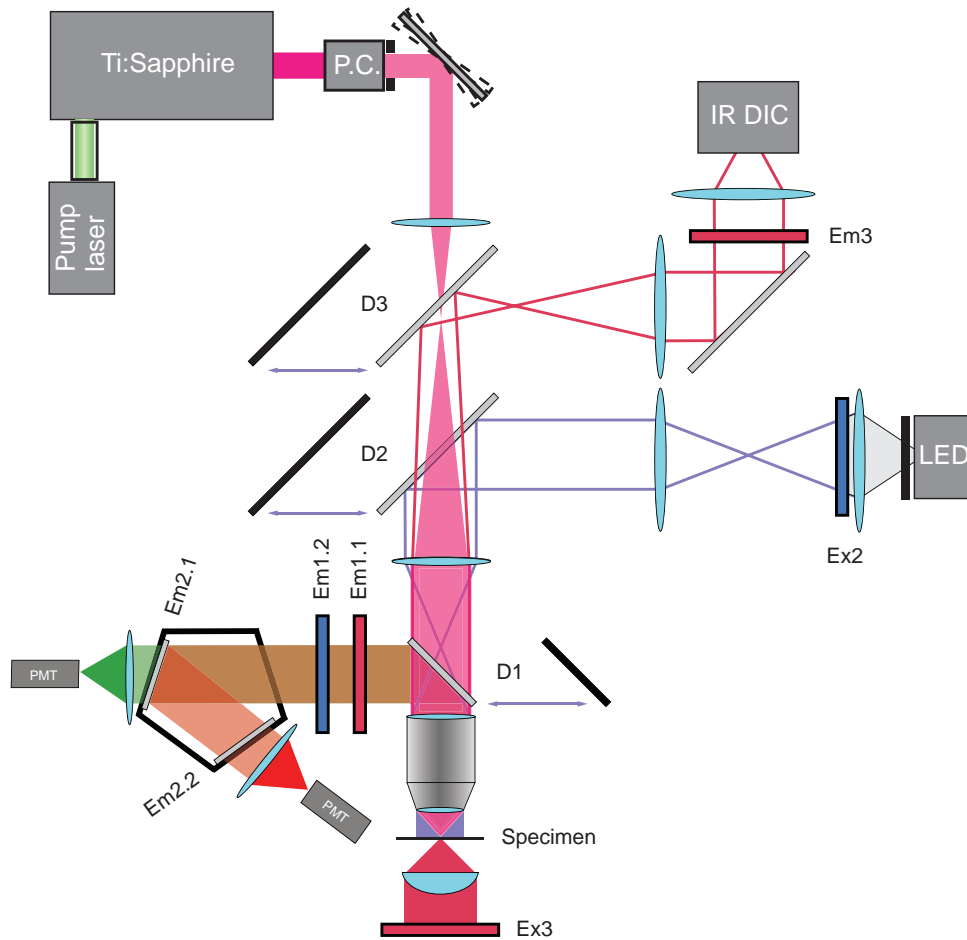
Figure 2: Schematic diagram of the beam path of the microscope equipped for simultaneous two-photon laser scanning micrsocopy, IR DIC imaging, and whole-field stimulation with blue LED light.

Two-Photon laser scanning microscopy:
- Dichroic: 725 nm longpass with a second band at 450 - 500 nm (D1)
- Protective: Calflex X (Em1.1), Razoredge 488 nm longpass (Em1.2)
- Emission: YC: 515/30 nm or 510/50 nm bandpass (En2.1)
               Rhod-2:   610/75 nm bandpass (Em2.2)

Blue light LED excitation:
- Dichroic: 700 nm longpass (D2)
- Excitation: 470/22 nm bandpass (Ex2)

IR DIC imaging:
- Dichroic: 800 nm longpass (D3)
- Excitation: 730 - 830 nm bandpass filter (Ex3)
- Protective: 740/80 nm blocking filter (Em3)

Objective: 20x water immersion objective (NA: 0.95)

P.C.:   Pockel's cell

time window starting just after response onset was chosen. Regions of interest corresponding to mitral cell somata were assigned manually based on the raw YC fluorescence images. Mean response amplitudes were calculated on the same time windows as the odor response maps.

For each fish, mitral cell responses to sets of 3 – 4 odors were recorded. Each stimulus was presented twice and responses were averaged. In each experiment, mitral cells from 1 – 3 focal planes were measured. Responses were recorded before, during and after application of dopamine. The drug was administered for at least 10 minutes before measurements started. Accordingly, dopamine was allowed to wash out for at least 15 minutes.

Electrophysiological recordings

Electrophysiological measurements of mitral cells in the ventrolateral olfactory bulb were performed by whole-cell patch clamp recordings. Spontaneous activity and evoked responses were recorded both in current clamp and in single-electrode continuous voltage clamp mode using a Multiclamp 700B amplifier (Molecular Devices, Sunnyvale, CA, USA). In current clamp, bridge balance was routinely compensated, as was electrode capacity in voltage clamp configuration. Data were filtered with an analogue 4-pole Bessel filter at a cut-off frequency of 4 kHz and digitized at 10 kHz using a National Instruments data acquisition card (Austin, TX, USA). Data were recorded by using custom-written software (Ephus; Svoboda Lab, Cold Spring Harbor Laboratory and Janelia Farm Researc Campus; https://openwiki.janelia.org/wiki/display/SvobodaLab/; Suter et al, 2010). Borosilicate patch pipettes (5.6 – 18 MΩ) were produced on a laser-based electrode puller (Sutter, Novato, CA, USA). Intracellular pipette solution contained (in mM) 130 K-gluconate, 10

Na-gluconate, 10 Na-phosphocreatine, 4 NaCl, 4 Mg-ATP, 0.3 Na-GTP, and 10 HEPES (pH 7.25). Alexa Fluor 594 (50 µM) was added to determine cell morphology.

Experiments were performed in HuC:YC, HuC:itTA/Ptet:ChR2YFP, and Dlx4/6:itTA/Ptet:ChR2YFP zebrafish lines. In the HuC lines expressing a fluorophore in mitral cells, neurons were targeted by a combination of IR DIC imaging and by two-photon targeted patching utilizing 515/30 nm or 510/50 nm bandpass emission filters. In a few cases, whole-field fluorescent camera imaging was used to identify mitral cells (excitation: 510/20 nm bandpass, emission: 540 nm longpass, dichroic: 530 nm longpass). In the Dlx4/6:itTA/Ptet:ChR2YFP line, mitral cells were targeted by IR DIC using the location and size of their somata as an indicator. Identity was confirmed based on the morphological features after establishing whole-cell configuration and filling with Alexa Fluor 594.

Mitral cell responses to several different types of stimuli were recorded in different experiments. To examine the effect of dopamine on mitral cells, 2 s current step injections of variable amplitude (-100 pA to +100 pA) were used. In addition, also responses to a single amino acid or a mixture of several amino acids were recorded in these cells. Each stimulus was repeated 3 times. For establishing the effect of dopamine on membrane potential, spontaneous firing rate, and input resistance, only cells were included that did not require any holding currents. For odor responses, small holding currents to stabilize the recordings (mean -17.2 ± 31.5 pA) were accepted. The absolute amplitudes of odor responses were calculated in a 500 ms time window starting just after stimulus onset. For relative amplitudes, a 500 ms pre-stimulus baseline was subtracted.

For establishing the capabilities of ChR2 in HuC:itTA/Ptet:ChR2YFP, sustained light stimuli (1 s duration) and trains of light pulses (10 – 15 ms) with constant (1 s duration, 5 – 40 Hz) and Poisson distributed (10 s duration, λ = 100 – 200 ms) inter-spike time intervals were applied in current clamp mode. In addition, responses to sustained light pulses (1 s) were also measured in voltage-clamp mode. In the Dlx4/6:itTA/Ptet:ChR2YFP line, trains of light pulses at frequencies of 20 – 50 Hz and with durations of up to 10 s were tested both in current and voltage clamp mode. Only data for 10 s pulse trains at 50 Hz are shown as no D2-receptor mediated effects were observed for any other condition. In a separate set of experiments, mitral cell responses to 10 s pulse trains at 50 Hz of variable spatial pattern were analyzed. Spatial patterns consisted of a round center of variable diameter with either the center ('Center', 40 – 100 μm, usually 2-3 different diameters tested per cell) or the periphery ('Surround', 40 – 200 μm, usually 2-3, up to 5 different diameters tested per cell) being illuminated. For each mitral cell, spatial stimulus patterns were individually centered onto the approximate center of their dendritic tuft. In all cases, stimuli were repeated 3 – 5 times. For experiments using LED whole-field illumination, responses were first averaged over all repetitions. Resulting traces in the presence and absence of sulpiride were subtracted to obtain the D2 receptor-mediated current. Amplitudes of the effect were measured by computing the mean holding current in a 250 ms time window just before stimulus offset relative to a corresponding time window starting 250 ms after stimulus onset. This baseline was chosen to compensate for offset effects. As sulpiride was not applied in those experiments exploring the effect of spatial patterns onto the effect of dopamine the response amplitude was estimated by calculating the difference in mean for a 1 s time window starting 1 s after stimulus offset relative to a corresponding time window just before stimulus onset.

When the effect of pharmacological agents was tested, measurements were taken before, during and after the application of the substance. Drugs were washed in for at least 5 minutes and washed out for 10 minutes, respectively, before starting the recordings.

Immunohistochemistry

Zebrafish brains were fixed in 2% paraformaldehyde in 1x phosphate buffered saline (PBS) and incubated over night at 4°C. Tissue was then rinsed three times (15 minutes) in 1x PBS, transferred to 30% sucrose in 1x PBS solution and kept over night at 4°C. Brains were placed in M-1 embedding matrix (Thermo Fisher Scientific, Waltham, MA, USA), quickly frozen and cut into 20 µm sections with a cryostat. Sections were allowed to adjust to room temperature for at least 2 hours prior to further processing. Slides were stained using a Discovery XT (system and chemicals: Ventana, Tucson, AZ, USA). Sections were pre-fixed for 8 minutes with RiboFix and incubated with the primary and secondary antibody for 60 and 32 minutes, respectively. In between each step slides were rinsed with Reaction Buffer. After the staining procedure slides were washed three times with reaction buffer, two times with 1x PBS and briefly with distilled water. In a final step slides were mounted using ProLong Gold antifade reagent (Invitrogen, Carlsbad, CA, USA). Slides were allowed to dry at room temperature for 24 hours before further processing. Rabbit anti-TH primary antibody was used at a dilution of 1:140 (antibody provided by W Driever). Anti-rabbit secondary antibody was conjugated to Alexa-633 (Molecular Probes, Eugene, OR, USA) and used at a dilution of 1:200. Antibodies were diluted in AB diluting solution (Ventana, Tucson, AZ, USA).

Images were taken with an LSM 510 inverted confocal laser scanning microscope equipped with a Plan-Neofluar 40x oil immersion objective (NA: 1.3, Zeiss, Jena, Germany). Alexa-633 and GFP were excited at 633 nm and 488 nm and emission was detected using a 650 longpass and a 505 – 530 bandpass filter, respectively. Individual channels were recorded in successive scans.

Data analysis

Data were analyzed offline using IgorPro (Wavemetrics, Lake Oswego, OR, USA) and MATLAB (Mathworks, Natick, MA, USA). For electrophysiological recordings, the mean membrane potential and spontaneous firing rates were calculated on recordings of spontaneous activity (5 repeats, 10 s each). The input resistance was measured from hyperpolarizing current injections in current clamp mode as voltage-clamp recordings were not routinely included for all cells. In each case, the smallest hyperpolarizing stimulus was chosen (-10 to -25 pA) and the resulting shift in membrane potential was calculated by taking the mean over a 1 s time window starting 1 s after stimulus onset relative to pre-stimulus baseline. Results obtained from voltage-clamp recordings yielded similar results (data not shown). To determine the input-output curves for mitral cells, firing rates in response to depolarizing and hyperpolarizing current injections were calculated on a 1 s time window starting 1 s after stimulus onset. This time window was chosen to obtain a steady-state estimate of firing rates, but qualitatively similar results were also obtained for other time windows. For each mitral cell, the rising phase of the mean input-output curves was fitted with a line. For this purpose curves were first interpolated using a piecewise cubic Hermite interpolation algorithm. As response curves were not always increasing monotonically, data points on the right of the maximum firing rate were excluded, as were data points left to the first zero

point. Linear fits were calculated for the interval comprising 10% – 90% of the maximum amplitude. Several other fitting strategies were tested that generally produced similar results, but were usually more sensitive to outliers.

Peristimulus time histograms (PSTHs) were calculated by convolving spike trains with a Gaussian kernel (Odor-evoked responses: σ = 50 ms, responses to Poisson-distributed pulses of blue light: σ = 100 ms) and averaged over all repetitions. PSTHs for odor responses were aligned manually to the onset of the earliest response observed within the same fish before averaging. Differences in PSTHs were tested for significance using a Wilcoxon sign rank test for paired samples on mean firing rates in consecutive time windows with a width of 50 ms (other values gave similar results).

If not mentioned otherwise, significance tests were performed using a Wilcoxon sign rank test for paired samples.

Pearson correlation coefficients were averaged by first performing a Fisher transformation and computing mean ± standard deviation (SD) on the resulting z-values. Values were then transformed back to correlation coefficients. Similarly, correlations coefficients for different correlation clusters of the matrix and testing of statistical significance were performed on the z-transformed values. In these cases a Student's t-test was applied for significance tests.

Results

Dopaminergic targeting of olfactory nerve terminals

In the past it has been proposed that dopamine acts as a feedback signal to directly decrease sensory input to the olfactory bulb (Hsia et al, 1999; Wachowiak and Cohen, 1999; Berkowicz and Trombley, 2000; Ennis et al, 2001; Maher and Westbrook, 2008). Several studies, however, have argued for a purely postsynaptic action of dopamine (Nowycky et al, 1983; Gurski and Hamilton, 1996; Duchamp-Viret et al, 1997). To distinguish between these two options I first analyzed the effect of dopamine on the afferent input to the olfactory bulb. In rodents, neurotransmitter release from ON terminals is proportional to the change in presynaptic calcium concentration (Bozza et al, 2004; Murphy et al, 2004). Furthermore, dopamine has been shown to directly attenuate calcium influx into the nerve terminals of turtles (Wachowiak and Cohen, 1999). I therefore performed calcium-sensitive dye imaging of sensory input to the olfactory bulb of adult zebrafish brain. For this purpose ORNs were selectively labeled with Oregon-Green BAPTA-1 dextran by injections into the nasal cavity (n = 10 fish). Odor-evoked changes in fluorescence were measured by CCD camera imaging under whole-field illumination (Friedrich and Korsching, 1997; Tabor et al, 2004; Tabor et al, 2008). Relative changes in fluorescence in response to odor stimulation were first measured in absence of any pharmacological agents. Drugs were then introduced into the continuous stream of ACSF for at least 10 minutes and responses to the original set of odors were measured again. Afterwards, drugs were washed out for at least 15 minutes and measurements were repeated. I tested the effects of dopamine (100 µM), the selective D1
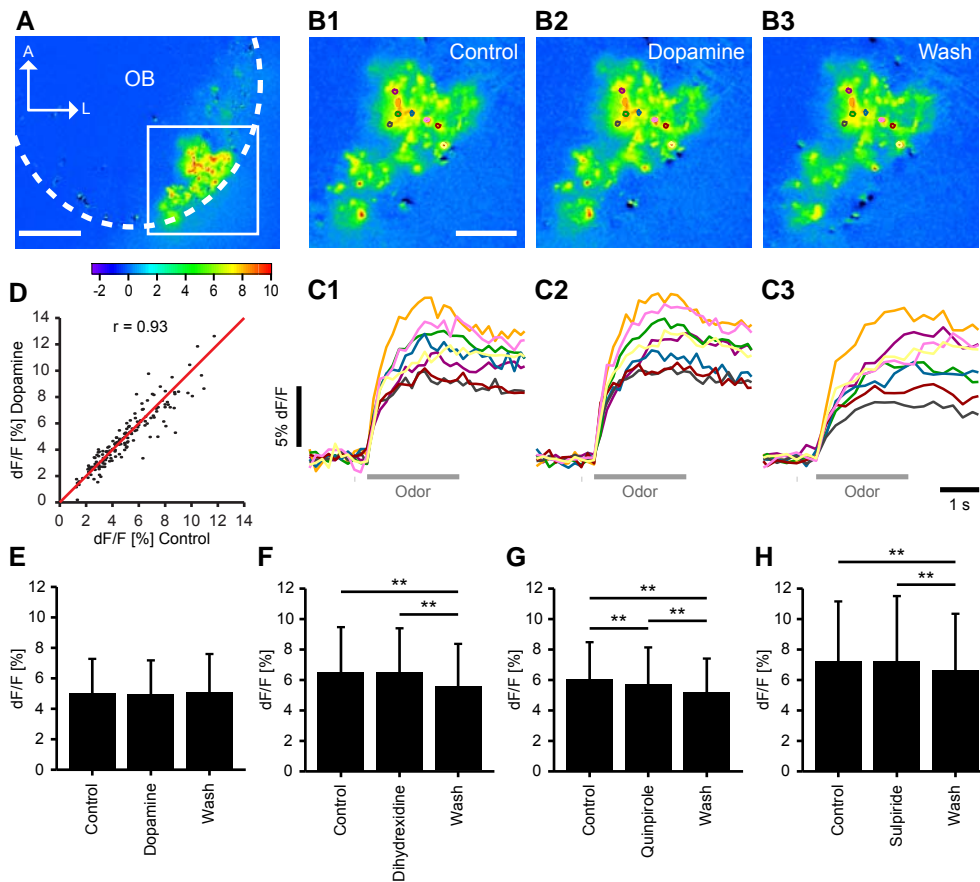
Figure 3: Dopamine has no effect on odor evoked signals in OSN terminals.

Change in presynaptic glomerular calcium signal in response to stimulation with an amino acid mixture. (A) Overview (scale bar: 100 µm). The white box indicates the area shown in (B). Glomerular activity pattern before drug application (B1), during application of dopamine (B2), and after wash-out of dopamine (B3). Seven individual glomeruli are outlined. Scale bar: 50 µm. (C) The time course of the odor response for the regions highlighted in (B). Grey bar indicates odor stimulation. (D) Comparison of the odor-evoked change in fluorescence the same glomeruli before and during application of dopamine. (E-H) Average response amplitude (± SD) in the presence of (E) dopamine (n = 157 glomeruli in 6 fish, p > 0.05), (F) the selective D1-receptor agonist dihydrexidine (n = 58 glomeruli in 2 fish, p > 0.05), (G) the selective D2-receptor agonist quinpirole (n = 56 glomeruli in 2 fish p < 0.001), and (H) the selective D2-receptor antagonist sulpiride (n = 154 glomeruli in 5 fish, p > 0.05). Odors were applied twice and responses were averaged. In each fish 18 – 53 regions of interest were defined according to raw fluorescence image and response pattern. ** P < 0.001 (Sign rank test).

(dihydrexidine, 10 µM) and D2 (quinpirole, 10 µM) receptor agonists, as well as the selective D2 receptor antagonist (sulpiride, 50 µM).

Under control conditions, odor stimulation caused strong activation of the ventrolateral part of the olfactory bulb (Fig. 3A), consistent with an earlier study by Friedrich and Korsching (1997). Generally, none of the tested drugs altered the spatial patterns of input as correlations between glomerular activity patterns under control conditions and during drug application remained high (Dopamine: r = 0.93; Dihydrexidine: r = 0.98; Quinpirole: r = 0.96; Sulpiride: r = 0.98, Fig. 3B-C). The mean amplitudes of the responses remained unchanged in the presense of dopamine (Fig. 3E, Control: 4.96 ± 2.25; Dopamine: 4.89 ± 2.21, p > 0.05, n = 157 glomeruli in 6 fish), dihydrexidine (Fig. 3F, Control: 6.46 ± 2.94, Dihydrexidine: 6.45 ± 2.87, p > 0.05, n = 58 glomeruli in 2 fish) and sulpiride (Fig. 3H, Control: 7.20 ± 3.89; Sulpiride: 7.18 ± 4.25, p > 0.05, n = 154 glomeruli in 5 fish), respectively. For quinpirole, a small but significant reduction in mean response amplitude was observed (Fig. 3G, Control: 6.00 ± 2.40, Quinpirole: 5.66 ± 2.41, p < 0.001, n = 56 glomeruli in 2 fish). This effect was not reversed upon wash-out of the D2 agonist, but became even more pronounced (Wash-out: 5.15 ± 2.19), suggesting a run-down.

To confirm that input to the olfactory bulb is not reduced, I also analyzed the effect of dopamine on spontaneous postsynaptic currents and odor-evoked input to mitral cells in voltage-clamp configuration (command voltage: -70 mV). Under resting conditions, application of dopamine reduced the mean holding current in mitral cells by approximately 32.1% (n = 16; Control: -68.2 ± 71.2 pA; Dopamine: -46.3 ± 65.4 pA, p < 0.0038, Fig. 4A). In addition, the variance in membrane currents also dropped significantly (Fig. 4B, Control: 354.3 ± 313.9; Dopamine: 150.5 ± 108.2, p < 0.0004).
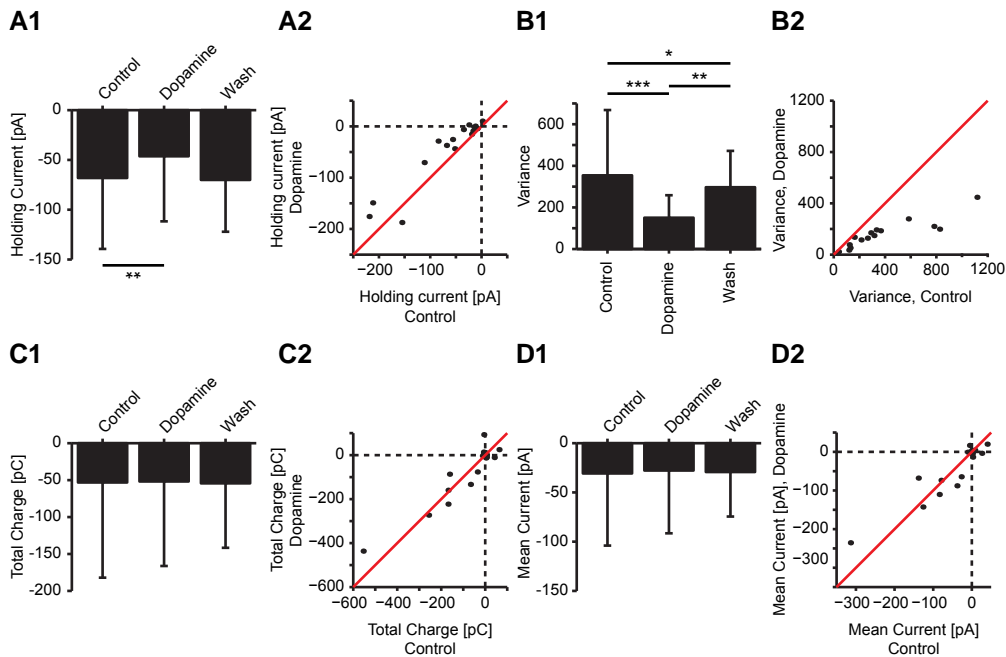
Figure 4: The effect of dopamine on spontaneous and evoked membrane currents.

(A, B) Voltage-clamp recordings in mitral cells under resting conditions (n = 16), command potential: -70 mV. (A1) Mean (± SD) holding current before, during and after application of dopamine. (A2) Cell-wise comparison between holding currents before and during wash-in of dopamine. The red line indicates the diagonal with slope 1. (B) Mean (± SD) variance in membrane currents (B1) and corresponding cell-wise comparison (B2) represented as in (A). (C, D) Voltage-clamp recordings of odor-evoked activity im mitral cells (n = 25), command potential: -70 mV. (C) Mean (± SD) total charge induced by odor stimulation calculated for the first 2 s of stimulation (C1) and corresponding cell-wise comparison (C2) represented as in (A). (D) Mean (± SD) odor-evoked membrane current under steady-state conditions calculated for a 1 s time window starting 1 s after stimulus onset (D1) and corresponding cell-wise comparison (D2) represented as in (A). * P < 0.05 ** P < 0.01 *** P < 0.001 (Sign rank test).

However, the high rate of spontaneous input to mitral cells prevented a more thorough analysis of unitary postsynaptic events as it was impossible to clearly identify individual events. I therefore also recorded odor evoked currents in mitral cells (n = 25). Under control conditions odors induced a total charge of -53.2 ± 128.9 pC within the first 2 s of the odor response (Fig. 4C). The mean amplitude of membrane currents was -30.8 ± 73.2 pA (Fig. 4D). Application of dopamine did not have an effect on either transmitted charge (-51.8 ± 114.5, p > 0.05) or membrane currents (-27.8 ± 63.7 pA, p > 0.05).

In summary, results obtained by calcium imaging and voltage-clamp recordings indicate that, in zebrafish, dopamine does not exert a prominent effect on afferent input to the olfactory bulb.

Biophysical properties of mitral cells

I next focused on mitral cells the other potential target of dopamine (Nowycky et al, 1983; Gurski and Hamilton, 1996; Duchamp-Viret et al, 1997). In order to analyze the intrinsic properties of mitral cells, neurons were recorded in whole-cell patch clamp configuration using a zebrafish line expressing the transgenic marker yellow cameleon selectively in mitral cells under control of the HuC promoter (Higashijima et al, 2003, Li et al, 2005).

To investigate whether dopamine modulates mitral cell properties I recorded spontaneous activity in current clamp configuration (n = 18 cells in 15 fish). In the intact brain, mitral cells receive spontaneous input from the receptor nerve terminals and are spontaneously active (Friedrich and Laurent, 2004, Tabor and Friedrich, 2008, Tabor et al 2008). Under control conditions, mitral cells spontaneously fired at 2.6 ± 2.6 Hz and exhibited a mean membrane potential of -56.2 ± 4.6 mV (Fig. 5A1, B1). These spontaneous firing rates were similar to
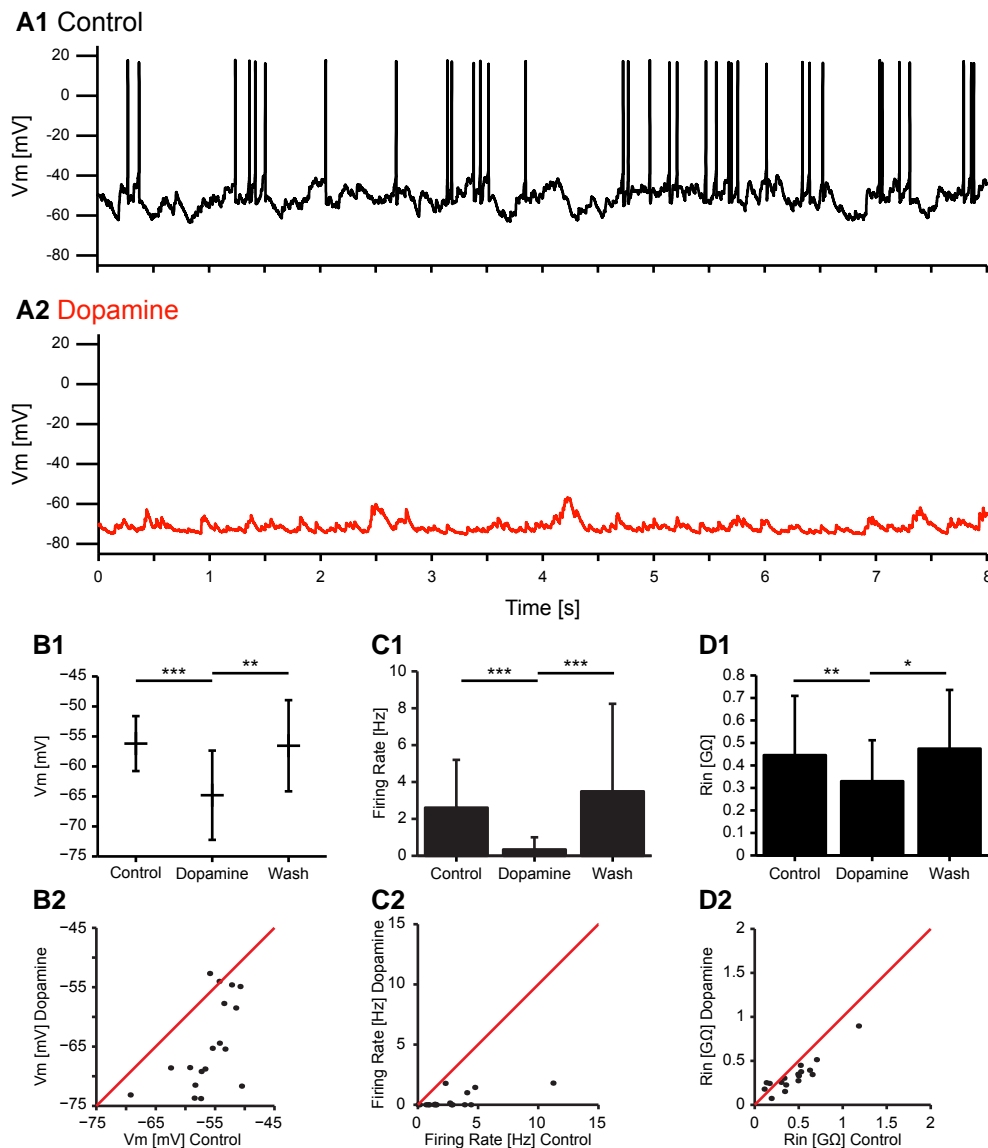
Figure 5: Dopamine exerts a hyperpolarizing effect on mitral cells.
Whole-cell recordings of spontaneous activity in a mitral cell before (A1) and during (A2) wash-in of dopamine. (B1) Mean (± SD) membrane potential before, during and after dopamine application (n = 18). (B2) Comparison of the membrane potential in the same mitral cells before and during application of dopamine. (C) Corresponding graphs for firing rate (n = 18) and (D) input resistance (n = 17). To calculate the input resistance small hyperpolarizing current steps (2 s, -25 pA) were applied and the mean membrane potential in a 1 s window starting 1 s after stimulus onset was compared to a corresponding time window just before stimulus onset. * P < 0.05 ** P < 0.01 *** P < 0.001 (Sign rank test).

those reported previously using whole-cell patch clamp recordings (Tabor and Friedrich, 2008; Tabor et al, 2008) but slightly lower than firing rates measured in cell-attached mode (Friedrich and Laurent, 2004), presumably because small negative holding currents were used (Tabor and Friedrich, 2008; Tabor et al, 2008). Upon bath application of dopamine, mitral cells hyperpolarized to a mean membrane potential of -64.8 ± 7.4 mV (Fig. 5A2, B, $p < 0.0004$). This effect was apparent in all but two out of 18 recorded cells. As a consequence, spontaneous firing was reduced in all mitral cells, with 11 out of 18 cells becoming essentially silent (Fig. 5C, mean firing rate 0.3 ± 0.7 Hz, $p < 0.0003$). In addition, the mean input resistance (R_{in}) dropped from 445.8 ± 263.3 MΩ to 329.8 ± 182.1 MΩ (Fig. 5D, $p < 0.0042$).

To examine whether dopamine acts directly on mitral cells, I repeated the experiment in pharmacologically isolated mitral cells. Glutamatergic synaptic transmission was blocked by NBQX (5 μM) and AP5 (50 μM), thereby blocking input from receptor neurons (Berkowicz et al, 1994; Ennis et al, 1996; Tabor and Friedrich, 2008), as well as glutamatergic input to interneurons and hence recurrent inhibition (Isaacson and Strowbridge, 1998; Schoppa et al, 1998). Under these conditions, subthreshold membrane fluctuations were virtually absent and most mitral cells did not fire action potentials. In a subset of experiments, GABAergic inhibition was blocked as well by additionally applying the GABA$_A$ receptor antagonist Gabazine (5 μM) and the GABA$_B$ receptor antagonist CGP 54626 (5 μM) (Tabor et al, 2008). Since glutamate and GABA are the two major neurotransmitters in the olfactory bulb, this abolished most of the network interactions (Berkowicz et al, 1994; Ennis et al, 1996; Edwards and Michel, 2002; Shepherd et al., 2004; Tabor and Friedrich, 2008; Tabor et al, 2008). In the presence of these synaptic blockers, mitral cells exhibited a mean membrane potential of
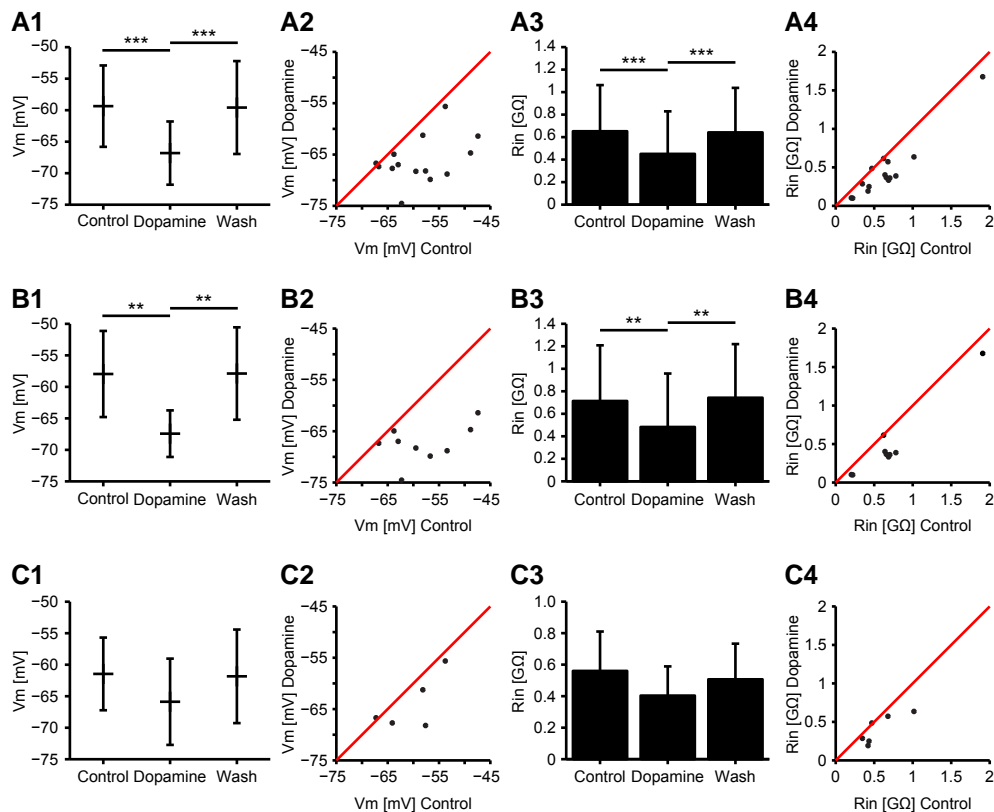
Figure 6: The effect of dopamine on mitral cells is independent of excitatory and inhibitory synaptic interactions.

(A) Mean (± SD) membrane potential (A1) and input resistance (A3) before, during and after dopamine application in the presence of blockers of glutamatergic (NBQX, AP5) or glutamatergic and GABAergic (Gabazine, CGP 54626) synaptic transmission (n = 15). (A2) Comparison of the membrane potential in the same mitral cells before and during application of dopamine. (A4) Corresponding graph for input resistance. (B) Subset of the mitral cells shown in (A) that were recorded in the presence of NBQX and AP5 (n = 9). (C) Subset of the mitral cells shown in (A) that were recorded in the presence of NBQX, AP5, Gabazine, and CGP 54626 (n = 6; membrane potential: p = 0.625; input resistance: p = 0.065). To calculate the input resistance small hyperpolarizing current steps (2 s, -25 pA) were applied and the mean membrane potential in a 1 s window starting 1 s after stimulus onset was compared to a corresponding time window just before stimulus onset. ** P < 0.01 *** P < 0.001 (Sign rank test).
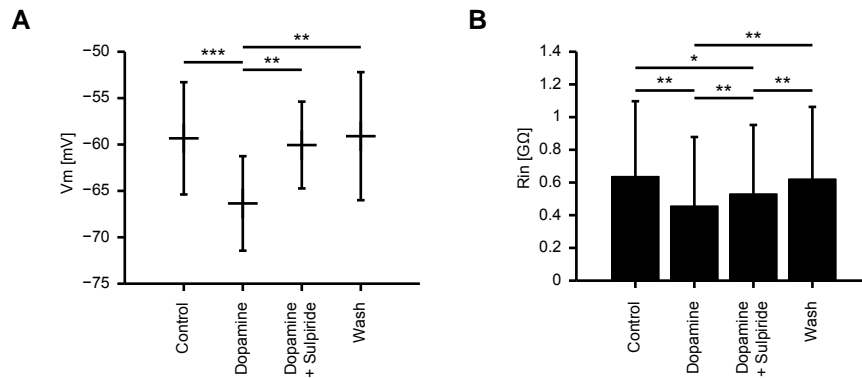
Figure 7: The effect of dopamine on mitral cells is at least partially mediated by D2 receptors.

Mean (± SD) membrane potential (A) and input resistance (B) before and during application of dopamine, in the presence of dopamine and the selective D2 receptor antagonist sulpiride, and after wash-out of dopamine and sulpiride (n = 12). Measurements were performed in the presence of synaptic blockers of glutamate (n = 7) or glutamate and GABA receptors (n = 5). To calculate the input resistance small hyperpolarizing current steps (2 s, -25 pA) were applied and the mean membrane potential in a 1 s window starting 1 s after stimulus onset was compared to a corresponding time window just before stimulus onset. * P < 0.05 ** P < 0.01 *** P < 0.001 (Sign rank test).

-59.3 ± 6.5 mV (n = 15 cells in 5 fish) and showed only little spontaneous activity (mean firing rate: 0.3 ± 0.6 Hz). Wash-in of dopamine still caused a pronounced hyperploarization of membrane potential (Fig. 6A1-2, V_m = -66.8 ± 5.0 mV, p < 0.0001). The firing rate dropped to zero in all cells, but as spontaneous activity was very low initially this effect did not become significant (p = 0.125). In addition, the dopaminergic effect on input resistance also persisted in the presence of the receptor blockers (Fig. 6A3-4, Control: 652.4 ± 401.1 MΩ, Dopamine: 451.2 ± 377.7 MΩ, p < 0.0002).

A similar trend was observed when analyzing the two conditions separately. When blocking only glutamatergic input to mitral cells (Fig. 6B, n = 9 cells in 3 fish), dopamine evoked a hyperpolarization of membrane potential (Control: -58.0 ± 6.8 mV, Dopamine: -67.4 ± 3.7 mV, p < 0.0039) and a reduction in input resistance (Control: 713.8 ± 494.7 MΩ, Dopamine: 483.0 ± 474.7 MΩ, p < 0.0039). When additionally blocking GABAergic transmission, membrane potential and input resistance shifted in a similar manner (Fig. 6C, n = 6 cells in 2 fish; mean V_m control: -61.4 ± 5.7 mV, dopamine: -65.9 ± 6.8 mV, p = 0.0625; mean R_{in} control: 560.3 ± 249.9 MΩ, dopamine: 403.4 ± 185.4 MΩ, p = 0.0625).

Taken together these results strongly support a direct modulation of mitral cell properties by dopamine. In other species, the major effect of dopamine has been attributed to the action of D2 receptors (Duchamp-Viret et al, 1997; Hsia et al, 1999; Berkowicz and Trombley, 2000; Ennis et al, 2001; Maher and Westbrook, 2008). To verify that in zebrafish the effect of dopamine is also D2 receptor mediated, I added the selective D2 receptor antagonist sulpiride (50 µM) to the bath solution after application of dopamine in a subset of the recordings (n = 12 cells, 7 cells with glutamate blockers only, 5 cells with both GABA and glutamate blockers). Sulpiride reliably
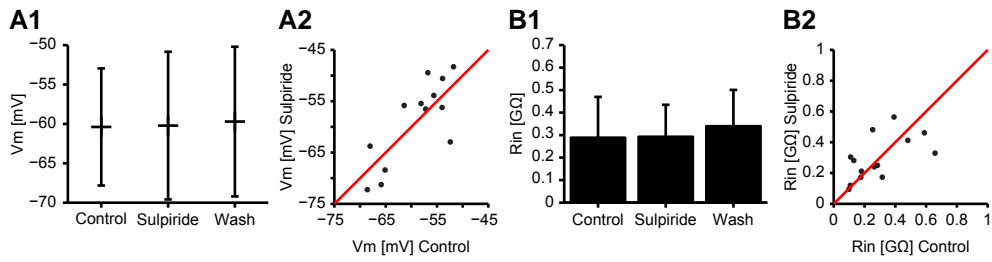
Figure 8: No tonic D2 receptor mediated effect on mitral cells in the absence of glutamatergic input to the system.
(A) Mean (± SD) membrane potential (A1) and input resistance (B1) before, during and after sulpiride application in the presence of blockers of glutamatergic (NBQX, AP5) and GABAergic (Gabazine, CGP 54 626) synaptic transmission (n = 14). (A2) Comparison of the membrane potential in the same mitral cells before and during application of sulpiride. (B2) Corresponding graph for input resistance. To calculate the input resistance small hyperpolarizing current steps (2 s, -25 pA) were applied and the mean membrane potential in a 1 s window starting 1 s after stimulus onset was compared to a corresponding time window just before stimulus onset. No significant effects found (Sign rank test).

reversed the effect of dopamine on the mean membrane potential (Dopamine: -66.4 ± 5.1 mV, Dopamine+Sulpiride: -60.1 ± 4.7 mV, p < 0.0015, Fig. 7A) and partially blocked the effect on input resistance (Dopamine: 456.1 ± 422.6 MΩ, Dopamine+Sulpiride: 530.4 ± 422.1 MΩ, p < 0.0024, Fig. 7B).

Several authors have described intrinsic pacemaker properties in mammalian dopaminergic periglomerular cells, causing neurons to fire action potentials at regular intervals in the absence of external stimulation (Pignatelli et al, 2005; Puopolo et al, 2005). I therefore also used sulpiride to test for a tonic effect of dopamine onto mitral cells in a separate set of cells (n = 14). In the absence of glutamatergic and GABAergic synaptic transmission sulpiride had no effect on the mean membrane potential (Fig. 8A, Control: -60.4 ± 7.4 mV, Sulpiride: -60.2 ± 9.4 mV, p > 0.05) or the mean input resistance (Fig. 8B, Control: 288.5 ± 181.4 MΩ, Sulpiride: 292.8 ± 142.1 MΩ, p > 0.05).

Dopaminergic modulation of olfactory bulb output

After having established the effect of dopamine on the biophysical properties of mitral cells I proceeded to analyze the influence of dopaminergic modulation on the computations performed within the microcircuit.

As a first approximation of the dopamine-mediated effect on the output I directly measured the transfer function for mitral cells by applying depolarizing and hyperpolarizing current steps and measuring the resulting firing rates in whole-cell current-clamp recordings in a time window starting 1 s after stimulus onset to obtain a steady state estimate of firing rates. A total of nine different stimulus amplitudes were tested ranging from -100 pA to +100 pA

(Fig. 9A). During control measurements, action potential firing was close to zero for hyperpolarizing current injections below -25 pA. For depolarizing current steps, mean firing rates increased almost linearly up to a maximum mean firing rate of 42.5 ± 12.8 Hz (Fig. 9B, n = 17 mitral cells). Bath application of dopamine increased the amount of current required to drive mitral cells to firing threshold and limited spiking to current injections ≥ 25 pA (Fig. 9B). As a consequence, the mean firing rates in response to stimuli between -25 pA and +50 pA were reduced. For higher stimulus amplitudes mean responses were also lower, but this effect was less pronounced.

Simple changes of input-output functions may be attributed to two effects: a multiplicative effect altering the slope of the curve and an add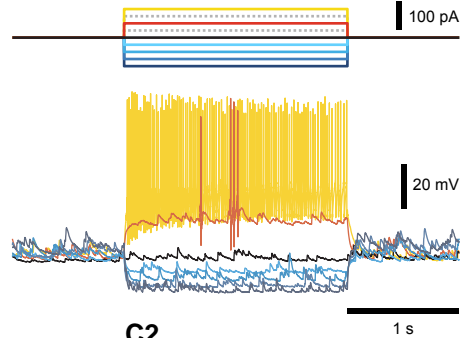itive effect shifting the curve along the axis. Multiplicative modulation corresponds to a scaling of the response and hence results in a change in the dynamic range of the neuron. Additive modulation represents a shift in response threshold and thus introduces an offset in the curve but does not affect the dynamic range of the cell. From the average input-output function, dopamine appears to selectively alter the response offset without affecting the slope. To test for this hypothesis I fitted the rising phase of each individual mitral cell response curve with a line and directly compared the resulting slopes and x-intercepts (n = 16, Fig. 9C). In the unperturbed network this approach produced mean slopes of 0.50 ± 0.22 Hz/pA and x-offsets of -9.90 ± 20.70 pA. Application of dopamine shifted the mean x-offset to 22.94 ± 18.00 pA (Fig. 9E, $p <$ 0.0004), corresponding to an increase in response threshold by 32.84 ± 25.60 pA. In addition, dopamine also increased the steepness of the curve in 11 out of 16 mitral cells (Fig. 9D, 0.71 ± 0.33 Hz/pA, $p < 0.0437$).
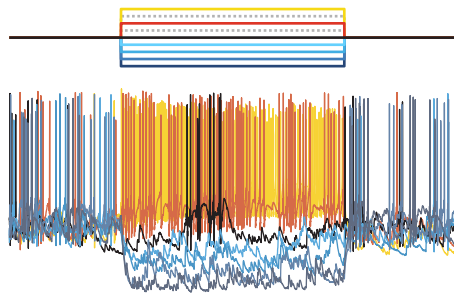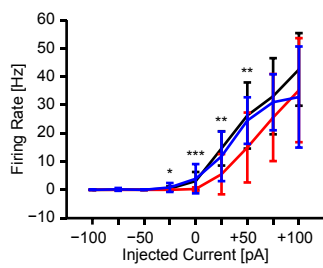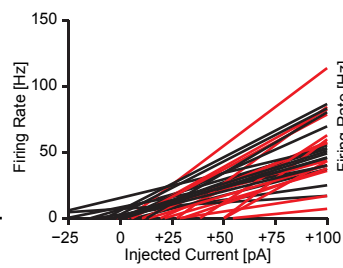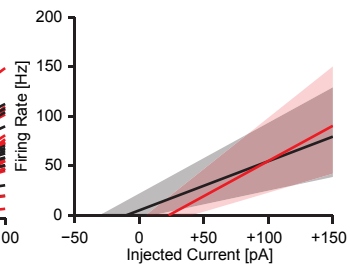
A1 Control **A2 Dopamine**
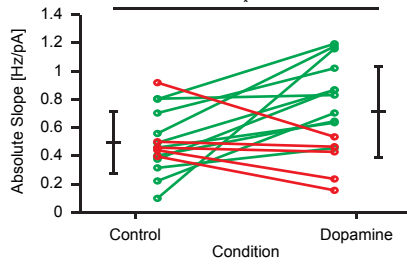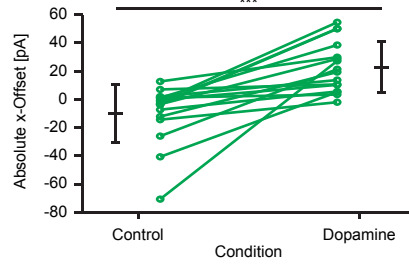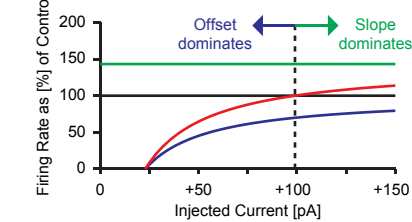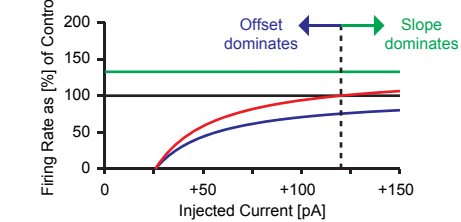
Figure 9: The effect of dopamine on the input-output function of mitral cells.
(A) Whole cell recordings of a mitral cell in response to 2 s current injections at different amplitudes (-100 pA to +100 pA) before (A1) and during (A2) bath application of dopamine. Stimulus intensities are color coded as indicated in the top panel. For illustration purposes responses to two depolarizing stimuli (+25 pA and and +75 pA, respectively) are omitted. (B) Mean (± SD) firing rate in response to current injections before (black), during (red), and after (blue) application of dopamine (n = 17). Asterisks denote conditions with a significant change in firing rate as a results of dopamine wash-in. (C1) For a subset of these mitral cells (n = 16) the response curve was fitted with a line in the interval 10% - 90% of the maximum amplitude. Lines represent individual fits for each mitral cell before (black) and during (red) application of dopamine. (C2) Solid lines show the averaged fits. Shaded areas depict the range defined by mean slope ± SD and mean x-offset ± SD. (D) Mean (± SD) slope obtained from the fits. Lines indicate values for individual mitral cells with increased (green) and decreased (red) values under dopamine, respectively. (E) Mean (± SD) x-offset illustrated as in (D). (F, G) Firing rate relative to control conditions when modulating slope only (green), x-offset only (blue), or both parameters (red). The solid black line indicates firing rates equal to control conditions. The dotted line marks the intersection between the firing rates before (black) and during (red) application of dopamine. (F) shows data obtained in the intact network. (G) Corresponding data calculated from mitral cell responses recorded in the presence of synaptic blockers (n = 12; NBQX, AP5: n = 7; Gabazine, CGP 54626 in addition, n = 5). To compute the input-output function current steps (2 s, -100 - +100 pA in 25 pA steps) were applied and the mean spike rate in a 1 s window starting 1 s after stimulus onset was calculated. * $P < 0.05$ ** $P < 0.01$ *** $P < 0.001$ (Sign rank test).

As both slope and offset were modulated by dopamine in opposing directions I examined the contribution of the two effects onto the output of neurons. For this purpose I computed the expected firing rates when only manipulating one of the two variables on the basis of the fitted parameters. Figure 9F illustrates the ratio of the calculated firing rates relative to the firing rate under control conditions. Selectively elevating the slope of the response function increased the ratio by a constant factor (Fig. 9F, green trace). In contrast, selectively varying the offset caused an input-dependent decrease in the ratio with the effect being strongest for small stimulation amplitudes (Fig. 9F, blue trace). For stronger inputs the curve asymptotically approached a ratio of one (Fig. 9F, black trace). When changing both parameters, i.e. simulating firing rates under dopamine, the curve also exhibited an asymptotical behavior, but approached a value defined by the ratio of the slopes during and before application of dopamine (Fig. 9F, red trace). Hence, for high inputs dopamine increases mitral cell firing rates by approximately 42%. Furthermore, the curve intersected the line of equal ratios at 99.02 pA. For smaller inputs the shift in offset dominated the output, while for larger inputs the effect on the slope was more prominent.

To address the question to which extent these results are dependent on network interactions I also recorded input-output functions in pharmacologically isolated mitral cells (n = 12, all experiments in the presence of NBQX and AP5, for five cells also Gabazine and CGP 54626 were added). The parameters obtained from fitting these curves were similar to those from the intact system yielding a small increase in slope (Control: 0.60 ± 0.26 Hz/pA, Dopamine: 0.80 ± 0.26 Hz/pA, $p < 0.021$) and a pronounced shift in offset (Control: -4.98 ± 14.46 pA, Dopamine: 25.75 ± 23.33 pA, $p < 0.0005$). The dopamine-induced increase in steepness became dominant for inputs beyond approximately 120 pA (Fig. 9G).

As a result, my data indicate that dopaminergic modulation causes a prominent lateral shift the input-output function. This effect is partially antagonized by an increase in the slope of the response curve. For smaller inputs the dominant effect of dopamine is an increase in firing threshold, for larger inputs the augmentation in steepness prevails.

In contrast to current injections into individual neurons, natural stimuli tend to activate larger proportions of the network and, thus, emphasize lateral interactions within the microcircuit (Friedrich et al, 2009). Simple transformations in mitral cell response functions might, thus, alter interactions within the system in a more complex fashion. Furthermore, it is possible, that additional, yet unidentified, targets of dopamine exist within the olfactory bulb that contribute at the network level. I therefore directly measured mitral cell responses to natural odors that are known to induce complex patterns of activity in the bulb (Friedrich and Korsching, 1997, 1998; see also Fig. 3).

Odor-evoked activity was measured in a total of 30 mitral cells. Under control conditions, both excitatory and inhibitory changes in firing rate were commonly observed. Examples for three different mitral cell responses are shown in figures 10 – 12. Responses peaked approximately 250 ms after stimulus onset and were analyzed within a 500 ms time window around the peak. Odors increased the mean firing rate by 4.6 ± 11.1 Hz relative to baseline (n = 30, Fig. 13A, D). As before, application of dopamine reduced spontaneous activity in mitral cells. In addition, odor-evoked activity was elevated. Absolute firing rate (Control: 8.1 ± 11.6 Hz, Dopamine: 9.7 ± 20.2 Hz, $p > 0.05$) and the relative amplitude (Control: 4.6 ± 11.1 Hz, Dopamine: 7.7 ± 18.6 Hz, $p > 0.05$) were slightly, but not significantly increased. As dopamine had a heterogeneous effect on odor-evoked activity, I also analyzed excitatory and inhibitory odor
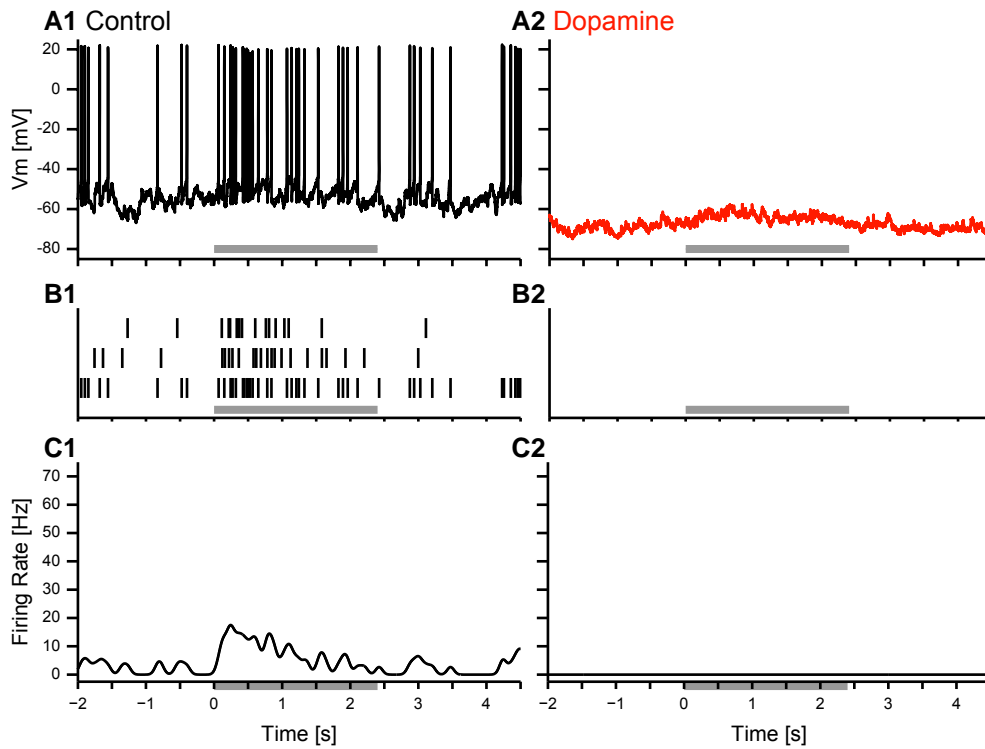
Figure 10: Effect of dopamine on weak excitatory odor responses.
Whole-cell recordings of a mitral cell odor response before (A1) and during
(A2) wash-in of dopamine. (B) Raster plots for three successive applications
of the odor before (B1) and during (B2) application of dopamine. Ticks
indicate individual spikes. Traces shown in (A) correspond to the bottom
rows. (C) Corresponding PSTHs averaged over all repetitions. Grey bar
indicates the odor stimulus.
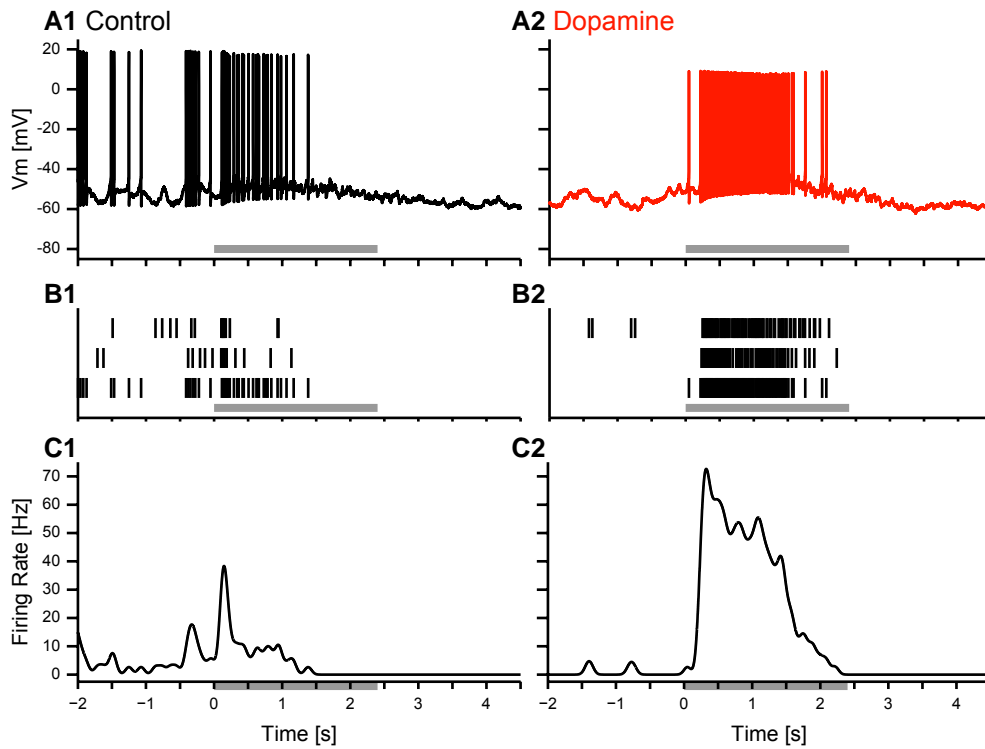
Figure 11: Effect of dopamine on strong excitatory odor responses.
Whole-cell recordings of a mitral cell odor response before (A1) and during
(A2) wash-in of dopamine. (B) Raster plots for three successive applications
of the odor before (B1) and during (B2) application of dopamine. Ticks
indicate individual spikes. Traces shown in (A) correspond to the bottom
rows. (C) Corresponding PSTHs averaged over all repetitions. Grey bar
indicates the odor stimulus.
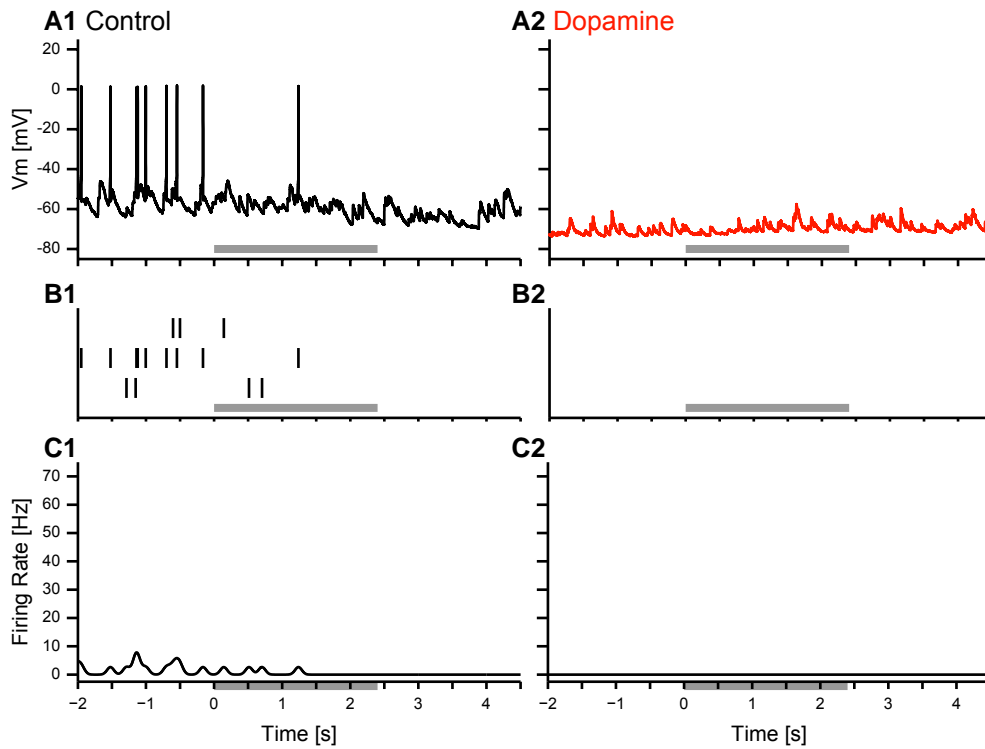
Figure 12: Effect of dopamine on inhibitory odor responses.
Whole-cell recordings of a mitral cell odor response before (A1) and during
(A2) wash-in of dopamine. (B) Raster plots for three successive applications
of the odor before (B1) and during (B2) application of dopamine. Ticks
indicate individual spikes. Traces shown in (A) correspond to the bottom
rows. (C) Corresponding PSTHs averaged over all repetitions. Grey bar
indicates the odor stimulus.

responses separately. Under control conditions excitatory responses increased mitral cell mean firing rates in the initial 500 ms time window by 12.7 ± 12.7 Hz (n = 13, Fig. 13B). Upon bath application of dopamine the mean amplitude of odor responses increased to 17.9 ± 25.3 Hz (p > 0.05). This trend was also observed in the absolute firing rates in response to odor stimulation (Control: 17.0 ± 13.1 Hz, Dopamine: 20.3 ± 27.4 Hz, p > 0.05). However, none of these effects became significant. In addition to the change in amplitude, responses were slightly delayed by approximately 30 ms and prolonged by more than 1.3 s.

When directly analyzing individual excitatory odor responses, it became apparent that dopamine selectively reduced responses in some cells, while enhancing firing in others. Weak to intermediate odor responses failed to trigger action potentials after wash-in of dopamine (Fig. 10). In these cells, synaptic input was still present in the membrane potential fluctuations (see Fig. 10A2) but remained subthreshold, presumably due to the more hyperpolarized state of the cell. In contrast, strong excitatory odor responses remained suprathreshold under dopamine and even became boosted in several cases (Fig. 11).

For odor responses dominated by inhibition, the absolute firing rates in response to an odor were not altered much by dopamine (Control: 1.5 ± 1.0 Hz; Dopamine: 0.2 ± 0.4 Hz, Fig. 13C) as mitral cells were almost silent even under control conditions. Due to the decrease in spontaneous firing rates, however, the relative response amplitude of inhibitory odor responses was more strongly reduced by dopamine (Control: -4.4 ± 4.5 Hz; Dopamine: -1.2 ± 2.6 Hz). Consequently, inhibitory odor responses became almost undetectable in the PSTH (Fig. 12).
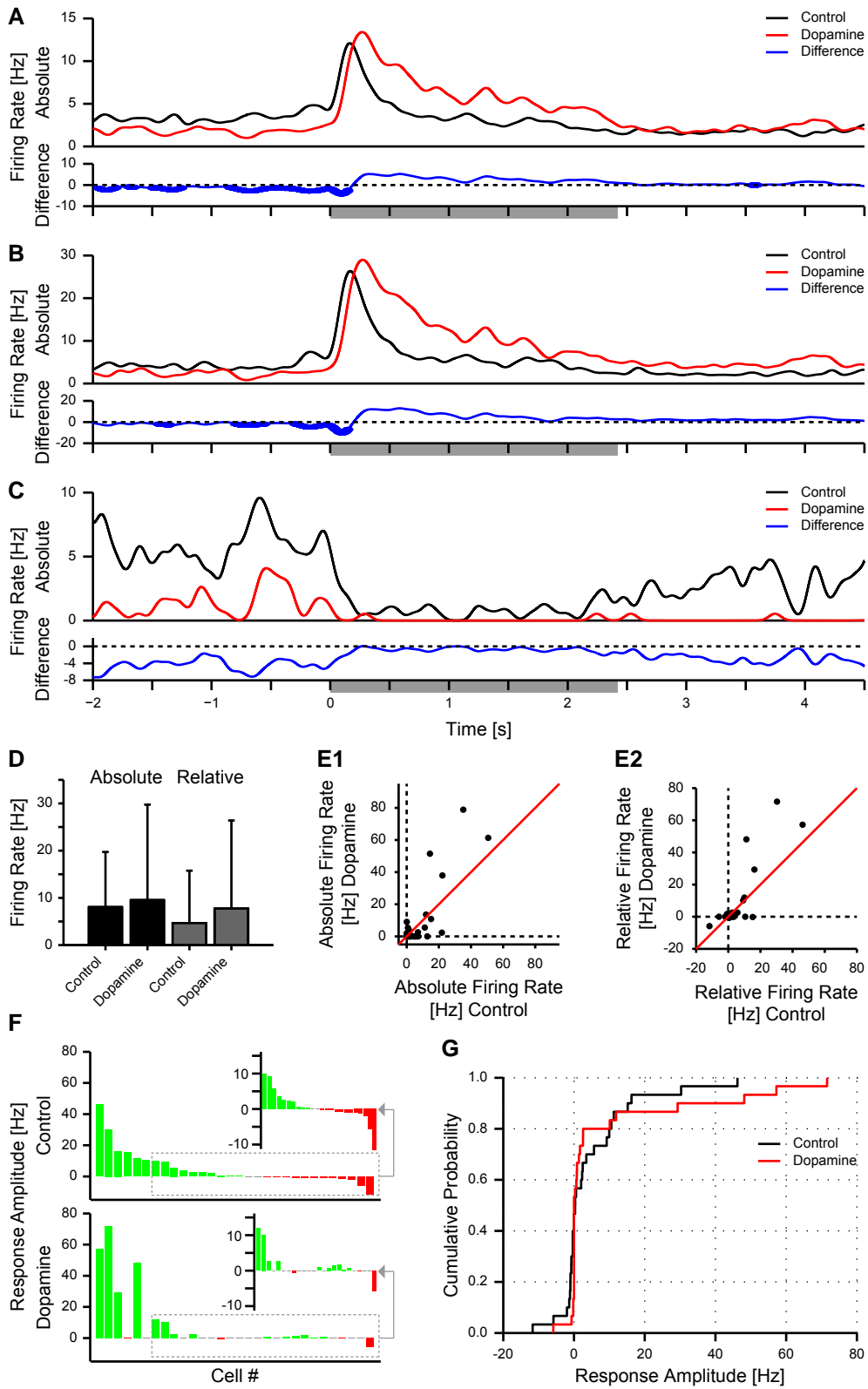
Figure 13: Effect of dopamine on odor responses.
(A) Top: Avgerage PSTH for mitral cell odor responses (n = 30) before (black) and during (red) application of dopamine. Bottom: Difference between the two conditions. Thick portions depict time bins significantly different (Sign rank test, P < 0.05). Grey bar indicates odor stimulus. Dashed line denotes the zero baseline. (B) Average PSTH for excitatory odor responses (> 1% increase in firing rate, n = 13) only. Conventions as in (A). (C) Avgerage PSTH for inhibitory odor responses (> 1% decrease in firing rate, n = 5) only. Conventions as in (A). (D) Mean (± SD) firing rate in response to odor stimulation (n = 30). Black bars: absulute firing rates, grey bars: response amplitude relative to pre-stimulus baseline (Sign rank test, both p > 0.05). (E) Comparison of firing rates before and during application of dopamine in the same mitral cells for absolute (E1) and relative (E2) amplitudes. (F) Mitral cell odor responses ranked according to the change in firing rate before (top) and during (bottom) application of dopamine (n = 30). Green and red indicate excitatory and inhibitory odor responses, respectively. Inset shows a subset of the cells at a larger scale. (G) Cumulative probabilty distribution for odor-evoked firing rate changes in mitral cells before (black) and during (red) bath application of dopamine (n = 30). Firing rates were always calculated for a 500 ms time window starting at stimulus onset. For PSTHs significance was tested for successive time windows averaged over 50 ms.

When comparing the odor response pattern across all mitral cells it becomes apparent that dopamine selectively diminished weak to intermediate excitatory as well as inhibitory responses (Fig. 13E, F). Most of these responses were completely abolished. This effect was particularly prominent for the relative response amplitudes (Fig. 13E2) and in the cumulative response amplitude plot as the slope for small amplitudes became very steep, indicating the lack of intermediate response amplitudes (Fig. 13G). As a consequence, the population response of mitral cells became more narrowly tuned with less cells responding to a given odor stimulus. In addition, no prominent case of a sign inversion in the odor response was observed. In summary, these findings are in good agreement with the observed effects of dopamine on offset and slope of the transfer function.

Effect of dopamine on odor-evoked activity patterns

While patch-clamp recordings provide very good temporal resolution and permit to analyze subthreshold fluctuations in membrane potentials, they do not allow for simultaneous acquisition of odor responses from a large number of neurons. It is thus impossible to directly assess the effect of dopamine on activity patterns. I therefore decided to perform two-photon calcium-sensitive dye imaging by bolus loading of the olfactory bulb with the red-fluorescent calcium-indicator, Rhod-2-AM (Brustein et al, 2003, Stosiek et al, 2003, Yaksi and Friedrich, 2006). The somatic calcium-signal mesured by this approach reflects action potential firing and, hence, the output of the cell and permits stable recordings for several hours (Yaksi and Friedrich 2006, Yaksi et al, 2007). Mitral cells were identified using a transgenic zebrafish-line expressing the mitral cell marker HuC:YC (Higashijima et al, 2003, Li et al, 2005). Rhod-2 and YC signals were detected simultaneously in separate channels. Mitral cell responses
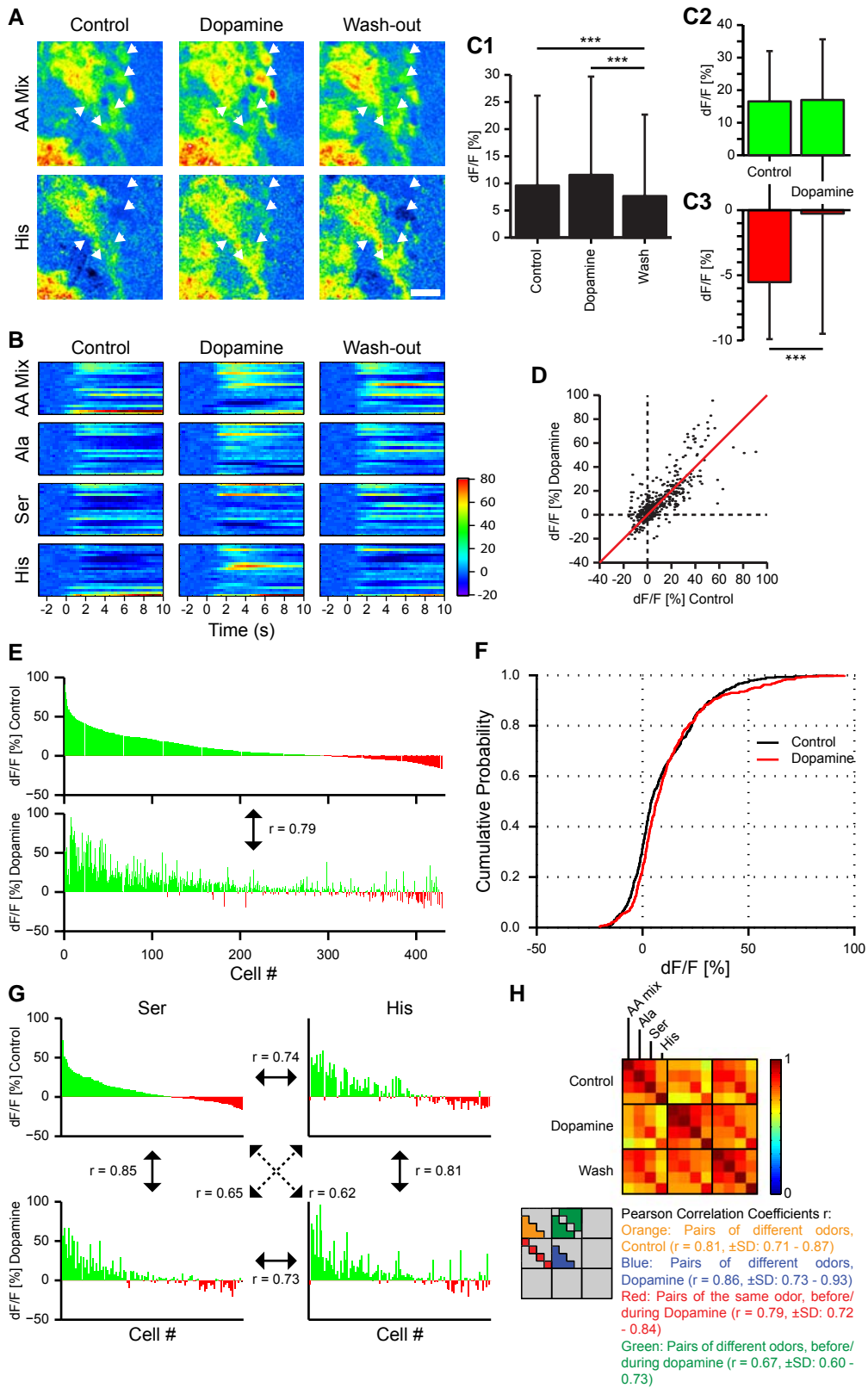
Figure 14: Effect of dopamine on mitral cell odor responses measured by two-photon calcium-sensitive dye imaging.
(A) Time-averaged change in calcium signal evoked by two different odors (Top: AA mix, Bottom: His) before (left), during (middle), and after (right) application of dopamine. White arrow heads indicate the location of six mitral cells. Scale bar: 20 μm. (B) Time-resolved odor response for a set of 20 mitral cells (including those shown in (A)) recorded in the same fish. 0 s time point corresponds to the switching of the odor valve. (C) Mean (± SD) odor-evoked change in somatic calcium signal before, during, and after application of dopamine averaged over all responses (n = 429 odor response in 112 mitral cells, C1), and excitatory (n = 294, C2) and inhibitory (n = 135, C3) odor responses only, respectively. *** $P < 0.001$ (Sign rank test). (D) Pairwise comparison of odor response amplitudes before and during application of dopamine. Each dot depicts a single odor-mitral cell pair (n = 429 response pairs in 112 mitral cells). (E) Comparison of mitral cell population response pattern. Top: Mitral cell odor responses ranked according to their magnitude before application of dopamine. Green and red bars indicate excitatory and inhibitory odor responses, respectively. Bottom: Responses of the same mitral cells in the presence of dopamine. (F) Cumulative probability distribution of calcium signals before (black) and during (red) wash-in of dopamine. (G) Comparison of odor-evoked response patterns for two different amino acids (left: Ser, right: His) before (top row) and during (bottom row) application of dopamine (n = 112 mitral cells). Conventions as in (E). (H) Pearson correlation coefficients of odor-evoked population activity patterns in response to four different stimuli (AA mix, Ala, Ser, His, n = 93 mitral cells). Means (± SD) are calculated for four different clusters as depicted in the diagram (bottom left): pairs of two different odors before (r = 0.81, Mean ± SD: 0.71 - 0.87, yellow) and during (r = 0.86, Mean ± SD: 0.73 - 0.93, blue) application of dopamine, and pairs of the same odor (r = 0.79, Mean ± SD: 0.72 - 084, red) or different odors (r = 0.67, Mean ± SD: 0.60 - 0.73, green) before and during application of dopamine. Pearson correlation coefficients were transformed using a Fisher z-transformation for calculating means and standard deviations. Odors were applied twice and responses were averaged for the analysis.

were quantified by calculating the relative change in fluorescence (ΔF/F) and averaging over a time 4.9 s time window starting 0.9 s after response onset.

I measured responses to 3 – 4 different odors in a total of 112 mitral cells (n = 8 fish) before, during and after bath application of dopamine. Stimulation with odors evoked strong changes in fluorescence signal both within the neurophil and cell somata (Fig. 14A, white arrow heads). When comparing odor-evoked response-maps based on ΔF/F for control conditions and during wash-in of dopamine, there was a small, but significant increase in neuropil responses (n = 4 fish, Control: 12.3 ± 12.4% ΔF/F, Dopamine: 17.0 ± 13.2% ΔF/F, p < 0.0001). However, visual inspection did not yield apparent dopamine-induced differences in the general distribution (Fig. 14A) and the coarse temporal pattern of activity, respectively (Fig. 14B).

Mitral cells also showed a small increase in mean ΔF/F change that did not become significant (Fig. 14C1, n = 429 odor responses in 112 cells, Control: 9.6 ± 16.6% ΔF/F; Dopamine: 11.6 ± 18.1% ΔF/F, p > 0.05). This effect was much more pronounced for odor responses dominated by inhibition (Fig. 14C3, n = 135, Control: -5.5 ± 4.4% ΔF/F, Dopamine: -0.3 ± 9.2% ΔF/F, p < 0.0001) than for excitatory odor responses (Fig. 14C2, n = 294, Control: 16.5 ± 15.5% ΔF/F; Dopamine: 17.0 ± 18.6% ΔF/F, p > 0.05).

When directly comparing the response amplitude under control and dopamine, it became apparent that inhibitory odor responses were preferentially reduced, while for excitatory odor responses both increases and decreases were observed (Fig. 14E). Generally, only few sign switches in response amplitudes were observed upon wash-in of dopamine. Furthermore, the number of inhibitory and weak

excitatory odor responses was decreased as indicated by a right-shift for in the cumulative amplitude distributions for responses below approximately 10% ΔF/F (Fig. 14F). Strong amplitudes, on the other hand, were more commonly observed in the presence of dopamine than under control conditions. Overall, however, dopamine did not have a prominent effect on population response pattern across the array of mitral cells as the correlation coefficient for the two conditions remained high (Fig. 14E, Pearson correlation coefficient r = 0.79).

To verify that the global pattern of activity was not affected by dopamine, I directly compared population odor responses to chemically similar amino acids (Fig. 14G, H). Activity patterns evoked by the same odors before and during dopamine application remained highly correlated (r = 0.79; Mean ± SD: 0.72 – 0.84, Fig. 14H, diagram: red shading). In addition, in almost all cases, odor-evoked patterns under control conditions were more closely related to the patter of the same odor (diagram: red shading) than to patterns evoked by different odors during dopamine application (r = 0.67, Mean ± SD: 0.60 – 0.73; diagram: green shading). However, odor responses under control conditions (r = 0.81, Mean ± SD: 0.71 – 0.87; diagram: orange shading) were generally more similar to each other than to responses during dopamine application (diagram: green shading; p < 0.0011, Student's t-test). Correspondingly, odor-evoked patterns under dopamine (r = 0.86, Mean ± SD: 0.73 – 0.93; blue shading) were also more similar amongst each other (p < 0.0065, Student's t-test). Nevertheless, within each condition the relation between the different odor response patterns with respect to each other remained preserved as indicated by a high correlation coefficient between the correlation matrices under control conditions (diagram: orange shading) and during wash-in of dopamine (diagram: blue shading; r = 0.87).

Taken together, the data obtained by two-photon calcium imaging generally support the findings from the electrophysiological recordings. In addition, they indicate that dopamine does not have a profound effect on global activity patterns.

Optogenetic stimulation of mitral cells

So far I always tested the effect of dopamine onto the network by bath application at high concentrations. It is unlikely, however, that this long-lasting, global presence of dopamine occurs under physiological conditions. I therefore decided to investigate the endogenous availability of dopamine within the system and the dynamics of the effect from endogenous sources by directly triggering release from dopaminergic periglomerular cells using an optogenetic approach.

A powerful tool to selectively stimulate specific populations of neurons is provided by optogenetic methods. As a first step I therefore explored the possibilities of this approach in a transgenic zebrafish line that utilizes the Tet system to express ChR2YFP in mitral cells under Ptet control (HuC:itTA/Ptet:ChR2YFP Line 03; Fig. 15A). To establish the response characteristics of mitral cells upon optical wide-field stimulation by a blue LED (470 nm; total power at sample < 0.3 mW; average power per area < 0.25 mW/mm2) I performed whole-cell patch-clamp recordings (n=6). Sustained stimulation for 1 s evoked strong depolarizations in ChR2YFP-positive cells that triggered pronounced action potential firing (Fig. 15B). Light-evoked spiking adapted over time. Similarly, in voltage-clamp mode, large rapidly-adapting inward-currents were measured upon light stimulation (Fig. 15C). This adaptation in ChR2-mediated membrane currents has been described previously in neuronal cell cultures (Boyden et al, 2005).

A

HuC:itTA/Tet07:ChR2YFP
Mitral cells

B Sustained light stimulus

20 mV

200 ms

C Sustained light stimulus

50 pA
250 ms

D 2-Photon activation
Scanning, 256 ms interval

20 mV

+ hyperpol.
Current

1 s

F1

Number of spikes

Frequency [Hz]

F2

Jitter throughout train [ms]

Frequency [Hz]

E1 Light pulses (15 ms)

5 Hz

10 Hz

20 Hz

30 Hz

40 mV

200 ms

E2 Light pulses (15 ms)

5 Hz

10 Hz

20 Hz

30 Hz

G1 Poisson train, λ = 200 ms

KYN

Spontaneous
Activity

Poisson train, λ = 100 ms

20 mV

20 mV

G2

KYN

KYN

20 Hz

20 mV

20 Hz

G3

No blockers

No blockers

20 Hz

20 mV

20 Hz

1 s

1 s

1 s

Figure 15: Optical manipulation of neuronal activity in mitral cells expressing channelrhodopsin-2.

(A) Two-photon image of mitral cells expressing the ChR2YFP construct under control of the HuC promoter (Image provided by Peixin Zhu). (B) Current clamp recording of a mitral cell response to sustained illumination with blue light. (C) Voltage-clamp recording of a mitral cell response to blue light stimulation. (D) Mitral cell membrane potential in response to continuous scanning with a two-photon laser at 256 ms intervals with (grey) and without (black) hyperpolarizing current injections. Spikes are truncated for better representation. (E1) Individual mitral cell responses to stimulation with trains of light pulses (15 ms) at constant frequencies. (E2) illustrates response patterns for multiple repetitions of the stimuli in the same cell. Each row represents a single trial. Ticks denote individual action potentials. Other mitral cells exhibited similar response characteristics (n = 3). (F1) Number of action potentials (mean ± SD) evoked by regular light stimulation as a function of frequency (n = 3 mitral cells). (F2) Jitter in timing of action potentials (mean ± SD) as a function of stimulus frequency (n = 3 mitral cells). (G) Mitral cell responses to Poisson trains of light pulses (15 ms) with different mean inter-spike intervals (left: 200 ms, right: 100 ms). (G1) Example of a whole-cell recording in current-clamp in the presence of kynurenic acid (KYN; 2 mM). (G2) Responses to five repeats of the same temporal strimulation pattern in the presence of kynurenic acid (KYN; 2 mM). Blue ticks: individual light pulses, black ticks: individual action potentials. Bottom: Mean firing rate as a function of time. Spike trains were convolved with a Gaussian kernel (sigma: 100 ms) and averaged. Gray shading indicates SD; dashed blue trace illustrates event rate of the pulse train. Other mitral cells showed very similar responses (n = 3). Middle (red): current-clamp recording of mitral cell membrane potential in the presence of kynurenic acid. (G3) Responses of the same mitral cell as in (G2) in the absence of kynurenic acid, resulting in a background of high spontaneous activity (center, black).

In order to assess the reliability and precision of light-induced spiking I measured action potential firing in response to short (5 – 15 ms) blue light pulses. Under physiological conditions mitral cells are spontaneously active at a high rate and exhibit strong glutamate-mediated sub- and suprathreshold activity (Tabor and Friedrich, 2008). To obtain unconfouded measurements of the characteristics of ChR2 stimulation I suppressed spontaneous activity either by blocking of glutamatergic transmission by kynurenic acid (2 mM) or by cutting the ON. In the absence of spontaneous input individual light pulses reliably triggered action potentials with a delay of approximately 20 ms after stimulus onset (n = 3 cells, Fig. 15E). Mitral cells faithfully followed pulse trains at constant frequencies up to 20 Hz. At higher frequencies response failures to individual pulses occurred and caused a saturation of the output (Fig. 15F1). Excess spikes were only rarely observed. Spike time precision was high with a jitter on the order of a few milliseconds (Fig. 15F2). In addition, the jitter in inter-spike intervals increased only slightly with higher stimulus frequencies.

Mitral cells also followed more complex temporal stimulus patterns. In the absence of spontaneous activity, spike trains in response to series of blue light pulses with Poisson-distributed inter-stimulus intervals were highly reproducible and closely resembled the actual stimulus pattern (n = 3, Fig. 15G1, G2). In the absence of synaptic blockers and with intact ON, mitral cells still followed complex temporal stimulus patterns despite strong synaptic input and high spontaneous activity. Hence, ChR2-mediated optical stimulation applying Tet-transgenic lines can be used to impose defined activity patterns onto neurons in the olfactory bulb (Fig. 15G3)

For precise optogenetic manipulation of neuronal activity patterns within the intact microcircuit not only temporal, but also spatial

precision in stimulation is critical. As neurons are embedded within the tissue, the spatially precise stimulation of individual neurons is a technical challenge. Single-photon excitation by blue light bears the disadvantage that stimulation of ChR2 is not limited to the focal plane, but occurs within the entire light-path. In addition, light scattering due to the optical properties of the tissue lowers the xy-resolution for stimulation. Both problems can potentially be circumvented by utilizing multiphoton activation of ChR2. In cultured neurons, it had been demonstrated that it was in principle possible to trigger action potentials by two-photon stimulation, however, evoked currents were generally very small and rapidly saturated (Rickgauer and Tank, 2009). In addition, in hippocampal slice cultures two-photon stimulation at high power (>150 mW power) only yielded subthreshold membrane depolarizations ≤ 1.5 mV and failed to elicit action potentials in ChR2 expressing cells (Zhang and Oertner, 2007). Furthermore, due to the long lifetime of the conducting state of ChR2 high excitation powers are capable of saturating currents even in out-of-focus membrane patches and consequently impair spatial resolution (Rickgauer and Tank, 2009). A possibility to facilitate the efficacy of multiphoton-driven excitation of neurons in the intact network therefore is the increase of expression levels of ChR2 rather than the increase in excitation intensity. Hence, the Tet system provides a potential solution to this problem. I performed initial test experiments on the feasibility of two-photon excitation of mitral cells. Imaging of the somatic region of HuC:itTA/Ptet:ChR2YFP positive cells caused strong, rhythmic depolarizations that were synchronized with the scanning pattern of the microscope and were capable to trigger action potentials (n = 3, Fig. 15D) (Zhu et al, 2009).
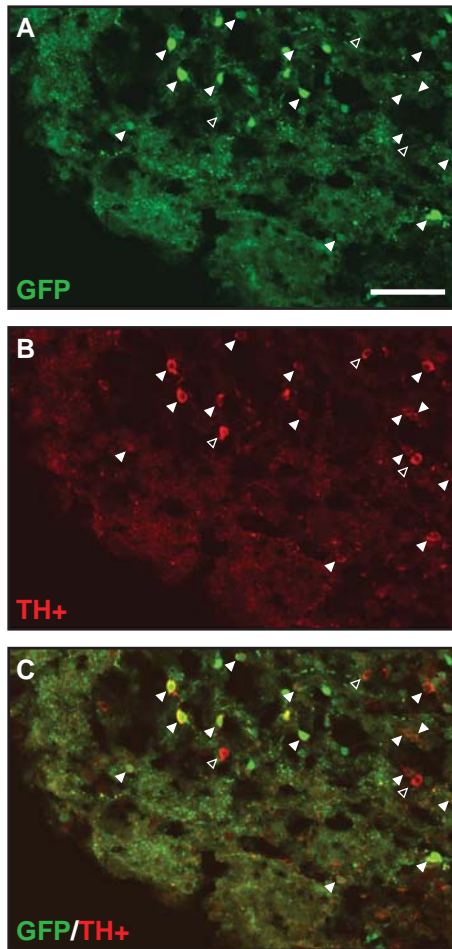
Figure 16: Colocalization of tyrosine hydroxylase immunofluorescence and GFP signal in the DLX4/6:eGFP zebrafish line. Pseudo-colored confocal laser scanning microscopy image in DLX4/6:eGFP fish. (A) The intrinsic GFP signal (green). (B) Tyrosine hydroxylase immunoreactivity (TH+, red). (C) Overlay. Solid arrow heads indicate cells positive for both GFP and tyrosine hydroxylase, empty arrow heads indicate cells only positive for tyrosine hydroxylase. Scale bar: 50 µm.

Endogenous release of dopamine

To optically stimulate dopaminergic periglomerular cells I used a transgenic zebrafish line that specifically expresses ChR2 in a subpopulation of interneurons under the Dlx4/6 promoter (Dlx4/6:itTA/Ptet:ChR2YFP line 1, Zhu et al, 2009). This line shows preferential labeling of the outer layers of the olfactory bulb and hence, of the periglomerular network. In mice, Dlx5/6, the murine homologue of Dlx4/6, is expressed in periglomerular cells including the dopaminergic subpopulation (Allen et al, 2007; Kohwi et al, 2007). To verify that Dlx4/6 also targets expression to dopaminergic neurons in zebrafish I performed immunohistochemical stainings in Dlx4/6:GFP zebrafish that exhibit a very similar expression pattern to the Dlx4/6:itTA/Ptet:ChR2YFP line 1. The majority of TH immunoreactive neurons was also GFP-positive (Fig. 16) thus confiming previous findings in mouse. I therefore used the Dlx4/6:itTA/Ptet:ChR2YFP line to directly activate dopaminergic periglomerular cells.

To measure light-evoked responses in mitral cells I performed patch-clamp recordings both in current-clamp and voltage-clamp configuration. Mitral cells were initially identified by the location and size of their somata. After achieving whole-cell configuration cells were filled with Alexa Fluor 594 to confirm their identity. Twelve out of 15 cells were unambiguously identified as mitral cell by their characteristic morphology. In addition, two cells clearly showed the features of ruffed cells, another type of projection neurons in the teleost olfactory bulb (Kosaka, 1979; Kosaka, 1980; Fuller and Byrd, 2005). To reduce spontaneous activity within the network glutamatergic transmission was blocked by NBQX (5 µM) and AP5 (50 µM) in all the experiments. I routinely tested light-

Figure 17: The effect of dopamine released endogenously by optical stimulation of interneurons onto mitral cells.

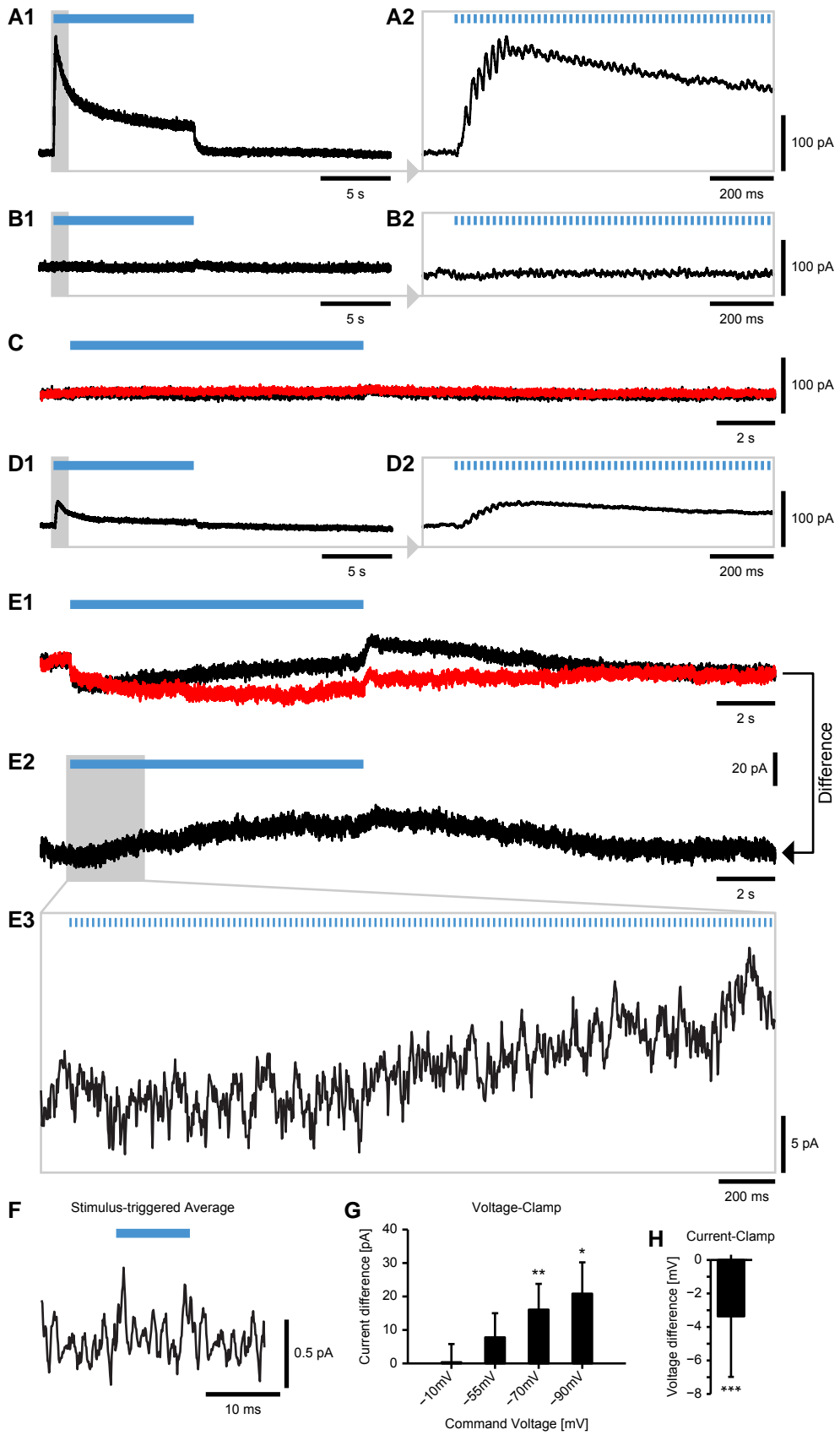(A-C) Whole-cell recordings of a mitral cell in voltage-clamp configuration at a holding potential near the reversal of excitatory synapses (Vcommand = -10 mV). (A1) Mitral cell response to 10 s trains of blue light pulses (10 ms pulse duration) at 50 Hz in the absence of blockers of synaptic transmission. (A2) shows the first second of light stimulation at larger magnification. (B) Response to the same stimulus in the presence of blocker of excitatory (NBQX, AP5) and inhibitory (Gabazine, CGP 54626) synaptic transmission. (C) Responses as in (B) before (black) and during (red) application of the D2-receptor antagonist sulpiride. (D-E) Whole-cell recordings of a mitral cell voltage-clamped to -70 mV. (D) Response in the absence of synaptic blockers. (E1) Response in the presences of synaptic blocker before (black) and during (red) the application of sulpiride. The sulpiride-sensitive component corresponding to the difference between the two conditions is shown in (E2, entire length) and (E3, initial 2.5 s of the stimulation). Blue bars indicate time of light stimulation. Grey areas highlight time windows shown at higher magnification. Traces shown are averages of 4 - 5 successive repetitions of the same stimulus. (A-E2) were median-filtered (5th order) to remove fast transients induced by triggering of the LED. Trace in (E3) was lowpass filtered with an eighth-order Chebyshev Type I filter with a cutoff frequency of 200 Hz and downsampled to 500 Hz. Traces shown in (C) and (E1) were offset subtracted for better comparison. (F) Stimulus-triggered average calculated for the trace shown in (E1). (G) Mean (± SD) amplitude of the sulpiride-sensitive current as a function of the command signal mitral cells were clamped to (Command voltage: -10 mV, n = 5; -55 mV, n = 3; -70 mV, n = 14; -90 mV, n = 7). (H) Mean (± SD) amplitude of the sulpiride-sensitive component measured in current-clamp (n = 15). The amplitude of the effect was calculated by first computing the difference between the mean responses in the presence and absence of sulpiride and then comparing the average amplitudes over a 250 ms time window just before stimulus offset relative to a corresponding time window starting 250 ms after stimulus onset. The latter was chosen to exclude potential offset shifts between different conditions. For recordings at a command potential of -55 mV an additional hyperpolarizing voltage step was applied during the pre-stimulus baseline. To compensate for capacitive transients the falling flank of the response to the voltage step was fitted with an exponential and subtracted before calculating the amplitude of the sulpiride-sensitive current. * $P < 0.05$ ** $P < 0.01$ *** $P < 0.001$ (Sign rank test)

induced currents in response to trains of light pulses (10 ms) at 20 – 50 Hz and durations of up to 10 s.

In the absence of $GABA_A$ and $GABA_B$ receptor antagonists, optical stimulation evoked strong synaptic input to mitral cells, confirming that stimulation was effective (n = 7). At depolarized holding potentials (V_{hold} = -10 mV) whole-field stimulation with blue light induced large outward currents that summed during the first few pulses and adapted at a slower rate (Fig. 17A). During the rising flank of the response, currents closely followed the train of light pulses (Fig. 17A2). These currents were attenuated, but still pronounced even at holding potentials close to the reversal potential for inhibitory synapses (Fig. 17D; V_{hold} = -70 mV) and were completely abolished by application of Gabazine (5 – 8 µM) and CGP 54626 (5 µM). At depolarized holding potentials (V_{hold} = -10 mV) no light-induced changes in holding current were detectable under these conditions (Fig. 17C). At a holding potential of -70 mV, however, a biphasic current was observed (Fig. 17E1, black trace). This current had a small excitatory component that in some cases was strong enough to elicit action potentials in current clamp recordings. The most likely source of these inward currents is gap-junction coupling between periglomerular cells and mitral cells (Kosaka and Kosaka, 2003; Kosaka and Kosaka, 2005b, 2005c; Kosaka et al, 2005; for a review see: Kosaka and Kosaka, 2005a). In addition, prolonged optical stimulation evoked a slow outward current with long tail after stimulus offset. Because this current developed slowly, it was not prominent during short trains of light pulses at 20 Hz (1 – 100 pulses), but became prominent during long stimulus trains (50 Hz for 10 s). In most cells, the net current measured at -70 mV therefore changed gradually from an inward to an outward current during prolonged optical pulse trains.

To examine whether any of these currents depend on dopamine, I examined the effect of D2 receptor antagonist, sulpiride (n = 15 mitral cells). Sulpiride had no obvious effect on the inward current. However, the slow outward current evoked by prolonged optical stimulation was completely blocked (V_{hold} = -70 mV; Fig. 17E). The sulpiride-sensitive current (control – sulpiride, Fig. 17E2) had a very slow rise time and was gradually building up over the entire time course of the 10 s stimulation. In addition, it also had a very long decay time constant. Furthermore, in contrast to fast events GABA-mediated currents that closely followed the stimulation for several pulses no temporal structure was observed in the sulpiride-sensitive current (Fig. 17E3). Overall, the effect was small and reached a mean maximum amplitude of 16.1 ± 7.7 pA (p < 0.0001, n = 14) after 10 s of stimulation (Fig. 17F). When examining the effect of the holding voltage onto the size of the sulpiride-sensitive current, the amplitude gradually decreased for holding potentials closer to the reversal of excitatory synapses (V_{hold} = -10 mV: 0.3 ± 5.4 pA, p > 0.05, n = 5; V_{hold} = -55 mV: 7.8 ± 7.2, p > 0.05, n = 3), but was increased for more hyperpolarized holding potentials (V_{hold} = -90 pA: 20.8 ± 9.4 pA, n = 7). When calculating the sulpiride-induced change in membrane potential in current clamp recordings in a corresponding time window, light-stimulation yielded a small but significant hyperpolarization (n = 15, -3.4 ± 3.6 mV, p = 0.0156).

Analysis of light-induced currents in ruffed cells (n = 2, data not shown) did not reveal any slow sulpiride-sensitive component, indicating that the effect was at least to some extent specific to mitral cells.

Spatial distribution of endogenous dopamine release

To explore the spatial extend of dopaminergic interactions within the glomerular layer, I stimulated periglomerular cells with spatially structured stimulus patterns. For this purpose I used a microscope equipped with a digital micromirror device that permits rapid switching of individual micromirrors in and out of the beam path and hence to control the spatial pattern of blue light excitation. A blue laser was employed to provide collimated stimulation light. Mitral cells were identified by the location and size of their somata and identity was confirmed upon achieving whole-cell configuration by filling the cells with Alexa Fluor 594. A total of 9 cells were clearly characterized as mitral cell by their morphological features. For each mitral cell, spatial stimulus patterns were individually centered onto the approximate center of their dendritic tuft (Fig. 18-20, panel A). Spatial patterns consisted of concentric circles of variable diameter with either the center (40 – 100 µm, usually 2-3 different diameters tested per cell) or the surround (40 – 200 µm, usually 2-3, up to 5 different diameters tested per cell) being illuminated. As the dopaminergic effect only became prominent for long stimulation I used 10 s trains of light pulses (10 ms) at a regular frequency of 50 Hz. All recordings were performed in the presence of glutamate (NBQX: 5 µM, AP5: 50 µM) and GABA (Gabazine: 5 µM, CGP 54626: 5 µM) receptor antagonists.

When stimulating only the central region of the dendritic field most mitral cells (7 out of 9 cells) exhibited pronounced tail currents that slowly decayed back to baseline and clearly resembled the time course previously measured for the sulpiride-sensitive component (Fig. 18-19, panels B, C3). No obvious differences were observed for stimuli with different diameters. In rare cases (n = 2 out of 9 mitral cells), an additional early outward current was detected that started

Figure 18: Dopamine release in response to spatially structured light stimulation.

(A1) Two-photon image of the recorded mitral cell filled with Alexa-594 fluor. The center position used to spatially allign light stimuli is marked by a red dot. Scale bar: 50 µm. The different diameters of center/surround stimuli used are depicted in (A2) Warm and cold colors indicate center-ON and surround-ON stimuli, respectively. The white box outlines the borders of the image shown in (A1). Scale bar: 50 µm. (B) Whole-cell recordings of the mitral cell holding current (command voltage: -70 mV) in response to center/surround stimuli of different size in the presence of blockers of excitatory (NBQX, AP5) and inhibitory (Gabazine, CGP 54626) synaptic transmission. Colors as in (A2). The black trace corresponds to whole-field illumination. Traces were averaged over five repetitions and baseline corrected. For illustration purposes traces were lowpass filtered with an eighth-order Chebyshev Type I filter with a cutoff frequency of 40 Hz and downsampled to 100 Hz. Blue ticks denote timing of pulses of blue light (10 ms pulses at a frequency of 50 Hz, 10 s duration). Dotted line indicates baseline. Grey boxes highlight time windows presented in more detail in (C). (C1-2) Initial 6 s of the traces shown in (B) for center-ON (C1) and surround-ON (C2) stimuli, respectively. (C3-4) Traces as in (B) for a 6 s time window starting 1 s before stimulus offset shown seperately for center-ON (C3) and surround-ON (C4) stimulation. The mitral cell response to stimulation with whole-field illumination (black) is presented as a reference. Blue ticks indicate timing of blue light stimulation. (D). Mean amplitude of the tail current computed for a 1 s time window starting 1 s after stimulus offset and measured relative to pre-stimulus baseline. Colored boxes above bars indicate the type and diameter of the stimulus.

shortly after stimulus onset and peaked approximately 1 s later (Fig. 19-20, panels B, C1). In contrast, when stimulating the surround or the entire field of view, a very pronounced initial outward current was observed in many of the cells (n = 5 out of 9 cells). This component usually decayed over the time course of the stimulus (Fig. 19-20, panel B). In all cases its amplitude decreased for increasing diameters of the dark center (Fig. 19-20, panel C2). When using LED whole-field stimulation this early component had been observed only in a few cells and was generally less pronounced. The reason for the less frequent occurrence in these experiments was probably related to the fact that stimulation light was spatially restricted to the field of view when using LED stimulation (see methods). Generally, in those cases tested the early outward current was insensitive to sulpiride (data not shown). In addition to the early component, stimulation of the periphery also elicited a slow outward current with a long tail (Fig. 18-20B, C4). However, in contrast to tail currents evoked by center stimulation that were usually maximal just after stimulus offset, outward currents in response to surround stimulation often increased slowly after stimulus offset (Fig. 19C4). This was particularly pronounced for global stimulation (Fig. 19-20, panels C3-4, black trace) and might be related to the existence of an additional inward current in these traces. As a consequence of the altered time course, a reasonable analysis of slow outward currents in response to surround stimulation was prohibited in three cells (Fig. 20C4). However, the remaining four cells all exhibited tail currents that decreased slowly with increasing diameter of the dark center (Fig. 18-19, panel C4) indicating that dopamine release can also be triggered by stimulation of remote areas.
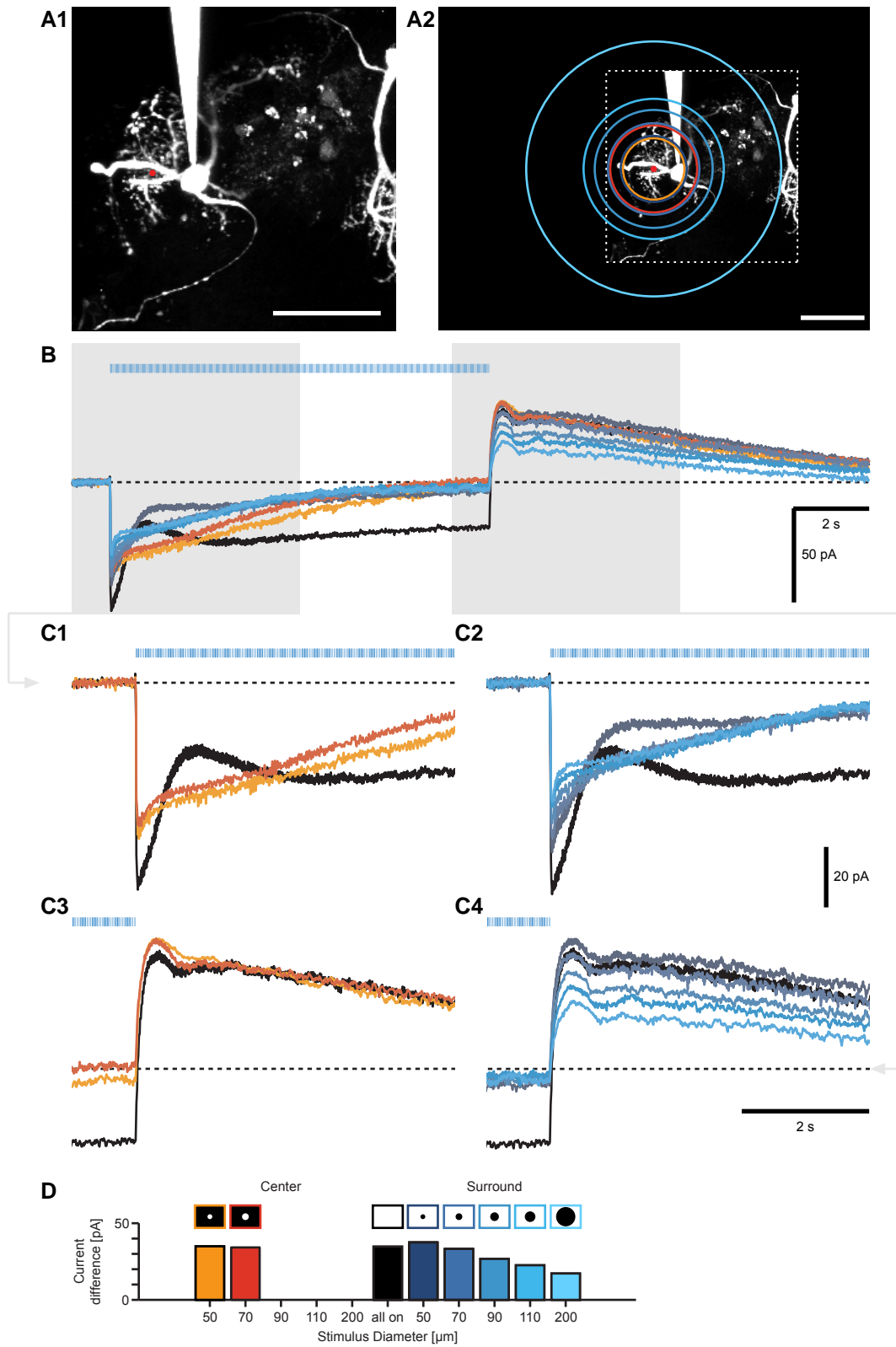
Figure 19: Dopamine release in response to spatially structured light stimulation.

(A1) Two-photon image of the recorded mitral cell filled with Alexa-594 fluor. The center position used to spatially allign light stimuli is marked by a red dot. Scale bar: 50 µm. The different diameters of center/surround stimuli used are depicted in (A2) Warm and cold colors indicate center-ON and surround-ON stimuli, respectively. The white box outlines the borders of the image shown in (A1). Scale bar: 50 µm. (B) Whole-cell recordings of the mitral cell holding current (command voltage: -70 mV) in response to center/surround stimuli of different size in the presence of blockers of excitatory (NBQX, AP5) and inhibitory (Gabazine, CGP 54626) synaptic transmission. Colors as in (A2). The black trace corresponds to whole-field illumination. Traces were averaged over five repetitions and baseline corrected. For illustration purposes traces were lowpass filtered with an eighth-order Chebyshev Type I filter with a cutoff frequency of 40 Hz and downsampled to 100 Hz. Blue ticks denote timing of pulses of blue light (10 ms pulses at a frequency of 50 Hz, 10 s duration). Dotted line indicates baseline. Grey boxes highlight time windows presented in more detail in (C). (C1-2) Initial 6 s of the traces shown in (B) for center-ON (C1) and surround-ON (C2) stimuli, respectively. (C3-4) Traces as in (B) for a 6 s time window starting 1 s before stimulus offset shown seperately for center-ON (C3) and surround-ON (C4) stimulation. The mitral cell response to stimulation with whole-field illumination (black) is presented as a reference. Blue ticks indicate timing of blue light stimulation. (D). Mean amplitude of the tail current computed for a 1 s time window starting 1 s after stimulus offset and measured relative to pre-stimulus baseline. Colored boxes above bars indicate the type and diameter of the stimulus.
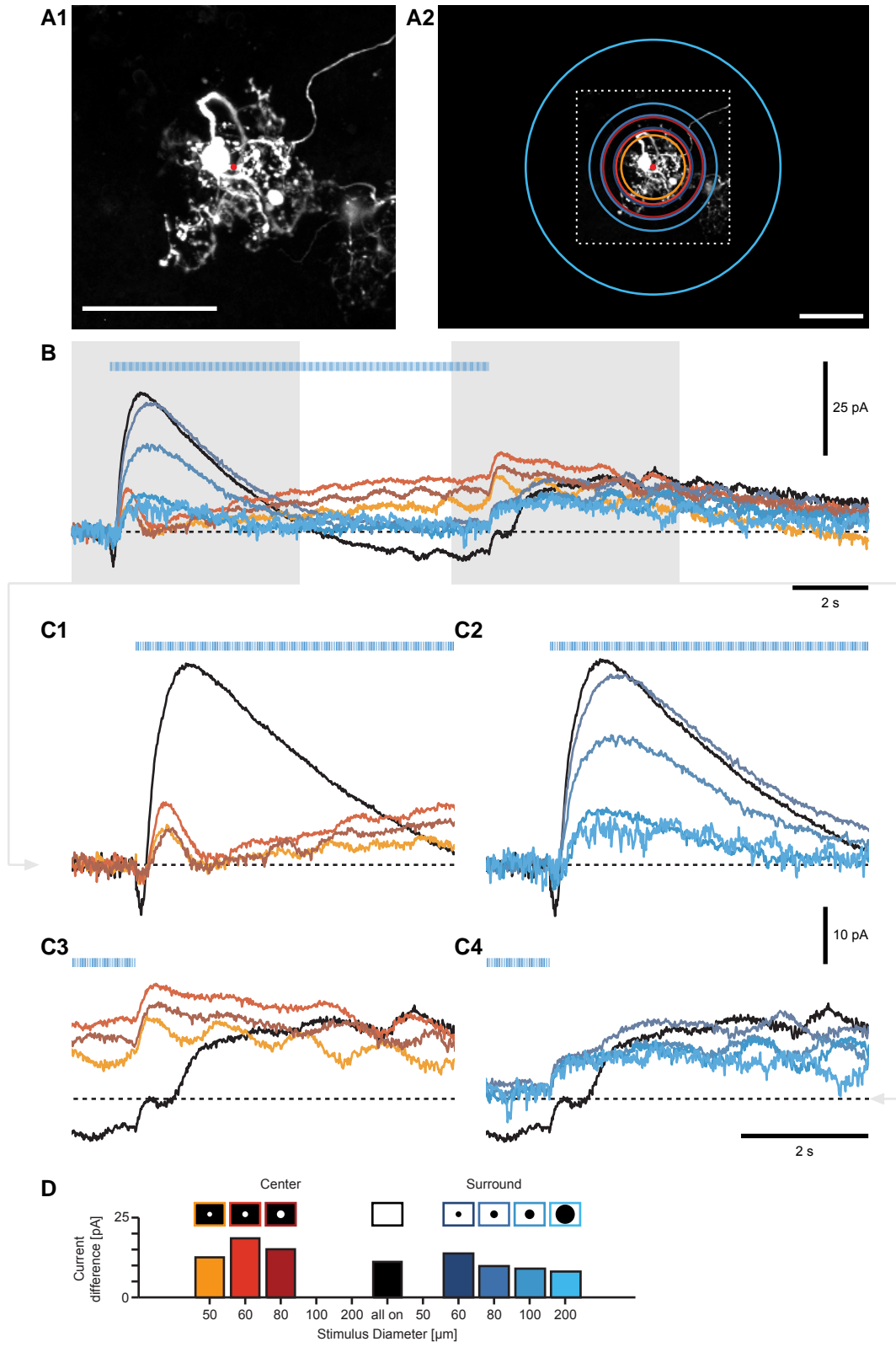
Figure 20: Dopamine release in response to spatially structured light stimulation.
(A1) Two-photon image of the recorded mitral cell filled with Alexa-594 fluor. The center position used to spatially allign light stimuli is marked by a red dot. Scale bar: 50 µm. The different diameters of center/surround stimuli used are depicted in (A2) Warm and cold colors indicate center-ON and surround-ON stimuli, respectively. The white box outlines the borders of the image shown in (A1). Scale bar: 50 µm. (B) Whole-cell recordings of the mitral cell holding current (command voltage: -70 mV) in response to center/surround stimuli of different size in the presence of blockers of excitatory (NBQX, AP5) and inhibitory (Gabazine, CGP 54626) synaptic transmission. Colors as in (A2). The black trace corresponds to whole-field illumiation. Traces were averaged over five repetitions and baseline corrected. For illustration purposes traces were lowpass filtered with an eighth-order Chebyshev Type I filter with a cutoff frequency of 40 Hz and downsampled to 100 Hz. Blue ticks denote timing of pulses of blue light (10 ms pulses at a frequency of 50 Hz, 10 s duration). Dotted line indicates baseline. Grey boxes highlight time windows presented in more detail in (C). (C1-2) Initial 6 s of the traces shown in (B) for center-ON (C1) and surround-ON (C2) stimuli, respectively. (C3-4) Traces as in (B) for a 6 s time window starting 1 s before stimulus offset shown seperately for center-ON (C3) and surround-ON (C4) stimulation. The mitral cell response to stimulation with whole-field illumination (black) is presented as a reference. Blue ticks indicate timing of blue light stimulation. (D). Mean amplitude of the tail current computed for a 1 s time window starting 1 s after stimulus offset and measured relative to pre-stimulus baseline. Colored boxes above bars indcate the type and diameter of the stimulus.
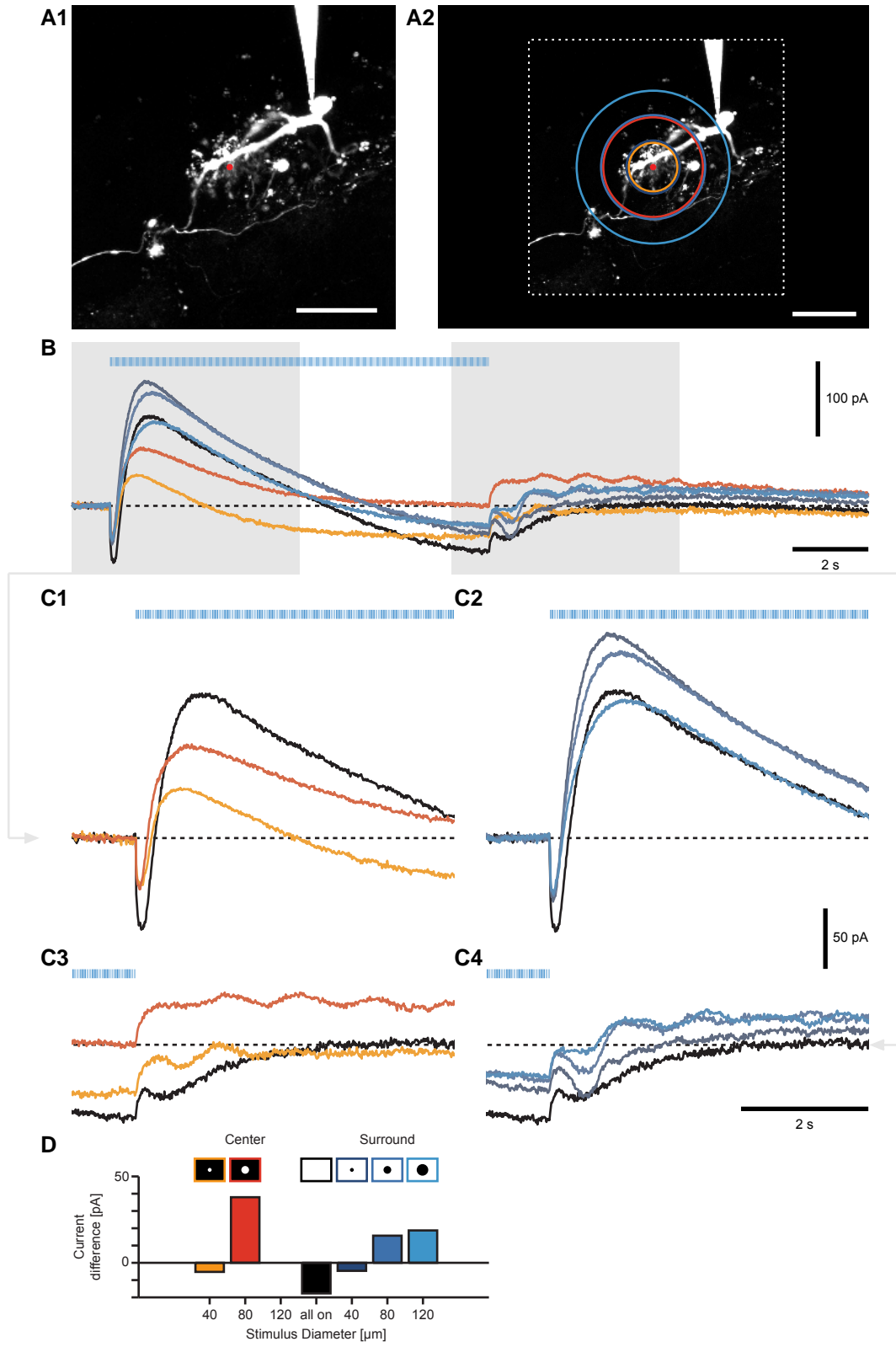
Discussion

Dopaminergic innervation of the olfactory bulb is exceptional. Most brain regions receive dopaminergic innervation via long-distance projections from brain stem systems such as the substantia nigra and the ventral tegmental area (Björklund and Dunnett, 2007). In contrast, in the olfactory bulb dopamine is released by a subpopulation of GABAergic interneurons and is thought to participate in local processing of odor information (Halász et al, 1977a, 1977b, 1978; Kosaka et al, 1985; Gall et al, 1987). However, its precise role in information processing in the olfactory bulb is poorly understood. In this study I analyzed the function of dopamine within the olfactory bulb of zebrafish by calcium-sensitive dye imaging and electrophysiological recordings in combination with traditional pharmacological manipulations and optogenetic stimulation, to gain insight as to how this local dopaminergic circuitry modulates olfactory processing.

The targets of dopamine in the olfactory bulb

Absence of dopaminergic effects on the afferent input

Dopamine may exert its effect in the olfactory bulb by modulating the afferent ORN input, or by influencing the intra-bulbar processing, with these possibilities being mutually non-exclusive.

Previous studies on the effect of bulbar dopamine on presynaptic ORN input have been fragmented and the results obtained are ambiguous. In mammals and reptiles, anatomical and functional evidence points to a presynaptic effect of dopamine by decreasing glutamate release from the ORNs (Palacios et al, 1981; Mansour et al, 1990; Nickell et al, 1991; Guthrie et al, 1991; Levey et al, 1993; Mania-Farnell et al, 1993; Coronas et al, 1999; Hsia et al, 1999;

Koster et al, 1999; Vargas and Lucero, 1999, 2002; Wachowiak and Cohen, 1999; Berkowicz and Trombley, 2000; Ennis et al, 2001; Maher and Westbrook, 2008). However, several studies in amphibians and reptiles suggest that dopamine affects primarily mitral cells, indicating the potential existence of phylogenetic differences (Nowycky et al, 1983; Gurski and Hamilton, 1996; Duchamp-Viret et al, 1997). I therefore directly examined the effect of dopamine on the afferent nerve terminals in zebrafish by calcium sensitive dye imaging. In other species this approach has been used previously to detect dopaminergic modulation of the afferent nerve fibers (Wachowiak and Cohen, 1999). Furthermore, in zebrafish the method has been applied successfully to investigate $GABA_B$-mediated presynaptic inhibition (Tabor et al, 2008). My results revealed no effect of dopamine on odor-evoked afferent activity (Fig. 3). This was true for both D1 and D2 receptor agonists as well as for the selective D2 receptor antagonist sulpiride, ruling out the possibility that the effect of dopamine is masked by an antagonistic action of D1 and D2 receptors and saturating levels of dopamine in the tissue, respectively.

Dopamine has been proposed to exert its effect on ORNs by modulating either membrane excitability or calcium influx, both leading to changes in stimulus evoked calcium currents (Vargas and Lucero, 1999, 2002; Wachowiak and Cohen, 1999). However, as dopamine receptors modulate adenylyl cyclase activity, dopamine might in principle also alter targets downstream of calcium influx, such as the vesicular release machinery (Sheng, 2009). In this case, calcium sensitive dye imaging would be inadequate for measuring changes in transmitter release. To exclude this possibility I analyzed both spontaneous and odor-evoked activity in mitral cells by whole-cell voltage-clamp recordings. Upon bath application of dopamine, I observed a decrease in mitral cell holding currents and in fluctuations

of the membrane current (Fig. 4A-B). This could result either from a reduction in synaptic input or as a consequence of changes in postsynaptic conductances. However, as dopamine did not alter the total charge conveyed by odor-evoked membrane currents (Fig. 4C), a postsynaptic site of action is likely. In summary, my experiments therefore argue against a prominent effect of dopamine on the afferent input.

Characterization of the dopaminergic effect on mitral cells

My electrophysiological recordings revealed a strong dopamine-induced hyperpolarization of mitral cells that was accompanied by a reduction in input resistance. As a result, spontaneous action potential firing was abolished in most of the measured mitral cells. My results imply intra-bulbar effects of dopamine such as a direct action on mitral cells or an indirect action by increasing tonic inhibitory input onto mitral cells. As the majority of inhibitory interactions in the olfactory bulb are GABA-mediated (Shepherd et al, 2004) I also added $GABA_A/GABA_B$-receptor antagonists in a subset of the patch-clamp recordings together with glutamate blockers. Application of GABA-blockers did not significantly change the results, indicating that dopamine acts directly on mitral cells.

In the olfactory bulb dopaminergic action has generally been attributed to an activation of D2 receptors. Consistently, in my experiments, the selective D2 receptor antagonist sulpiride completely reversed the hyperpolarization of mitral cell membrane potential caused by dopamine. Moreover, the decrease in input resistance was partially antagonized by sulpiride. My experiments therefore suggest that D2 receptors play a prominent role in controlling mitral cells in zebrafish.

In conclusion, my results provide clear evidence that in the zebrafish dopamine exerts a prominent effect directly onto mitral cells. My results argue against a pronounced effect of dopamine on afferent input to the olfactory bulb. While a few studies in amphibians and reptiles have suggested a similar mechanism (Nowycky et al, 1983; Gurski and Hamilton, 1996; Duchamp-Viret et al, 1997), direct functional evidence for a purely postsynaptic action of dopamine had so far been missing.

Unresolved aspects

I have provided strong evidence for a direct D2 receptor-mediated effect of dopamine onto mitral cells. Nevertheless, there might be further dopaminergic effects within the network. A few studies have described additional effects of dopamine such as a modulation of lateral spread of activity from mitral cells onto interneurons (Brünig et al, 1999; Davida et al, 2003; Davison et al, 2004; Gutièrrez-Mecinas et al, 2005) and a targeting of interneurons directly (Brünig et al, 1999; Gutièrrez-Mecinas et al, 2005). However, as blocking of glutamatergic and GABAergic transmission did not have a prominent effect on the outcome of my experiments the contribution of additional mechanisms should be limited. Similarly, there are rare reports about D1 receptor mediated effects in the olfactory bulb (Brünig et al, 1999; Coronas et al, 1999; Davida et al, 2003). As sulpiride did not completely rescue the decrease in input resistance observed in current-clamp recordings from mitral cells (Fig. 7B), a small residual D1 receptor mediated component might indeed exist. Therefore, while I cannot rule out the existence of such mechanisms, my results do not yield any evidence for further strong effects of dopamine. It is well possible, though, that dopamine also serves functions beyond a modulation of neuronal activity within the network. A regulation of synaptic plasticity might be a potential

candidate as extracellular dopamine levels are elevated during odor preference learning (Coopersmith et al, 1991).

In addition, my experiments only allow for a limited analysis of the underlying cellular mechanism in mitral cells. A possible way to explain both hyperpolarization and decreased input resistance would be to assume that activation of D2 receptors (a metabotropic receptor; see Beaulieu and Gainetdinov, 2011) opens a hyperpolarizing conductance. I also measured endogenous dopaminergic currents in mitral cells evoked by photostimulation of interneurons (Fig. 17G). In these experiments the response amplitude in mitral cells decreased with increasing depolarization, in contrast to what might be expected from a hyperpolarizing conductance in which the driving force should increase with depolarization. How can one reconcile the hyperpolarizing, conductance increasing effect of dopamine on mitral cells with the negative dependence of the induced current on depolarization? There are several possibilities that could account for my findings: one potential mechanism would be a D2 receptor-mediated modulation of several conductances including a reduction in inward currents and an increase in hyperpolarization-activated inward rectifying potassium currents that are inactivated by depolarization. Further experiments will be required to elucidate the precise cellular mechanisms of dopaminergic action in mitral cells.

Interestingly, light-stimulation of periglomerular cells also revealed additional currents that were insensitive to sulpiride and GABA-blockers (e.g. Fig. 20). A potential neurotransmitter mediating the observed early outward current could be glycine (Trombley and Shepherd, 1994) that might be co-released by a subpopulation of GABAergic periglomerular cells (Kosaka et al, 1998, preliminary

results). It will be informative to learn more about the function of these additional circuits.

Dopaminergic effect on bulbar output

To evaluate the consequences of dopaminergic modulation on the output of the system I analyzed mitral cell responses to two different types of stimuli. I first measured the input-output relationship in single mitral cells directly by applying current injections. Application of dopamine had two effects. First, mitral cell response curves were shifted towards higher inputs (Fig. 9B-C). This essentially corresponds to a shift in response threshold and is likely to be a direct consequence of the dopamine-induced decrease in membrane potential as well as input resistance. Second, dopamine slightly increased the gain of the I-F curve. This effect can, in principle, result from a modulation of intrinsic properties as well as from changes in network interactions such as recurrent inhibition. Blocking of synaptic transmission did not abolish the observed increase in gain, suggesting that the modulation in the I-F curve results from changes in mitral cell intrinsic properties. Some modeling studies have demonstrated that a decrease in input resistance can cause a shift in response threshold and, in addition, also increase the gain by a scaling of noise (Doiron et al, 2001; Azouz, 2005; for a review see Silver, 2010). Such a mechanism might participate in the effects. However, as blocking glutamatergic input and thus, presumably, a strong reduction in synaptic noise did not abolish the dopamine-induced increase in gain, it is unlikely to account for the results.

From fitting the I-F curves of mitral cells before and during dopamine application, it became apparent that the increase in gain was only effective for inputs beyond approximately 100 pA (Fig. 9F). How does this relate to the size of natural inputs? At the odor concentrations used in my experiments (10 – 60 µM), voltage-clamp recordings

indicate that the steady-state input rarely exceeds 100 pA, and is on average only about 30 pA in size (Fig. 4D). It is therefore likely that under normal conditions, the dopamine-induced gain modulation has a rather small impact compared to the shift in threshold.

Current injections do not induce strong activity in the microcircuit and are unlikely to engage pronounced lateral inhibitory interactions between mitral cells. Therefore, I tested whether the previous findings also hold true for the processing of more complex natural stimuli, by using patch clamp recordings and calcium imaging of odor responses. As expected from the observed thresholding effect on the input-output function, dopamine abolished only weak, but not strong excitatory odor responses in mitral cells. In electrophysiological recordings input was still detectable for weak responses, but activity remained subthreshold. In addition, strong excitatory odor responses became boosted both in response amplitude and duration. This amplification can be a direct result of the dopamine-induced increase in gain in the input-output function of mitral cells. However, as measured odor-evoked membrane currents were usually below 100 pA (Fig. 4D), it is unclear whether the observed increase in gain can account for the boosting effect by itself. Another possible explanation for the augmentation of strong responses is an attenuation of lateral inhibition because, as both spontaneous and induced activity in the olfactory bulb are reduced, interneurons are expected to be less excitable in the presence of dopamine. It has also been suggested that dopamine can directly reduce excitatory synaptic transmission from mitral cells onto interneurons (Davida et al, 2003; Davison et al, 2004; Gutièrrez-Mecinas et al, 2005). Such mechanisms might facilitate the observed effects, however, would not be essential for explaining my results.

At the population level, the effect of dopamine is clearly seen in the cumulative distribution of odor response amplitudes (Fig. 13G): (a) a light tail for negative firing rate changes due to the decrease inhibitory responses; (b) a steep gradient around 0 Hz due to the loss in weak excitatory and inhibitory responses; and (c) a heavy tail for positive firing rate changes as a result of the increase in the strong responses. Similar results were also obtained for calcium imaging experiments, however, with a less pronounced increase in the gradient (Fig. 14F). Hence, the effect of dopamine can be interpreted as a form of contrast enhancement (Fig. 21B). This contrast enhancement can be accounted for, at least in part, by changes of the I-F curves in single neurons. In other sensory systems such as the retina, contrast enhancement is produced by lateral inhibitory interactions within networks of neurons (Cook and McReynolds, 1998). Contrast enhancement of activity patterns by dopamine in the olfactory bulb may therefore be achieved by different mechanisms.

When analyzing odor-evoked population response patterns obtained by calcium imaging it also becomes apparent that dopamine does not alter the general pattern of activity, as population odor responses remained highly correlated (Fig. 14H). Furthermore, differences in response patterns evoked by different odors were largely preserved. This is expected for several reasons: first, a change in threshold would not dramatically reorganize activity patterns, and second, results from mathematical and computational modeling have indicated that a reduction in spontaneous activity is likely to impair temporal decorrelation (Wiechert et al, 2010).

In summary, I have provided evidence that dopamine shifts the response threshold of individual mitral cells, with only a minor change in gain that becomes dominant only for strong input. Responses to natural stimuli exhibit very similar characteristics: weak excitatory

remain subthreshold while strong responses are augmented. In contrast, inhibitory odor responses are no longer apparent because spontaneous activity is nearly abolished. All of these features can, in principle, be directly accounted for by the dopaminergic modulation of the individual transfer functions. Nevertheless, additional effects within the network such as a reduction in lateral inhibition may also be involved.

Characteristics of endogenous release of dopamine

Tonic release

Previous studies in mice have argued that dopaminergic periglomerular cells exhibit intrinsic pacemaker currents and are thus spontaneously active even in the absence of external input (Pignatelli et al, 2005; Puopolo et al, 2005). These findings would indicate a persistent release of dopamine. As a first step I therefore explored the existence of tonic dopaminergic modulation in the presence of glutamate and GABA receptor antagonists. However, my findings argue against a prominent tonic effect of ambient dopamine levels as sulpiride had no additional effect on mitral cells. Release of dopamine is therefore more likely to be directly controlled by input to the olfactory bulb. This is in line with findings by Mahler and Westbrook (2008), who did not find a prominent tonic effect of dopamine in the mouse olfactory bulb.

Evoked release of endogenous dopamine

The effect of neurotransmitters within a system is traditionally examined by bath application of receptor agonists. The shortcoming of this approach is that it neglects aspects such as intrinsic availability of the transmitter as well as temporal dynamics and

spatial patterns of release. To gain a better understanding of the role of dopamine within the olfactory bulb it is therefore indispensable to analyze endogenous transmitter release. To my knowledge, only a single study tried to address this question by directly stimulating individual TH positive neurons in patch-clamp recordings (Maher and Westbrook, 2008). However, the authors could not identify any stimulation-evoked dopaminergic effects. I therefore investigated the characteristics of endogenous dopamine release by using optogenetics to simultaneously stimulate a large number of periglomerular cells including the TH-positive subpopulation.

Light stimulation of periglomerular cells evoked a number of overlapping currents in mitral cells. Under control conditions, GABA-mediated currents were dominant. Blockade of GABAergic transmission unmasked additional currents including an inward current that was possibly mediated by gap junctions between mitral cells and a subpopulation of periglomerular cells (Kosaka and Kosaka, 2003; Kosaka and Kosaka, 2005b, 2005c; Kosaka et al, 2005; for a review see: Kosaka and Kosaka, 2005a). In addition, application of the D2 receptor antagonist sulpiride revealed a very slow outward current. This current was specific to mitral cells and was not observed in ruffed cells, a type of projection neurons unique to the teleost olfactory bulb (Kosaka, 1979; Kosaka, 1980; Fuller and Byrd, 2005).

My data therefore indicate that dopaminergic effects on mitral cells have very slow kinetics and gradually build up over many seconds. In contrast, odor-evoked activity patterns in mitral cells have been shown to evolve over a few hundred milliseconds (Friedrich and Laurent, 2001, 2004; Yaksi et al, 2007; Niessing and Friedrich, 2010). Furthermore, behavioral experiments in mammals have demonstrated that odor identification takes between 200 ms and 2 s

(Wise and Cain, 2000; Uchida and Mainen, 2003; Rinberg et al, 2006; Kahn et al, 2007). It is therefore unlikely that dopamine participates in the processing of rapid odor stimuli. Rather, dopamine is likely to fulfill a modulating role by adapting the system to changes in the environment on a longer time scale.

Spatial aspects of dopamine release

An important factor for assessing the role of dopamine within the olfactory bulb is its spatial release characteristics. Therefore, I addressed the spatial properties of dopamine release by directly stimulating endogenous transmitter release using light-activation of ChR2. Slow, presumably dopamine mediated, tail currents were triggered both by stimulation of the center and the surround. In most cases, current amplitudes measured in response to surround stimuli with a small omitted center were similar to those obtained by stimulation of the center. For larger diameters of the center surround responses decreased gradually. These results could be explained by a poor spatial resolution in light stimulation patterns due to light scattering. However, as currents evoked by surround stimulation were sensitive to even small increases in center diameter at small radii (Fig. 18D), this cannot account for my findings. My results therefore suggest a relatively large effective range of influence of individual dopaminergic neurons.

This can be explained by two different concepts: either dopaminergic periglomerular cells possess large dendritic or axonal fields, or they are activated over long distances by excitatory interactions between periglomerular cells. A candidate mechanism for excitatory coupling between periglomerular neurons are gap junctions, which have been described extensively in rodent periglomerular cells (Kosaka and Kosaka, 2003; Kosaka and Kosaka, 2005b, 2005c; Kosaka et al,

2005; for a review see: Kosaka and Kosaka, 2005a). In addition, axonal projections of dopaminergic interneurons have been reported to possess extensive axonal projections and establish an interglomerular network (Aungst et al, 2003; Kosaka and Kosaka, 2008; Kiyokage et al, 2010; Kosaka and Kosaka, 2011). It is therefore likely that dopaminergic neurons can transmit signals over relatively large distances within the olfactory bulb. However, to date the location of dopamine-releasing sites within periglomerular cells is unknown. GABA and dopamine might be co-released at the same sites or spatially segregated and specifically allocated to dendodendritic or axonal synapses. As optogenetic methods are capable of both orthodromic and antidromic stimulation, it was not possible to localize release sites. Further experiments are required to assess the spatial constraints on dopamine release.

Functional implications of dopaminergic modulation

Dopamine and adaptation

A striking feature of the dopamine-mediated effects is their slow onset and decay over tens of seconds. This is in sharp contrast to the faster kinetics of GABAergic currents. What might be the functional role of the dopamine-mediated slow outward current? First, dopamine could act as a high-pass filter that selectively removes slow components such as changes in background odors. Second, adaptive processes with slow temporal dynamics also provide a mechanism to correct for variance within the input and higher-order statistical properties. As has been reported by Arganda and colleagues (2007), slow pump currents are capable of scaling neuronal responses to input statistics on the time scale of one minute. It is possible that in a natural environment, olfactory input to the nose is not constant, but temporally structured and presented in

odor plumes. In this case, fast GABAergic inhibition would have the tendency to follow these fluctuations. In contrast, dopamine could provide a mechanism to integrate them over time, allowing for adaptation to fluctuations. Dopamine might therefore be important for processes such as odor habituation that operate on long time scales in the olfactory bulb (McNamara et al, 2008; Chaudhury et al, 2010).

Under natural conditions new odors are perceived on a persistent background of other stimuli. However, background stimuli are likely to cause several problems to the olfactory bulb microcircuit: first, tonic input will increase mitral cell activity, thereby reducing their dynamic range. Second, interneurons will receive more input, hence, be more excitable. As a consequence, tonic input can potentially facilitate lateral spread of inhibition and thus would be capable of altering global activity patterns and temporal dynamics within the network. For simultaneous application of two odors it has in fact been demonstrated that new response patterns can emerge (Niessing and Friedrich, 2010). One way to account for persistent background would be a channel-autonomous offset subtraction that compensates for tonic increases in input in each glomerular unit. There are several mechanisms for how an offset subtraction could be implemented. One possibility would be an inhibitory feed-forward circuit with a slow onset that countervails afferent input with some temporal delay. Anatomical data in mammalian systems have provided evidence that TH-positive neurons belong to the population of type 2 periglomerular cells that receive direct input from the ON terminals and form dendodendritic synapses on mitral cells (Kosaka et al, 1997; Kosaka et al, 1998). They are therefore in a good position to provide feed-forward inhibition. In addition, temporal activity patterns in periglomerular cells closely resemble those of ORNs and do not exhibit pronounced dynamics as is the case for mitral cells (P. Zhu and R.W. Friedrich, unpublished observations). It is therefore feasible

A Background compensation mechanisms

B Contrast enhancement mechanisms
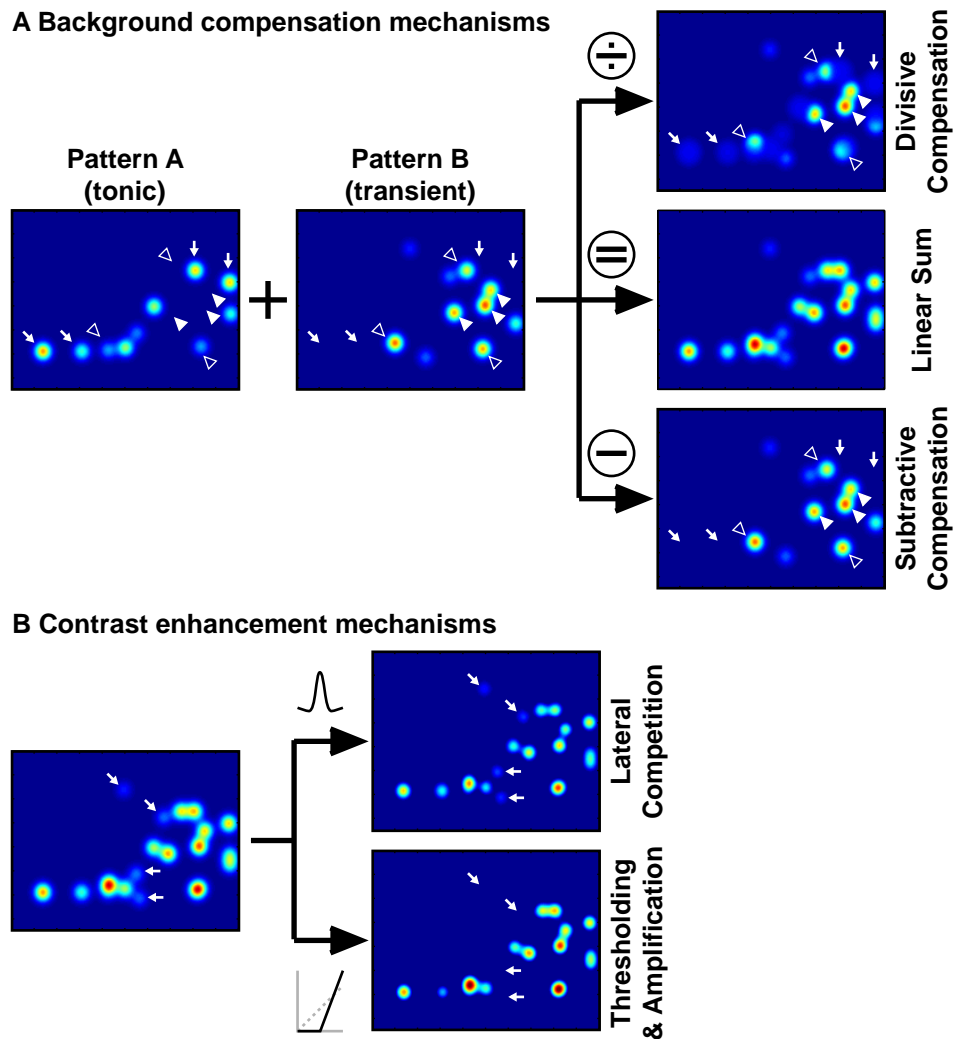
Figure 21: Potential functional implications of dopaminergic modulation.

(A) Illustration of different mechanisms compensating for a tonic background (pattern A). Both divisive and subtractive compensation mechanisms strongly reduce background (arrows). However, as a divisive compensation mechanism reduces background by decreasing the sensitivity of a channel, it also scales the new pattern accordingly (open arrow heads). Channels not receiving tonic background remain unchanged (closed arrow heads). In contrast, background subtraction does not reduce sensitivity and therefore preserves the original pattern of B.

(B) Illustration of different contrast enhancement mechanisms. Both lateral competition and thresholding increase the contrast within the pattern. However, lateral inhibition preserves all local maxima (arrows) while thresholding only preserves activity above threshold irrespective of spatial arrangement.

that dopaminergic neurons provide a negative copy of the receptor input to mitral cells. Importantly, as dopamine specifically increases the response threshold of mitral cell I-F curves but has only a weak effect on neuronal gain, it can potentially compensate for an increase in tonic input without compromising the sensitivity of mitral cells (Fig. 21A).

To function as a channel-autonomous background subtraction mechanism dopaminergic modulation should be restricted spatially to the activated glomerular unit. I cannot directly address this issue. In experiments using concentric on- or off-center light stimuli, effects were observed over an intermediate spatial range. This observation shows that some effects of periglomerular cells extend over a substantial spatial range. However, it does not preclude a local action of dopamine because optical stimulation may have caused long-range effects, such as antidromic action potential propagation in axons that do not occur under normal conditions. It is therefore possible that dopamine acts locally within an activated glomerulus or more globally across glomeruli. In fact, these two possibilities are not mutually exclusive. To resolve this issue it would be necessary to localize the sites dopamine release within periglomerular cells (axonal or dendritic) and to characterize the mode of release.

Dopamine as a potential mechanism for contrast enhancement

Another potential role of dopamine might be a biasing of olfactory processing according to the amount of input. My data have provided evidence that dopamine provides a way of cell-autonomous contrast enhancement that depends on increasing threshold and gain in the neuronal I-F curve. The dopaminergic network could therefore serve as a mechanism to enhance contrast in mitral cells that receive tonic input. It could potentially increase the signal-to-noise ratio within the

channel by decreasing spontaneous activity and selectively amplifying the more salient responses while suppressing less salient responses. This interpretation is in line with a study by Duchamp-Viret et al (1997) that also argued for a dopamine-mediated increase in signal-to-noise ratio. Furthermore, injection of a D2 receptor antagonist or reduction in TH expression by nostril occlusion increase both the total number of single units responding to an odor and the number of units responding to more than a single stimulus (Guthrie et al, 1990; Wilson and Sullivan, 1995). Experiments in mammals are therefore also consistent with the hypothesis that dopamine can modulate contrast in the olfactory bulb by sharpening neuronal tuning.

Traditionally, contrast enhancement is associated with the increase in spatial contrast within a low-dimensional continuous topographic representation, as is the case for retinotopic maps. In the retina, these mechanisms employ lateral competition between neighboring units, thereby reducing overlap among responses of neurons with similar tuning (Cook and McReynolds, 1998). However, odor space is high-dimensional and chemotopic maps are fragmented in the olfactory bulb (Friedrich and Korsching, 1997, 1998; Friedrich and Stopfer, 2001; Wachowiak and Cohen, 2001, Bozza et al, 2004), and it has been shown that similarity in odor tuning does not correlate well with proximity of glomerular units (Linster et al, 2005). Nevertheless, there is evidence that contrast enhancement also exists in the olfactory bulb (Yokoi et al, 1995).

It has been proposed that activity-dependent lateral inhibition can provide a form of contrast enhancement in the olfactory bulb by selectively suppressing mitral cell activity only in the intermediate range (Arevian et al, 2006). As a result of this mechanism the distribution of odor response amplitudes will become narrow, with

only a few strongly active cells. The observed modulation by dopamine closely resembles these characteristics and could therefore potentially allow for globally setting the contrast of the system (Fig. 21B). Furthermore, Cleland and Sethupathy (2006) have proposed a potential mechanism to circumvent the lack informative nearest-neighbor relations by employing non-topographic contrast enhancement that relies on two different prerequisites: first, it requires local feed-forward inhibition to suppress weakly activated mitral cells and second, global inhibitory feedback to compensate for differences in mean activity within the olfactory bulb. My data suggest that dopaminergic periglomerular cells could possibly meet these requirements by abolishing weak but not strong odor responses. Furthermore, as light stimulation of periglomerular cells affected mitral cells over a considerable spatial range, processes of dopaminergic neurons potentially extend over large distances. However, as the observed dopamine-mediated effects are clearly too slow to directly participate in odor processing, the role of the dopaminergic network might rather be an adjustment in response thresholds and hence, contrast enhancement mechanisms to persistent changes in input on a long time scale. Interestingly, in the retina, the only other system that features a local dopaminergic network, it has been suggested that one function of dopamine might be a modulation of spatial contrast by adjusting the receptive field size of horizontal cells (for a review see: Witkovsky, 2004; Bloomfield and Völgyi, 2009).

A recent study by Wiechert and colleagues (2010) has shown mathematically and by computational modeling that thresholding by itself produces pattern decorrelation. In recurrent networks, this decorrelation is amplified by feedback of the decorrelated patterns. In the olfactory bulb, dopamine increases the threshold of output neurons, which may have different effects depending on network

parameters. In weakly connected networks, an increased threshold would enhance pattern decorrelation. However, in sparsely but strongly connected networks, which are likely to include the olfactory bulb, it is expected that pattern decorrelation is reduced by an increase in response threshold. In fact, administration of a D2 receptor agonist into the olfactory bulb reduced odor discrimination performance in rats (Yue et al, 2004; Wei et al, 2006; Escanilla et al, 2009; but see Tillerson et al, 2006). Systemic dopamine application may therefore provide a tool to analyze mechanisms of pattern decorrelation in the olfactory bulb by direct predictions of a mathematical theory.

Generally, a local background subtraction and a more global contrast enhancement by dopamine are not mutually exclusive computational effects. In granule cells it has been shown that dendrodendritic synapses permit local transmitter release (Chen et al, 2000; Egger et al, 2003, 2005; Zelles et al, 2006). As periglomerular cells feature both dendrodendritic synapses (Toida et al, 2000) and axonal connections (Aungst et al, 2003; Kosaka and Kosaka, 2008; Kiyokage et al, 2010; Kosaka and Kosaka, 2011) it would in principle be feasible that dopaminergic periglomerular cells acted both locally as a channel-autonomous background subtraction mechanism and globally as an inhibitory mean subtraction for non-topographic contrast enhancement.

Conclusions and Outlook

My data have provided clear evidence for a direct dopaminergic modulation of mitral cells. Application of dopamine had a hyperpolarizing effect on mitral cells resulting in an increase in neuronal response threshold and consequently a suppression of spontaneous activity. Furthermore, dopamine also caused a thresholding of responses to natural odors essentially abolishing weak excitatory and inhibitory responses. In contrast, strong excitatory responses were amplified, possibly as a result of a decrease in network activity. The effect of dopamine can therefore be interpreted as a cell-autonomous form of contrast enhancement.

Importantly, my experiments demonstrate that dopaminergic effects are slow and occur on a much longer time scale than GABAergic currents. As a consequence, it seems unlikely that dopamine directly participates in processing of odor information but rather provides a mechanism to adapt the system to slow changes in the environment. Depending on the spatial extent of release the dopaminergic network could potentially serve as a circuit for channel-autonomous background subtraction or global adjustment of contrast.

Therefore, an important future target for investigations will be the spatial characteristics of dopamine release – particularly, whether dopamine is capable of acting as a channel-autonomous mechanism or whether it functions as a global signal. While my data provided first indications, an in-depth analysis of the distribution of dopaminergic effects would further elucidate the computational functions of dopamine. If released globally, dopamine would be expected cause cross-adaptation of mitral cells innervating distant glomeruli. On a fast time scale interglomerular inhibition has not been observed

(McGann et al, 2005). However, as dopamine acts on a slow temporal scale, cross-adaptation by prolonged stimulation of remote glomeruli could yield an interesting way to test for spatial dimensions of dopaminergic effects. Feasible approaches would be either tonic stimulation with an odor that does not evoke activity within the glomerulus or optogenetic stimulation of the olfactory receptor nerve terminals directly. These experiments would also provide insights into the physiological stimulus conditions promoting dopamine release. Also, recent publications have employed "false fluorescent neurotransmitters" to selectively label catecholaminergic vesicles (Gubernator et al, 2009; Lee et al, 2010). This approach could potentially allow for studying both spatial and temporal properties of neurotransmitter release within individual neurons and consequently provide insights into the cellular localization and the modes of dopamine release.

Importantly, dopaminergic neurons are known to also release GABA. To date, the role of co-release and the potential interactions between GABAergic and dopaminergic transmission have not addressed at all. However, due to the large number of GABAergic microcircuits within the olfactory bulb, a specific targeting of the dopaminergic subpopulation by optogenetic tools (see Knöpfel et al, 2010 for a review) would be desirable for a comprehensive analysis. Alternatively, dopaminergic neurons could also be targeted by selective neurotoxins such as 6-hydroxydopamine or MPTP (Anichtchik et al, 2004; Sallinen et al, 2009). However, such an approach would be prone to causing strong side effects within the system.

Furthermore, my results indicate a possible effect of dopamine on pattern decorrelation as a consequence of shifting the response threshold of mitral cells but potentially also as by impairing lateral

inhibitory interactions within the system. It would therefore be interesting to address this aspect in more detail by calcium sensitive dye imaging. If the effect of dopamine is really limited to mitral cells these experiments would also allow for a direct testing of the predictions made by the analytical model by Wiechert and colleagues (2010).

Acknowledgements

I would like to thank PD Dr. Rainer Friedrich for providing me with the opportunity to pursue my project in his laboratory and under his supervision and for his support and motivating discussions particularly in the final stage of my PhD. Furthermore, I am grateful to members the Friedrich lab, both past and present, for fruitful discussions (scientific and non-scientific) and for providing a warm and supportive working atmosphere.

I thank Prof. Dr. Andreas Lüthi for taking the time to review and evaluate my thesis and Prof. Dr. Silvia Arber to agree to officiate as the faculty responsible. In addition, I thank the Boehringer Ingelheim Fonds for supporting my project.

Furthermore, I would also like to thank my family and my friends for reminding me every now and then that there is a world beyond the lab. Thanks to all of you for being part of my life!

References

Adrian ED (1942). Olfactory reactions in the brain of the hedgehog. J Physiol, 100: 459 – 473.

Allen II ZJ, Waclaw RR, Colbert MC, Campbell K (2007). Molecular identity of olfactory bulb interneurons: transcriptional codes of periglomerular neuron subtypes. J Mol Hist, 38: 517 – 525.

Andres KH (1970). Anatomy and ultrastructure of the olfactory bulb in fish, amphibia, reptiles, birds and mammals. In: Ciba foundation symposium on taste and smell in vertebrates (Wolstenholme GEW, Knight J, eds), pp 177 – 196. London: Churchill Press.

Anichtchik OV, Kaslin J, Peitsaro N, Scheinin M, Panula P (2004). Neurochemical and behavioural changes in zebrafish Danio rerio after systemic administration of 6-hydroxydopamine and 1-methyl-4-phenyl-1,2,3,6-tetrahydropyridine. J Neurochem, 88, 443 – 453.

Arevian AC, Kapoor V, Urban NN (2008). Activity-dependent gating of lateral inhibition in the mouse olfactory bulb. Nat Neurosci, 11: 80 – 87.

Arganda S, Guantes R, de Polavieja GG (2007). Sodium pumps adapt spike bursting to stimulus statistics. Nat Neurosci, 10: 1467 – 1473.

Aroniadou-Anderjaska V, Zhou FM, Priest CA, Ennis M, Shipley MT (2000). Tonic and synaptically evoked presynaptic inhibition of sensory input to the rat olfactory bulb via GABA(B) heteroreceptors. J Neurophysiol, 84: 1194 – 1203.

Aungst JL, Heyward PM, Puche AC, Karnup SV, Hayar A, Szabo G, Shipley MT (2003). Centre-surround inhibition among olfactory bulb glomeruli. Nature, 426: 623 – 629.

Azouz R (2005). Dynamic spatiotemporal synaptic integration in cortical neurons: neuronal gain, revisited. J Neurophysiol, 94: 2785 – 2796.

Beaulieu JM, Gainetdinov RR (2011). The physiology, signaling, and pharmacology of dopamine receptors. Pharmacol Rev, 63: 182 – 217.

Berkowicz DA, Trombley PQ (2000). Dopaminergic modulation at the olfactory nerve synapse. Brain Res, 855: 90 – 99.

Berkowicz DA, Trombley PQ, Shepherd GM (1994). Evidence for glutamate as the olfactory receptor cell neurotransmitter. J Neurophysiol, 71: 2557 – 2561.

Björklund A, Dunnett SB (2007). Dopamine neuron systems in the brain: an update. Trends Neurosci, 30: 194 – 202.

Björklund H, Lindvall O (1984). Dopamine-containing systems in the CNS. In: Handbook of Neuroanatomy (Björklund A, Hökfelt T, eds), pp 55 – 122. Amsterdam: Elsevier.

Bloomfield SA, Völgyi B (2009). The diverse functional roles and regulation of neuronal gap junctions in the retina. Nat Rev Neurosci, 10: 495 – 506.

Bockamp E, Sprengel R, Eshkind L, Lehmann T, Braun JM, Emmrich F, Hengstler JG (2008). Conditional transgenic mouse models: from the basics to genome-wide sets of knockouts and current studies of tissue regeneration. Regen Med, 3: 217 – 235.

Bonino M, Cantino D, Sassoe-Pognetto M (1999). Cellular and subcellular localization of gamma-aminobutyric acidB receptors in the rat olfactory bulb. Neurosci Lett, 274: 195 – 198.

Boyden ES, Zhang F, Bamberg E, Nagel G, Deisseroth K (2005). Millisecond-timescale, genetically targeted optical control of neural activity. Nat Neurosci, 8: 1263 – 1268.

Boyson SJ, McGonigle P, Molinoff PB (1986). Quantitative autoradiographic localization of the D1 and D2 subtypes of dopamine receptors in rat brain. J Neurosci, 6: 3177 – 3188.

Bozza T, McGann JP, Mombaerts P, Wachowiak M (2004). In vivo imaging of neuronal activity by targeted expression of a genetically encoded probe in the mouse. Neuron, 42: 9 – 21.

Briggs CA, Pollock NJ, Frail DE, Paxson CL, Rakowski RF, Kang CH, Kebabian JW (1991). Activation of the 5-HT$_{1c}$ receptor expressed in Xenopus oocytes by the benzazepines SCH 23390 and SKF 38393. Br J Pharmacol, 104: 1038 – 1044.

Brünig I, Sommer M, Hatt H, Bormann J (1999). Dopamine receptor subtypes modulate olfactory bulb gamma-aminobutyric acid type A receptors. Proc Natl Acad Sci USA, 96: 2456 – 2460.

Brustein E, Marandi N, Kovalchuk Y, Drapeau P, Konnerth A (2003). "In vivo" monitoring of neuronal network activity in zebrafish by two-photon Ca(2+) imaging. Pflugers Arch, 446: 766 – 773.

Buck LB (2000). The molecular architecture of odor and pheromone sensing in mammals. Cell, 100: 611 – 618.

Byrd CA, Brunjes PC (1995). Organization of the olfactory system in the adult zebrafish: histological, immunohistochemical, and quantitative analysis. J Comp Neurol, 358: 247 – 259.

Camps M, Kelly PH, Palacios JM (1990). Autoradiographic localization of dopamine D 1 and D 2 receptors in the brain of several mammalian species. J Neural Transm Gen Sect, 80: 105 – 127.

Carr WES (1988). The molecular nature of chemical stimuli in the aquatic environment. In: Sensory biology of aquatic animals (Atema J, Fay RR, Popper AN, Tavolga WN, eds), pp 3 – 27. New York: Springer.

Chaudhury D, Manella L, Arellanos A, Escanilla O, Cleland TA, Linster C (2010). Olfactory bulb habituation to odor stimuli. Behav Neurosci, 124: 490 – 499.

Chen WR, Xiong W, Shepherd GM (2000). Analysis of relations between NMDA receptors and GABA release at olfactory bulb reciprocal synapses. Neuron, 25: 625 – 633.

Chu DC, Albin RL, Young AB, Penney JB (1990). Distribution and kinetics of GABAB binding sites in rat central nervous system: a quantitative autoradiographic study. Neuroscience, 34: 341 – 57.

Cleland TA, Sethupathy P (2007). Non-topographical contrast enhancement in the olfactory bulb. BMC Neurosci, 7: 7.

Cook PB, McReynolds JS (1998). Lateral inhibition in the inner retina is important for spatial tuning of ganglion cells. Nat Neurosci, 1: 714 – 719.

Coopersmith R, Weihmuller FB, Kirstein CL, Marshall JF, Leon M (1991). Extracellular dopamine increases in the neonatal olfactory bulb during odor preference training. Brain Res, 564: 149 – 153.

Coronas V, Krantic S, Jourdan F, Moyse E (1999). Dopamine receptor coupling to adenylyl cyclase in rat olfactory pathway: a combined pharmacological-radioautographic approach. Neuroscience, 90: 69 – 78.

Coronas V, Srivastava LK, Liang JJ, Jourdan F, Moyse E (1997). Identification and localization of dopamine receptor subtypes in rat olfactory mucosa and bulb: a combined in situ hybridization and ligand binding radioautographic approach. J Chem Neuroanat, 12: 243 – 257.

Davida NG, Blakemore LJ, Trombley PQ (2003). Dopamine modulates synaptic transmission between rat olfactory bulb neurons in culture. J Neurophysiol, 90: 395 – 404.

Davison IG, Boyd JD, Delaney KR (2004). Dopamine inhibits mitral/tufted--> granule cell synapses in the frog olfactory bulb. J Neurosci, 24: 8057 – 8067.

Denk W, Strickler JH, Webb WW (1990). Two-photon laser scanning fluorescence microscopy. Science 248: 73 – 76.

Diop L, Gottberg E, Brière R, Grondin L, Reader TA (1988). Distribution of dopamine D1 receptors in rat cortical areas, neostriatum, olfactory bulb and hippocampus in relation to endogenous dopamine contents. Synapse, 2: 395 – 405.

Doiron B, Longtin A, Berman N, Maler L (2001). Subtractive and divisive inhibition: effect of voltage-dependent inhibitory conductances and noise. Neural Comput, 13: 227 – 248.

Duchamp-Viret P, Coronas V, Delaleu JC, Moyse E, Duchamp A (1997). Dopaminergic modulation of mitral cell activity in the frog olfactory bulb: a combined radioligand binding-electrophysiological study. Neuroscience, 79: 203 – 216.

Duchamp-Viret P, Delaleu JC, Duchamp A (2000). GABA(B)-mediated action in the frog olfactory bulb makes odor responses more salient. Neuroscience, 97: 771 – 777.

Edwards JG, Michel WC (2002). Odor-stimulated glutamatergic neurotransmission in the zebrafish olfactory bulb. J Comp Neurol, 454: 294 – 309.

Egger V, Svoboda K, Mainen ZF (2003). Mechanisms of lateral inhibition in the olfactory bulb: efficiency and modulation of spike-evoked calcium influx into granule cells. J Neurosci, 23: 7551 – 7558.

Egger V, Svoboda K, Mainen ZF (2005). Dendrodendritic synaptic signals in olfactory bulb granule cells: local spine boost and global low-threshold spike. J Neurosci, 25: 3521 – 3530.

Ennis M, Zhou FM, Ciombor KJ, Aroniadou-Anderjaska V, Hayar A, Borrelli E, Zimmer LA, Margolis F, Shipley MT (2001). Dopamine D2 receptor-mediated presynaptic inhibition of olfactory nerve terminals. J Neurophysiol, 86: 2986 – 2997.

Ennis M, Zimmer LA, Shipley MT (1996). Olfactory nerve stimulation activates rat mitral cells via NMDA and non-NMDA receptors in vitro. Neuroreport, 7: 989 – 992.

Escanilla O, Yuhas C, Marzan D, Linster C (2009). Dopaminergic modulation of olfactory bulb processing affects odor discrimination learning in rats. Behav Neurosci, 123: 828 – 833.

Friedrich RF, Habermann CJ, Laurent G (2004). Multiplexing using synchrony in the zebrafish olfactory bulb. Nat Neurosci, 7: 862 – 871.

Friedrich RW, Korsching SI (1997). Combinatorial and chemotopic odorant coding in the zebrafish olfactory bulb visualized by optical imaging. Neuron, 18: 737 – 752.

Friedrich RW, Korsching SI (1998). Chemotopic, combinatorial, and noncombinatorial odorant representations in the olfactory bulb revealed using a voltage-sensitive axon tracer. J Neurosci, 18: 9977 – 9988.

Friedrich RW, Laurent G (2001). Dynamic optimization of odor representations in the olfactory bulb by slow temporal patterning of mitral cell activity. Science, 291: 889 – 894.

Friedrich RW, Laurent G (2004). Dynamics of olfactory bulb input and output activity during odor stimulation in zebrafish. J Neurophysiol, 91: 2658 – 2669.

Friedrich RW, Stopfer M (2001). Recent dynamics in olfactory population coding. Curr Opin Neurobiol, 11: 468 – 474.

Friedrich RW, Yaksi E, Judkewitz B, Wiechert MT (2009). Processing of odor representations by neuronal circuits in the olfactory bulb. Ann N Y Acad Sci, 1170: 293 – 297.

Fritschy JM, Mohler H (1995). GABAA-receptor heterogeneity in the adult rat brain: differential regional and cellular distribution of seven major subunits. J Comp Neurol, 359: 154 – 194.

Fuller CL, Byrd CA (2005). Ruffed cells identified in the adult zebrafish olfactory bulb. Neurosci Lett, 379: 190 – 194.

Gall CM, Hendry SHC, Seroogy KB, Jones EG, Haycock JW (1987). Evidence for coexistence of GABA and dopamine in neurons of the rat olfactory bulb. J Comp Neurol, 266: 307 – 318.

Ghanem N, Jarinova O, Amores A, Long Q, Hatch G, Park BK, Rubenstein JL, Ekker M (2003). Regulatory roles of conserved intergenic domains in vertebrate Dlx bigene clusters. Genome Res, 13: 533 – 543.

Gonzales A, Smeets WJAJ (1991). Comparative analysis of dopamine and tyrosine hydroxylase immunoreactivities in the brain of two amphibians, the Anuran Rana ridibunda and the Urodele Pleurodeles waltlii. J Comp Neurol, 303: 457 – 477.

Gorelova N, Seamans JK, Yang CR (2002). Mechanisms of dopamine activation of fast-spiking interneurons that exert inhibition in rat prefrontal cortex. J Neurophysiol, 88: 3150 – 3166.

Gossen M, Bujard H (1992). Tight control of gene expression in mammalian cells by tetracycline-responsive promoters. Proc Natl Acad Sci USA, 89, 5547 – 5551.

Gray CM (1994). Synchronous oscillations in neuronal systems: mechanisms and functions. J Comput Neurosci, 1: 11 – 38.

Gubernator NG, Zhang H, Staal RG, Mosharov EV, Pereira DB, Yue M, Balsanek V, Vadola PA, Mukherjee B, Edwards RH, Sulzer D, Sames D (2009). Fluorescent false neurotransmitters visualize dopamine release from individual presynaptic terminals. Science, 324: 1441 – 1444..

Gurski MR, Hamilton KA (1996). Effects of dopamine and fluphenazine on field potential amplitude in the salamander olfactory bulb. Exp Brain Res, 108: 236 – 246.

Guthrie KM, Pullara JM, Marshall JF, Leon M (1991). Olfactory deprivation increases dopamine D2 receptor density in the rat olfactory bulb. Synapse, 8: 61 – 70.

Guthrie KM, Wilson DA, Leon M (1990). Early unilateral deprivation modifies olfactory bulb function. J Neurosci, 10: 3402 – 3412.

Gutièrrez-Mecinas, Crespo C, Blasco-Ibánez JM, Gracia-Llanes FJ, Marqués-Marí AI, Nácher J, Varea E, Martínez-Guijarro FJ (2005). Distribution of D2 dopamine receptor in the olfactory glomeruli of the rat olfactory bulb. Eur J Neurosci, 22: 1357 – 1367.

Halabisky B, Friedman D, Radojicic M, Strowbridge BW (2000). Calcium influx through NMDA receptors directly evokes GABA release in olfactory bulb granule cells. J Neurosci, 20: 5124 – 5134.

Halász N, Hökfelt T, Ljungdahl A, Johannson O, Goldstein M (1977a). Dopamine neurons in the olfactory bulb. Adv Biochem Psychopharmacol, 16: 169 – 177.

Halász N, Ljungdahl A, Hökfelt T (1978). Transmitter histochemistry of the rat olfactory bulb. II. Fluorescence histocemical, autoradiographic and electron microscopic localization of monoamines. Brain Res, 154: 253 – 271.

Halász N, Ljungdahl A, Hökfelt T, Johansson O, Goldstein M, Park D, Biberfeld P (1977b). Transmitter histochemistry of the rat olfactory bulb. I. Immunohistochemical localization of monoamine synthesizing enzymes. Support for intrabulbar, periglomerular dopamine neurons. Brain Res, 126: 455 – 474.

Hara TJ (1994). The diversity of chemical stimulation in fish olfaction and gustation. Rev Fish Biol Fish, 4: 1 – 35.

Hardy A, Palouzier-Paulignan B, Duchamp A, Royet JP, Duchamp-Viret P (2005). 5-Hydroxytryptamine action in the rat olfactory bulb: in vitro electrophysiological patch-clamp recordings of juxtaglomerular and mitral cells. Neuroscience, 131: 717 – 731.

Higashijima S, Masino MA, Mandel G, Fetcho JR (2003). Imaging neuronal activity during zebrafish behavior with a genetically encoded calcium indicator. J Neurophysiol, 90: 3986 – 3997.

Hoyer D, Karpf A (1988). [125I]SCH 23982, a 'selective' D-1 receptor antagonist, labels with high affinity 5-HT1C sites in pig choroid plexus. Eur J Pharmacol, 150: 181 - 184.

Hsia AY, Vincent JD, Lledo PM (1999). Dopamine depresses synaptic inputs into the olfactory bulb. J Neurophysiol, 82: 1082 – 1085.

Huang CJ, Jou TS, Ho YL, Lee WH, Jeng YT, Hsieh FJ, Tsai HJ (2005). Conditional expression of a myocardium-specific transgene in zebrafish transgenic lines. Dev Dyn, 233: 1294 – 1303.

Isaacson JS (2001). Mechanisms governing dendritic gamma-aminobutyric acid (GABA) release in the rat olfactory bulb. Proc Natl Acad Sci U S A, 98: 337 – 342.

Isaacson JS, Strowbridge BW (1998). Olfactory reciprocal synapses: dendritic signaling in the CNS. Neuron, 20: 749 – 761.

Kaslin J, Panula P (2001). Comparative anatomy of the histaminergic and other aminergic systems in zebrafish (Danio rerio). J Comp Neurol, 440: 342 – 377.

Kasowski HJ, Kim H, Greer CA (1999). Compartmental organization of the olfactory bulb glomerulus. J Comp Neurol, 407: 261 – 274.

Khan RM, Luk CH, Flinker A, Aggarwal A, Lapid H, Haddad R, Sobel N (2007). Predicting odor pleasantness from odorant structure: pleasantness as a reflection of the physical world. J Neurosci,27: 10015 – 10023.

Kiyokage E, Pan YZ, Shao Z, Kobayashi K, Szabo G, Yanagawa Y, Obata K, Okano H, Toida K, Puche AC, Shipley MT (2010). Molecular identity of periglomerular and short axon cells. J Neurosci, 30: 1185 – 1196.

Knöpfel T, Lin MZ, Levskaya A, Tian L, Lin JY, Boyden ES (2010). Toward the second generation of optogenetic tools. J Neurosci, 30: 14998 – 15004.

Kohwi M, Petryniak MA, Long JE, Ekker M, Obata K, Yanagawa Y, Rubenstein JLR, Alvarez-Buylla A (2007). A subpopulation of olfactory bulb GABAergic interneurons is derived from Emx1- and Dlx5/6-expressing progenitors. J Neurosci, 27: 6878 – 6891.

Kosaka K, Aika Y, Toida K, Heinzmann CW, Hunziker W, Jacobowitz DM, Nagatsu I, Streit P, Visser TJ, Kosaka T (1995). Chemically defined neuron groups and their subpopulations in the glomerular layer of the rat main olfactory bulb. Neurosci Res, 23: 73 – 88.

Kosaka K, Aika Y, Toida K, Kosaka T (2001). Structure of intraglomerular dendritic tufts of mitral cells and their contacts with olfactory nerve terminals and calbindinimmunoreactive type 2 periglomerular neurons. J Comp Neurol, 440: 219 – 235.

Kosaka K, Kosaka T (2005a). Synaptic organization of the glomerulus in the main olfactory bulb: compartments of the glomerulus and heterogeneity of the periglomerular cells. Anat Sci Int, 80: 80 – 90.

Kosaka K, Toida K, Aika Y, Kosaka T (1998). How simple is the organization of the olfactory glomerulus?: the heterogeneity of so-called periglomerular cells. Neurosci Res, 30: 101 – 110.

Kosaka K, Toida K, Margolis FL, Kosaka T (1997). Chemically defined neuron groups and their subpopulations in the glomerular layer of the rat main olfactory bulb--II. Prominent differences in the intraglomerular dendritic arborization and their relationship to olfactory nerve terminals. Neuroscience, 76: 775 – 786.

Kosaka T (1979). Ruffed cell: a new type of neuron with a distinctive initial unmyelinated portion of the axon in the olfactory bulb of the goldfish (Carassius auratus) I. Golgi impregnation and serial thin sectioning studies. J Comp Neurol, 186: 301 – 319.

Kosaka T (1980). Ruffed cell: a new type of neuron with a distinctive initial unmyelinated portion of the axon in the olfactory bulb of the goldfish (Carassius auratus): II. Fine structure of the ruffed cell. J Comp Neurol, 193: 119 – 145.

Kosaka T, Deans MR, Paul DL, Kosaka K (2005). Neuronal gap junctions in the mouse main olfactory bulb: morphological analyses on transgenic mice. Neuroscience, 134: 757 – 769.

Kosaka T, Hataguchi Y, Hama K, Nagatsu I, Wu JY (1985). Coexistence of immunoreactivities for glutamate decarboxylase and tyrosine hydroxylase in some neurons in the periglomerular region of the rat main olfactory bulb: possible coexistence of gamma-aminobutyric acid (GABA) and dopamine. Brain Res, 343: 166 – 171.

Kosaka T, Kosaka K (2003). Neuronal gap junctions in the rat main olfactory bulb, with special reference to intraglomerular gap junctions. Neurosci Res, 45: 189 – 209.

Kosaka T, Kosaka K (2005b). Structural organization of the glomerulus in the main olfactory bulb. Chem Senses, 30 (suppl 1): i107 – i108.

Kosaka T, Kosaka K (2005c). Intraglomerular dendritic link connected by gap junctions and chemical synapses in the mouse main olfactory bulb: electron microscopic serial section analyses. Neuroscience, 131: 611 – 625.

Kosaka T, Kosaka K (2008). Tyrosine hydroxylase-positive GABAergic juxtaglomerular neurons are the main source of the interglomerular connections in the mouse main olfactory bulb. Neurosci Res, 60: 349 – 354.

Kosaka T, Kosaka K (2011). "Interneurons" in the olfactory bulb revisited. Neurosci Res, 69: 93 – 99.

Koster NL, Norman AB, Richtand NM, Nickell WT, Puche AC, Pixley SK, Shipley MT (1999). Olfactory receptor neurons express D2 dopamine receptors. J Comp Neurol 411: 666 – 673.

Lagier S, Carleton A, Lledo PM (2004). Interplay between local GABAergic interneurons and relay neurons generates gamma oscillations in the rat olfactory bulb. J Neurosci, 24: 4382 – 4392.

Laurent G (2002). Olfactory network dynamics and the coding of multidimensional signals. Nat Rev Neurosci, 3: 884 – 895.

Laurie DJ, Seeburg PH, Wisdem W (1992). The distribution of 13 GABAA receptor subunit mRNAs in the rat brain. II. Olfactory bulb and cerebellum. J Neurosci, 12: 1063 – 1076.
Laurent, 2002

Lee M, Gubernator NG, Sulzer D, Sames D (2010). Development of pH-responsive fluorescent false neurotransmitters. J Am Chem Soc, 132: 8828 – 8830.

Levey AI, Hersch SM, Rye DB, Sunahara RK, Niznik HB, Kitt CA, Price DL, Maggio R, Brann MR, Ciliax BJ (1993). Localization of D1 and D2 dopamine receptors in brain with subtype-specific antibodies. Proc Natl Acad Sci USA, 90: 8861 – 8865.

Li J, Mack JA, Souren M, Yaksi E, Higashijima S, Mione M, Fetcho JR, Friedrich RW (2005). Early development of functional spatial maps in the zebrafish olfactory bulb. J Neurosci, 25: 5784 – 5795.

Linster C, Sachse S, Galizia CG (2005). Computational modeling suggests that response properties rather than spatial position determine connectivity between olfactory glomeruli. J Neurophysiol, 93: 3410 – 3417.

Maher BJ, Westbrook GL (2008). Co-transmission of dopamine and GABA in periglomerular cells. J Neurophysiol, 99: 1559 – 1564.

Mania-Farnell BL, Farbman AI, Bruch RC (1993). Bromocriptine, a dopamine D2 receptor agonist, inhibits adenylyl cyclase activity in rat olfactory epithelium. Neuroscience, 57: 173 – 180.

Mansour A, Meador-Woodruff JH, Bunzow JR, Civelli O, Akil H, Watson SJ (1990). Localization of dopamine D2 receptor mRNA and D1 and D2 receptor binding in the rat brain and pituitary: an in situ hybridizationreceptor autoradiographic analysis. J Neurosci, 10: 2587 – 2600.

Mathieson WB, Maler L (1988). Morphological and electrophysiological properties of a novel in vitro preparation: the electrosenspry lateral line lobe brain slice. J Comp Physiol A, 163: 489 – 506.

McGann JP, Pírez N, Gainey MA, Muratore C, Elias AS, Wachowiak M (2005). Odorant representations are modulated by intra- but not interglomerular presynaptic inhibition of olfactory sensory neurons. Neuron, 48: 1039 – 1053.

McLean JH, Shipley MT (1988). Postmitotic, postmigrational expression of tyrosine hydroxylase in olfactory bulb dopaminergic neurons. J Neurosci, 8: 3658 – 3669.

McNamara AM, Magidson PD, Linster C, Wilson DA, Cleland TA (2008). Distinct neural mechanisms mediate olfactory memory formation at different timescales. Learn Mem, 15: 117 – 125.

Mengod G, Vilaró MT, Niznik HB, Sunahara RK, Seeman P, O'Dowd BF, Palacios JM (1991). Visualization of a dopamine D1 receptor mRNA in human and rat brain. Brain Res Mol Brain Res, 10: 185 – 191.

Miyawaki A, Llopis J, Heim R, McCaffery JM, Adams JA, Ikura M, Tsien RY (1997). Fluorescent indicators for Ca2+ based on green fluorescent proteins and calmodulin. Nature, 388: 882 – 887.

Mombaerts P (1999). Molecular biology of odorant receptors in vertebrates. Annu Rev Neurosci, 22: 487 – 509.

Monsma FJ Jr, Mahan LC, McVittie LD, Gerfen CR, Sibley DR (1990). Molecular cloning and expression of a D1 dopamine receptor linked to adenylyl cyclase activation. Proc Natl Acad Sci USA, 87: 6723 – 6727.

Morilak DA, Garlow SJ, Ciaranello RD (1993). Immunocytochemical localization and description of neurons expressing serotonin$_2$ receptors in the rat brain. Neuroscience, 54: 701 – 717.

Murphy GJ, Darcy DP, Isaacson JS (2005). Intraglomerular inhibition: signaling mechanisms of an olfactory microcircuit. Nat Neurosci, 8: 354 – 364.

Murphy GJ, Glickfeld LL, Balsen Z, Isaacson JS (2004). Sensory neuron signaling to the brain: properties of transmitter release from olfactory nerve terminals. J Neurosci, 24: 3023 – 3030.

Nickell WT, Norman AB, Wyaatt LM, Shipley MT (1991). Olfactory bulb DA receptors may be located on the terminals of the olfactory nerve. Neuroreport, 2: 9 – 12.

Niessing J, Friedrich RW (2010). Olfactory pattern classification by discrete neuronal network states. Nature, 465: 47 – 52.

Nowycky MC, Halász N, Shepherd GM (1983). Evoked field potential analysis of dopaminergic mechanisms in the isolated turtle olfactory bulb. Neuroscience, 8: 717 – 722.

Palacios JM, Niehoff DL, Kuhar MJ (1981). [^{3}H]Spiperone binding sites in brain: autoradiographic localization of multiple receptors. Brain Res, 213:277–289.

Petzold GC, Hagiwara A, Murthy VN (2009). Serotonergic modulation of odor input to the mammalian olfactory bulb. Nat Neurosci, 12: 784 – 791.

Pignatelli A, Kobayashi K, Okano H, Belluzzi O (2005). Functional properties of dopaminergic neurones in the mouse olfactory bulb. J Physiol, 564: 501 – 514.

Pinching AJ, Powell TP (1971a). The neuron types of the glomerular layer of the olfactory bulb. J Cell Sci, 9: 305 – 345.

Pinching AJ, Powell TP (1971b). The neuropil of the glomeruli of the olfactory bulb. J Cell Sci, 9: 347 – 377.

Pinching AJ, Powell TP (1971c). The neuropil of the periglomerular region of the olfactory bulb. J Cell Sci, 9: 379 – 409.

Pologruto TA, Sabatini BL, Svoboda K (2003). ScanImage: flexible software for operating laser scanning microscopes. Biomed Eng Online, 2: 13.

Puopolo M, Bean BP, Raviola E (2005). Spontaneous activity of isolated dopaminergic periglomerular cells of the main olfactory bulb. J Neurophysiol, 94: 3618 – 3627.

Rickgauer JP, Tank DW (2009). Two-photon excitation of channelrhodopsin-2 at saturation. Proc Natl Acad Sci USA, 106: 15025 – 15030.

Rinberg D, Koulakov A, Gelperin A (2006). Speed-accuracy tradeoff in olfaction. Neuron, 51: 351 – 358.

Rubin BD, Katz LC (1999). Optical imaging of odorant representations in the mammalian olfactory bulb. Neuron, 23: 499 – 511.

Sallinen V, Torkko V, Sundvik M, Reenilä I, Khrustalyov D, Kaslin J, Panula P (2009). MPTP and MPP+ target specific aminergic cell populations in larval zebrafish. J Neurochem, 108: 719 – 731.

Satou M (1990). Synaptic organization, local neuronal circuitry, and functional segregation of the teleost olfactory bulb. Prog Neurobiol, 34: 115 – 142.

Schneider SP, Macrides F (1978). Laminar distribution of interneurons in the main olfactory bulb of the adult hamster. Brain Res Bull, 3: 73 – 82.

Schoppa NE, Kinzie JM, Sahara Y, Segerson TP, Westbrook GL (1998). Dendrodendritic inhibition in the olfactory bulb is driven by NMDA receptors. J Neurosci, 18: 6790– 6802.

Schonig K, Bujard H (2003). Generating conditional mouse mutants via tetracycline-controlled gene expression. Methods Mol Biol, 209: 69 – 104.
Schoppa et al, 1998

Sheng ZH (2009). Modulation of neurotransmitter release and presynaptic plasticity by protein phosphorylation. In: Molecular mechanisms of neurotransmitter release (Wang ZW, ed). Pp 187 – 206. New York: Humana Press.

Shepherd GM, Chen WR, Greer CA (2004). Olfactory bulb. In: The synaptic organization of the brain (Shepherd GM, ed), pp 165 – 216. Oxford: Oxford University Press.

Siklos L, Rickmann M, Joo F, Freeman WJ, Wolff JR (1995). Chloride is preferentially accumulated in a subpopulation of dendrites and periglomerular cells of the main olfactory bulb in adult rats. Neuroscience, 64: 165 – 172.

Silver RA (2010). Neuronal arithmetic. Nat Rev Neurosci, 11: 474 – 489.

Smith TC, Jahr CE (2002). Self-inhibition of olfactory bulb neurons. Nat Neurosci, 5: 760 – 766.

Stopfer M, Bhagavan S, Smith BH, Laurent G (1997). Impaired odour discrimination on desynchronization of odour-encoding neural assemblies. Nature, 390: 70 – 74.

Stosiek C, Garaschuk O, Holthoff K, Konnerth A (2003). In vivo two-photon calcium imaging of neuronal networks. Proc Natl Acad Sci U S A, 100: 7319 – 7324.

Suter BA, O'Connor T, Iyer V, Petreanu LT, Hooks BM, Kiritani T, Svoboda K, Shepherd GMG (2010). Ephus: multipurpose data acquisition software for neuroscience experiments. Front Neurosci, 4: 53.

Tabor R, Friedrich RW (2008). Pharmacological analysis of ionotropic glutamate receptor function in neuronal circuits of the zebrafish olfactory bulb. PLoS One, 3: e1416.

Tabor R, Yaksi E, Friedrich RW (2008). Multiple functions of GABA A and GABA B receptors during pattern processing in the zebrafish olfactory bulb. Eur J Neurosci, 28: 117 – 127.

Tabor R, Yaksi E, Weislogel JM, Friedrich RW (2004). Processing of odor mixtures in the zebrafish olfactory bulb. J Neurosci, 24: 6611 – 6620.

Tillerson JL, Caudle WM, Parent JM, Gong C, Schallert T, Miller GW (2006). Olfactory discrimination deficits in mice lacking the dopamine transporter or the D2 dopamine receptor. Behav Brain Res, 172: 97 – 105.

Toida K, Kosaka K, Aika Y, Kosaka T (2000). Chemically defined neuron groups and their subpopulations in the glomerular layer of the rat main olfactory bulb – IV. Intraglomerular synapses of tyrosine hydroxylase-immunoreactive neurons. Neuroscience, 101: 11 – 17.

Toida K, Kosaka K, Heizmann CW,Kosaka T (1998). Chemically defined neuron groups and their subpopulations in the glomerular layer of the rat main olfactory bulb: III. Structural features of calbindin D28K-immunoreactive neurons. J Comp Neurol, 392: 179 – 198.

Trombley PQ, Shepherd GM (1994). Glycine exerts potent inhibitory actions on mammalian olfactory bulb neurons. J Neurophysiol, 71: 761 – 167.

Uchida N, Mainen ZF (2003). Speed and accuracy of olfactory discrimination in the rat. Nat Neurosci, 6: 1224 – 1229.

Uchida S, Akaike N, Nabekura J (2000). Dopamine activates inward rectifier K+ channel in acutely dissociated rat substantia nigra neurones. Neuropharmacology, 39: 191 – 201.

Vargas G, Lucero MT (1999). Dopamine modulates inwardly rectifying hyperpolarization-activated current (Ih) in cultured rat olfactory receptor neurons. J Neurophysiol, 81: 149 – 158.

Vargas G, Lucero MT (2002). Modulation by PKA of the hyperpolarization-activated current (Ih) in cultured rat olfactory receptor neurons. J Membr Biol, 188: 115 – 125.

Wachowiak M, Cohen LB (1999). Presynaptic inhibition of primary olfactory afferents mediated by different mechanisms in lobster and turtle. J Neurosci, 19: 8808 – 8817.

Wachowiak M, Cohen LB (2001). Representation of odorants by receptor neuron input to the mouse olfactory bulb. Neuron, 32: 723 – 735.

Wehr M, Laurent G (1996). Odour encoding by temporal sequences of firing in oscillating neural assemblies. Nature, 384: 162 – 166.

Wei CJ, Linster C, Cleland TA (2006). Dopamine D(2) receptor activation modulates perceived odor intensity. Behav Neurosci, 120: 393 – 400.

Wiechert MT, Judkewitz B, Riecke H, Friedrich RW (2010). Mechanisms of pattern decorrelation by recurrent neuronal circuits. Nat Neurosci, 13: 1003 – 1010.

Wilson DA, Sullivan RM (1995). The D2 antagonist spiperone mimics the effects of olfactory deprivation on mitral/tufted cell odor response patterns. J Neurosci, 15: 5574 – 5581.

Wise PM, Cain WS (2000). Latency and accuracy of discriminations of odor quality between binary mixtures and their components. Chem Senses, 25: 247 – 265.

Wise RA (2004). Dopamine, learning and motivation. Nat Rev Neurosci, 5: 483 – 494.

Witkovsky P (2004). Dopamine and retinal function. Doc Ophthalmol, 108: 17 – 40.

Woodward RM, Panicker MM, Miledi R (1992). Actions of dopamine and dopaminergic drugs on cloned serotonin receptors expressed in Xenopus oocytes. Proc Nati Acad Sci USA, 89: 4708 – 4712.

Yaksi E, Friedrich RW (2006). Reconstruction of firing rate changes across neuronal populations by temporally deconvolved Ca2+ imaging. Nat Methods, 3: 377 – 383.

Yaksi E, Judkewitz B, Friedrich RW (2007). Topological reorganization of odor representations in the olfactory bulb. PLoS Biol, 5: e178.

Yaksi E*, von Saint Paul F*, Niessing J, Bundschuh ST, Friedrich RW (2009). Transformation of odor representations in target areas of the olfactory bulb. Nat Neurosci, 12: 474 – 482. (* Equal conribution)

Yokoi M, Mori K, Nakanishi S (1995). Refinement of odor molecule tuning by dendrodendritic synaptic inhibition in the olfactory bulb. Proc Natl Acad Sci USA, 92: 3371 – 3375.

Yue EL, Cleland TA, Pavlis M, Linster C (2004). Opposing effects of D1 and D2 receptor activation on odor discrimination learning. Behav Neurosci, 118: 184 – 190.

Zelles T, Boyd JD, Hardy AB, Delaney KR (2006). Branch-Specific Ca2+ Influx from Na+-Dependent Dendritic Spikes in Olfactory Granule Cells. J Neurosci, 26: 30 – 40.

Zerucha T, Stuhmer T, Hatch G, Park BK, Long Q, Yu G, Gambarotta A, Schultz JR, Rubenstein JL, Ekker M (2000). A highly conserved enhancer in the Dlx5/Dlx6 intergenic region is the site of cross-regulatory interactions between Dlx genes in the embryonic forebrain. J Neurosci, 20: 709 – 721.

Zhang YP, Oertner TG (2007). Optical induction of synaptic plasticity using a light-sensitive channel. Nat Methods, 4: 139 – 141.

Zhu P, Narita Y, Bundschuh ST, Fajardo O, Schärer YP, Chattopadhyaya B, Bouldoires EA, Stepien AE, Deisseroth K, Arber S, Sprengel R, Rijli FM, Friedrich RW (2009). Optogenetic Dissection of Neuronal Circuits in Zebrafish using Viral Gene Transfer and the Tet System. Front Neural Circuits, 3: 21.

SEBASTIAN BUNDSCHUH

Address:	Friedrich Miescher Institute for Biomedical Research
	WRO-1066.4.62
	Maulbeerstrasse 66
	4058 Basel
	Switzerland
Email:	sebastian.bundschuh@fmi.ch
Date of Birth:	November 10, 1978
Born in:	Friedberg (Hessen), Germany
Marital Status:	Single
Citizenship:	Federal Republic of Germany

EDUCATIONAL BACKGROUND

08/2011
Doctor of Philosophy, Grade: magna cum laude (very good)
Report: PD Dr. Rainer W. Friedrich
Co-report: Prof. Dr. Andreas Lüthi
Faculty representative: Prof. Dr. Silvia Arber

04/2007–03/2011
Friedrich Miescher Institute for Biomedical Research,
Basel (Switzerland), Group of Dr. Rainer Friedrich
Ph.D. studies in neurobiology continued

04/2005–03/2007
Max Planck Institute for Biomedical Research, Heidelberg
(Germany), Group of Dr. Rainer Friedrich
Ph.D. studies in neurobiology started
Topic: Dopaminergic modulation of odor responses by local
interneurons in the zebrafish olfactory bulb

03/2005
Master of Science, Grade: B (very good)

11/2004–03/2005
Hertie Institute for Clinical Brain Research, Tübingen
(Germany), Dept. Cognitive Neurology, Supervisor: Dr. Volker
Gauck
Topic: Functional connectivity within the deep cerebellar nuclei

10/2002–03/2005
Eberhard Karls University, Tübingen (Germany)
Master studies in Neural and Behavioural Sciences

08/2001
Vordiplom (intermediate examination), Grade: 1.7 (good)

10/1999–09/2002
Dresden University of Technology, Dresden (Germany)
Diploma studies in Psychology

08/1995–06/1998
Friedrich-Dessauer-Gymnasium (high school),
Frankfurt/Main, (Germany), Grade: 1.5 (good)

LABORATORY ROTATIONS

11/**2003**–03/**2004**	**Max Planck Institute for Medical Research**, Heidelberg (Germany), Group of Dr. Rainer Friedrich Topic: Spatial distribution of fast oscillations in the olfactory bulb of zebrafish
08/**2003**–09/**2003**	**Eberhard Karls University,** Tübingen (Germany), Dept. Cellular Neurobiology, Supervisor: Dr. Andreas Mack Topic: Visualizing vesicle cycling in Mb bipolar cell terminals in goldfish retinal slices
09/**2001**–08/**2002**	**Duke University**, Durham (North Carolina, USA), Center for Cognitive Neuroscience, Group of Dr. Marty Woldorff Topic: The effect of jittered inter-stimulus intervals on the EEG signal of omitted stimuli

FELLOWSHIPS

04/**2006**–04/**2008**	Fellowship by Boehringer Ingelheim Fonds

PUBLICATIONS

Zhu P, Narita Y, Bundschuh ST, Fajardo O, Schärer YP, Chattopadhyaya B, Bouldoires EA, Stepien AE, Deisseroth K, Arber S, Sprengel R, Rijli FM, Friedrich RW (2009). Optogenetic dissection of neuronal circuits in zebrafish using viral gene transfer and the Tet System. Front Neural Circuits, 3: 21.

Yaksi E, von Saint Paul F, Niessing J, Bundschuh ST, Friedrich RW (2009). Transformation of odor representations in target areas of the olfactory bulb. Nat Neurosci, 12: 474–482.

Rinck M, Becker ES, Bundschuh S, Engler S, Mueller A, Wissmann J, Ellwart T, Hoyer J (2003). Spinnenangst-Screening (SAS). In Hoyer J and Margraf J (editors), Angstdiagnostik: Grundlagen und Testverfahren. Berlin: Springer.

Rinck M, Bundschuh S, Engler S, Müller A, Wissmann J, Ellwart T, Becker ES (2002). Reliabilität und Validität dreier Instrumente zur Messung von Angst vor Spinnen. Diagnostica, 48: 141–149.